UNIVERSITA' DEGLI STUDI DI PARMA

Dottorato di ricerca in FISICA

Ciclo XXIX

Transport modeling and measurements in solid state photo-detectors

Coordinatore:

Chiar.mo Prof. CRISTIANO VIAPPIANI

Tutor:

Chiar.ma Prof.ssa MAURA PAVESI

Dottorando: ANDREA SANTI

Dedicated to my family

Andrea Santi

Dept. of Physics and Earth Sciences, University of Parma, Italy

Viale G.P. Usberti 7/A, I-43100 Parma, Italy

e-mail: andrea.santi@studenti.unipr.it

INDEX

ABSTRACT

The research is part of a project to study the $II-VI$ semi-insulating materials and especially the binary compound $CdTe$ and the ternary compound $Cd_{1-x}Zn_xTe$(CZT). The great interest about these materials lies in their ability to solve high-energy photons from the spectroscopic point of view. With a very remarkable stopping power, due to the high atomic number of its components and a high signal to noise ratio, due to a resistivity of the order of $10^{11}\ \Omega\cdot$ cm, the CZT ranks as one of the best radiation detectors at room temperature. Furthermore, the charge collection efficiency is closely related to the product between mobility μ and the lifetime τ of the carriers (electrons and holes) and it depends strongly on the spatial profile of the electric field.

The non-uniformity of the electric field within the CZT is confirmed both by numerical simulations and by experimental evidence (Pockels effect). The spatial profile of the electric field, that governs the transport of the charge carriers, should be investigated.

The technique used to obtain information about the transport and the electric field inside the material is a technique TOF (time of flight) called Laser Excited-Transient Current Technique: (LE-TCT). The transient measurements performed on full-area detectors have involved the study and the comparison of different samples.

The analysis of current transients was made using a new model (2τ model) that allows to obtain both the transport parameters and the electric field profile within the material.

Recently, complex geometries such as pixelated detectors and strip detectors have been developed with the intention to couple a good spectroscopic performance to a good spatial resolution. In this way, a single device can identify the type of X and γ rays source, either to its location. A complex geometry, however, entails complications from the point of view of the calculation of the current signal.

A new model (1τ model), developed and proposed in this thesis, allows both to decouple the contribution of the weighting (geometrical field) from that due to the electric field (physical field), and to obtain the mobility and lifetime of the carriers.

Finally, a new diffusion model suitable for the study of the thermal spread of the carriers, a phenomenon assumed to be negligible in the previous models, is presented. The model allows to obtain the diffusion coefficient, directly proportional to the mobility of carriers which then can be calculated in two independent ways starting from the current transients.

1 INTRODUCTION

The first chapter introduces the main mechanisms through matter interacts with radiation (Paragraph 1.1) and the phenomena that lead to the study of the transport in semiconductors (Paragraph 1.2).

1.1 RADIATION MATTER INTERACTIONS

Electromagnetic radiation such as X-rays and γ rays can exchange energy with matter through three main mechanisms (Fig 1.1) [1]:

- Photoelectric effect
- Compton scattering
- Pair production

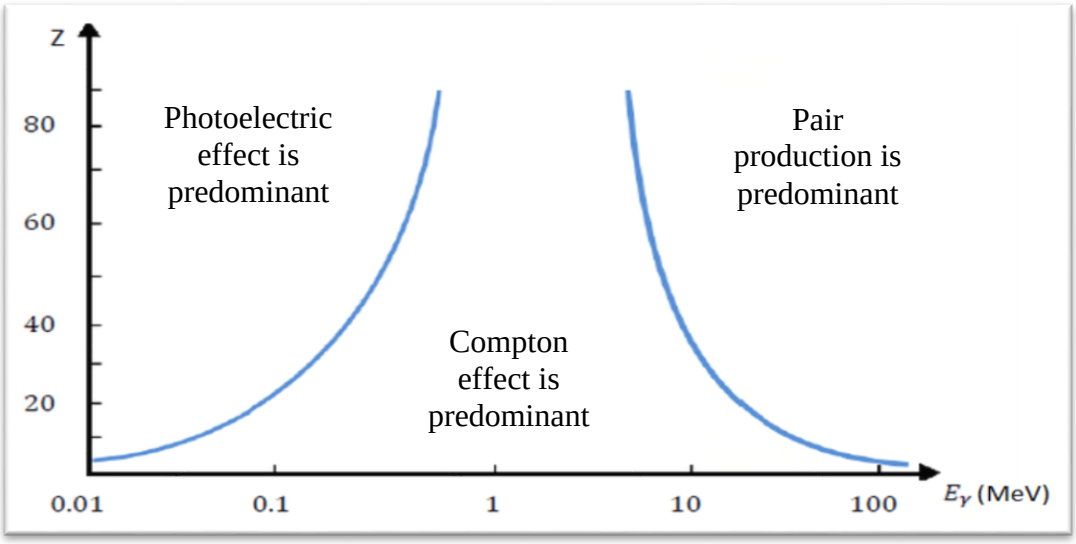

FIGURE 1.1 Main mechanisms of energy exchange between Radiation and Matter

PHOTOELECTRIC EFFECT

In the photoelectric (photon-electron) interaction, a photon transfers all its energy to an electron. Photoelectric interactions usually occur with electrons that are firmly bound to the atom, that is, those with a relatively high binding energy. Photoelectric interactions are most probable when the electron binding energy is only slightly less than the energy of the photon. If the binding energy is higher than the energy of the photon, a photoelectric interaction cannot occur. The photoelectric effect dominates for high values of the atomic number Z and for low photon energies $E_{PH} < 200$ keV.

In a metal, the conduction electrons are delocalized and they are bound to the metal through the metallic bond, an attractive Coulomb force from the metal positive ions: a photon with an energy equal or greater to the binding energy can rip away an electron from the metal.

In a semiconductor instead the electrons of the outer shells are located on the top of the valence band. These electrons can still absorb energy by photoelectric effect and they can be promoted into the conduction band if the photon energy matches with the energy gap. In the same time, the place left by the electron allows the valence electron to move if an electric field is applied. The place left free by the electron is described as a positive charge (hole) with its effective mass that depends on the interaction between valence electrons and the lattice. Photoelectric effect in a semiconductor can be interpreted as a pair production: a free negative charge in the conduction band and a free positive charge in the valence band.

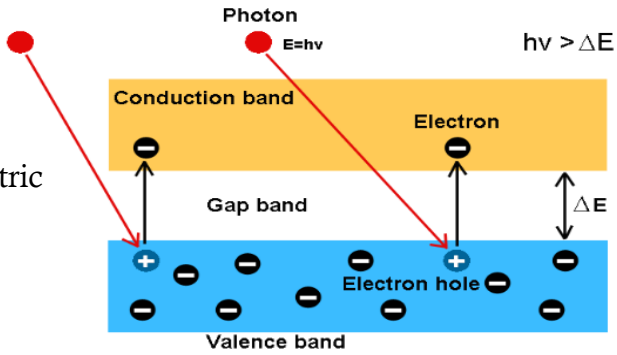

FIGURE 1.2 Photo-electric effect in semiconductors

COMPTON SCATTERING

In the Compton interaction only a portion of the energy of the incident photon is absorbed and a photon with lower energy is produced. This latter leaves the site of the interaction in a direction different from that of the incident photon. Because of the change in photon direction, this type of interaction is classified as a scattering process. In effect, a portion of the incident radiation is scattered by the material. This is significant in some situations because inside the material the primary X-ray beam becomes a secondary radiation source. Compton effect predominates for small values of the atomic number Z and for photon energy in the range $200keV < E_{PH} < 1\,MeV$.

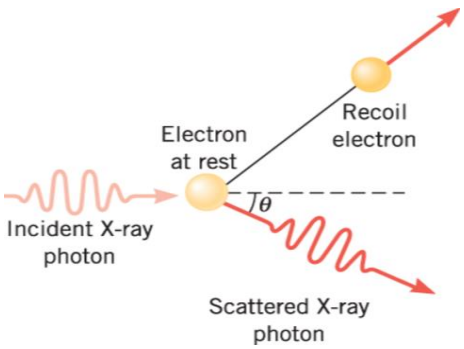

FIGURE 1.3 Compton scattering

PAIR PRODUCTION

Pair production is a photon-matter interaction that can occur only with photons with energies higher than $E_{PP} = 1.02\ MeV$. In a pair-production interaction, the photon interacts with the nucleus in such a manner that its energy is converted into matter. The interaction produces a pair of particles, an electron and a positron. These two particles have the same mass, equivalent to a rest mass energy of $0.51\ MeV$. The phenomenon dominates for high values of the atomic number Z.

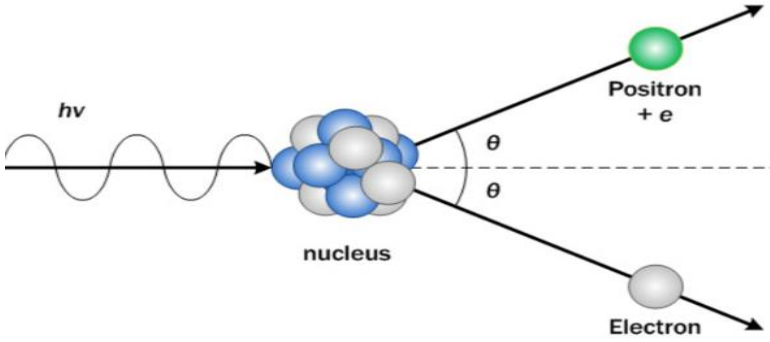

FIGURE 1.4 Production of an Electron-Positron pair

The photons' flux $\Phi(x)$ to a depth x inside the material is equal to:

$$\Phi(x) = \Phi(0)\, e^{-ux} \tag{1.1}$$

Where $u(\epsilon) = \mu_f + \mu_c + \mu_{pp}$ is the linear attenuation coefficient and it results from the sum of the contributions of the three above-mentioned effects.

The material used in our research, $CdZnTe$ or $CdTe$, has average atomic number close to 50. Furthermore the incident radiation used in our experiments has an energy of the order of $1\ eV$ so the dominant phenomenon is the photoelectric effect. Moreover, in our case, each absorbed photon produces one electron-hole pair.

1.2 CHARGE TRANSPORT IN SEMICONDUCTORS

The first Ohm law describes the passage of the current density $\vec{J}$ in a material when it is crossed by the electric field $\vec{E}$:

$$\vec{J} = \vec{J_e} + \vec{J_h} = (\sigma_e + \sigma_h)\vec{E} = \sigma\vec{E} = \frac{1}{\rho}\vec{E} \tag{1.2}$$

where:

- σ is the total conductivity, which is generally a tensor, but in condition of homogeneity and isotropy of the material it becomes a scalar term;
- ρ is the resistivity of the material;
- σ_e e σ_h are respectively the conductivity of electrons and holes, defined in the following way;

$$\begin{cases} \sigma_e = \mu_e\, n\, e \\ \sigma_h = \mu_h\, p\, e \end{cases} \tag{1.3}$$

where:

- e = 1.6 10^{-19} C
- μ_e e μ_h are respectively the mobility of electrons and holes;
  The mobility is of great interest because it's directly proportional to the velocity of the carriers:

$$\vec{v} = \mu\,\vec{E} \tag{1.4}$$

- n, p are the electrons density in the conduction band and the hole density in the valence band;
  In a semiconductor at the thermal equilibrium we can get the following relationships:

$$\begin{cases} n(T) = \int_{E_c}^{+\infty} D_c(E)\, F(E,T)\, dE = N_c\, e^{-\frac{(E_c - E_F)}{kT}} \\ p(T) = \int_{-\infty}^{E_v} D_v(E)\, [1 - F(E,T)]\, dE = N_v\, e^{-\frac{(E_F - E_v)}{kT}} \end{cases} \tag{1.5}$$

where:

- $D_c(E)$ and $D_v(E)$ are the density of states in the conduction band CB and in the valence band VB as a function of the energy;
- $F(E,T)$ is the Fermi function describing the occupancy probability of the energy level E and at the temperature T;
- N_c , N_v are the effective density of states of CB and VB;
- k is the Boltzmann constant. (at $T = 300\ °K$ the thermal energy is about $26\ mV$;
- E_v , E_F , E_c are respectively the VB maximum, the Fermi energy and the minimum of the CB

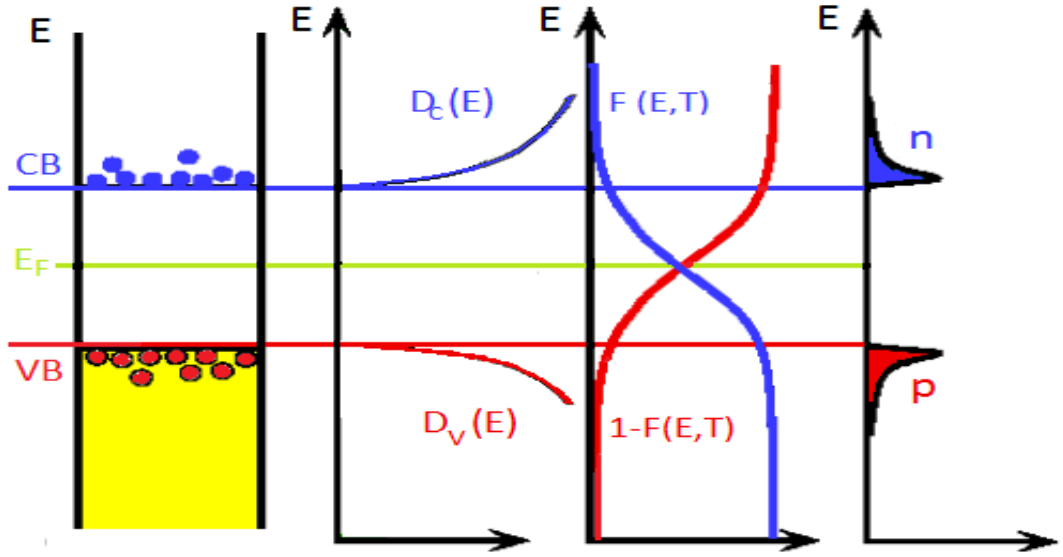

FIGURE 1.5. a) Bands' Diagram b) Density of states c) Fermi function d) Carriers' density

INTRINSIC SEMICONDUCTOR AT THE THERMAL EQUILIBRIUM

In an intrinsic semiconductor [2] the electron density in the CB and the density of holes in the VB must be equal:

$$n(T) = p(T) = \sqrt{N_c\, N_v}\; e^{-\frac{(E_c - E_v)}{kT}} \tag{1.6}$$

So the Fermi energy can be obtained using the (1.5):

$$E_{F\,intr} = \frac{E_c + E_v}{2} - \frac{kT}{2}\, ln\frac{N_C}{N_V} = \frac{E_c + E_v}{2} - \frac{kT}{2}\ln\left(\frac{m_e^*}{m_h^*}\right)^{\frac{3}{2}} \tag{1.7}$$

Where m_e^* and m_h^* are the effective masses of electrons and holes.

EXTRINSIC SEMICONDUCTOR AT THE THERMAL EQUILIBRIUM

The electrical properties of an intrinsic semiconductor crystal [2] can be modified inserting small controlled quantities of atoms of other species, thus obtaining an extrinsic (or doped) semiconductor. These atoms are replaced by the same number of atoms into the crystal without altering, ideally, the crystalline structure, but modifying the band structure. The purpose of the doping is to produce an excess of electrons (or holes) in the material. To understand how to carry out the doping of the n-type we consider the case of silicon (Si). The atoms of Si have four valence electrons, each of which is covalently linked to one of four adjacent Si atoms.

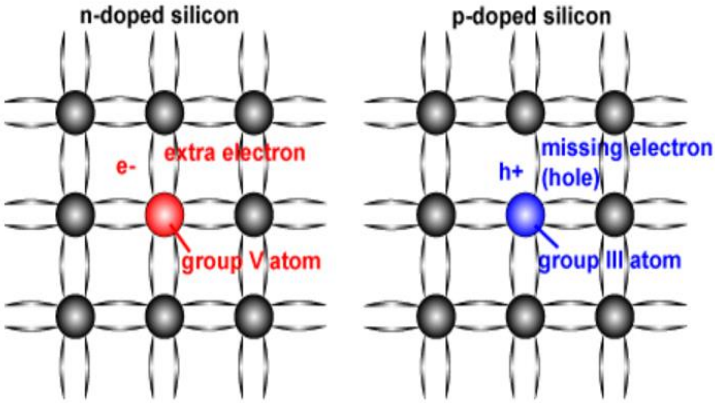

FIGURE 1.6 Example of n, p doped silicon

If an atom with five valence electrons, such as the phosphorous, is incorporated in the crystalline lattice in place of an atom of Si, then that atom will have four covalent bonds and an electron non-covalently linked bonds. This extra electron is only weakly bound to the atom and can easily be brought into the conduction band. In this case the electrons are the majority charge carriers and holes are the minority charge carriers.

The atoms with five valence electrons have then an electron to "donate", these atoms are indicated with the name of atoms "donor". In the same way atoms of group III, such as boron, yield holes to the valence band and are called "acceptor".

In a semiconductor extrinsic relations (1.6, 1.7) are obviously not valid anymore:

$$n + N_A = p + N_D \tag{1.8}$$

where N_A and N_D are the concentrations of ionized donors and acceptors. The Fermi energy is affected by these concentrations: if we add donors or acceptors to the semiconductor, the crystal will become extrinsic doped n or p, respectively, and the Fermi level will approach the CB or VB (figure 1.7)

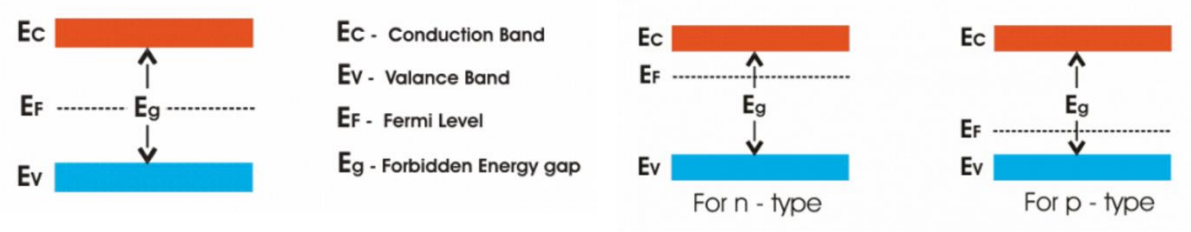

FIGURE 1.7 Fermi energy position in different types of semiconductors (intrinsic, n-doped and p-doped

THE RESISTIVITY IN CZT

A good radiation detector must have the minimum concentration of carriers thermally generated because these carriers disturb the collection of photo-generated carriers. Anyway when the CZT is not illuminated a flow of current through the material is observed. This noise contribution is called the dark current and it is due to the presence of unintentional free carriers (into extrinsic materials), generated by thermal energy or by cosmic rays.

However, to have a very low dark current:

- the energy gap must be high (in the CZT is about 1.57 eV). In this way the thermal promotion into the CB is suppressed;
- the resistivity has to be very high (in CZT ρ is equal to $10^{10\div11}\ \Omega\cdot cm$)

The semiconductor resistivity is closely link to the Fermi energy [3] : using the relations (1.2 ; 1.5) the resistivity becomes: (with $E_v = 0$)

$$\frac{1}{\rho} = e(\mu_e\, n(T) + \mu_h\, p(T)) = e(\mu_e\, N_c\, e^{-\frac{(E_c - E_F)}{kT}} + \mu_h\, N_v\, e^{-\frac{E_F}{kT}}) \qquad (1.9)$$

The value of the Fermi energy for which the resistivity assumes the maximum value is:

$$E_F = \frac{E_c}{2} - \frac{kT}{2} ln\left(\frac{m_e^*}{m_h^*}\right)^{\frac{3}{2}} - \frac{kT}{2}\, ln\frac{\mu_e}{\mu_h} \qquad (1.10)$$

And the maximum value of the resistivity results:

$$\rho_{MAX} = \frac{e^{+\frac{E_{gap}}{kT}}}{2e\sqrt{\mu_h \mu_e N_c\, N_v}} \qquad (1.11)$$

In $CdZnTe$ for example:

$$\begin{cases} \dfrac{\mu_e}{\mu_h} \sim 10 \quad \rightarrow per\ T = 300\ K \quad \dfrac{kT}{2}\ ln\dfrac{\mu_e}{\mu_h} \sim 0.03\ eV \\ \dfrac{m_e^*}{m_h^*} \sim 0.1 \quad \rightarrow per\ T = 300\ K \quad \dfrac{kT}{2} ln\left(\dfrac{m_e^*}{m_h^*}\right)^{\frac{3}{2}} \sim 0.04\ eV \\ \dfrac{E_c}{2} \sim 0.8\ eV \end{cases}$$

A well-known result is obtained: the resistivity has a maximum when the Fermi energy is located approximately in the middle gap. In Figure 1.8 the profile of the resistivity as a function of the Fermi energy, in the case of CZT:

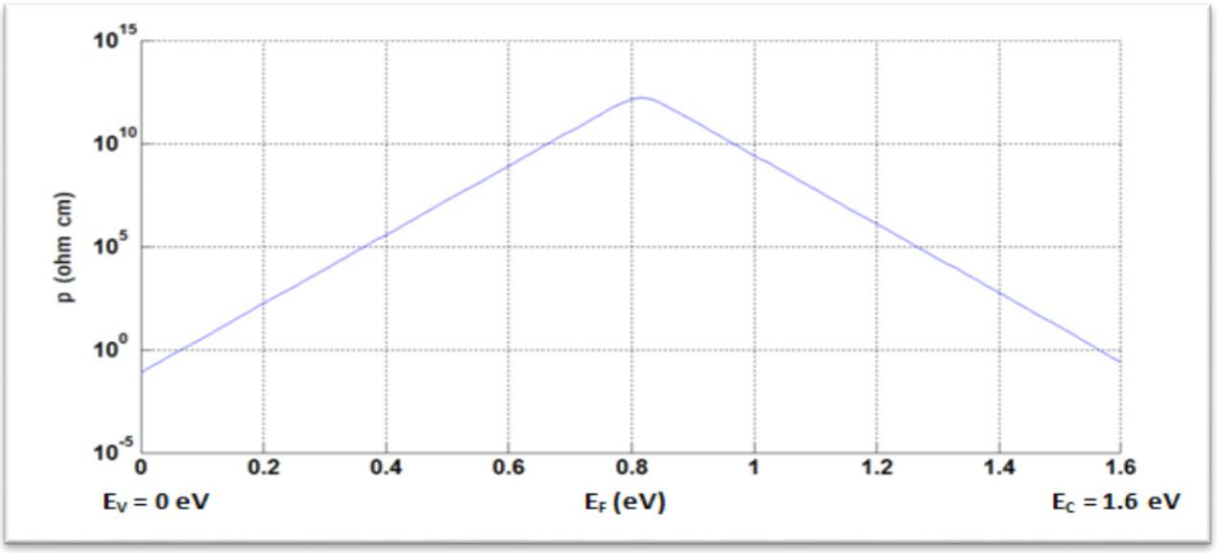

FIGURE 1.8 CZT resistivity as a function of the Fermi Energy. The resistivity shows a maximum value when the Fermi energy is located in the mid gap.

However, as described in Chapter 2, the CZT is not an intrinsic material. The material is a ternary alloy and inhomogeneities and an imperfect stoichiometry are responsible for a not intentional doping. The CZT grows naturally p-doped because of a non-congruent solidification and the presence of Cadmium vacancies. To obtain a high resistivity, the CZT is doped with chlorine and/or indium.

SEMICONDUCTOR IN THERMAL NON-EQUILIBRIUM

In the paragraphs discussed before, the concentration of the free carrier concentration is determined for semiconductor near the thermal equilibrium and, as a consequence, it depends only on the temperature and the doping concentration.

In semiconductors far from the thermal equilibrium [3], the carrier concentration it is also determined by external factors such as the injection of charge, due to injecting contacts or absorption of radiation due to the photo-electric effect.

In the case of CZT the photo-electric effect dominates: the density of the thermal carriers is negligible compared to the density of photo-generated carriers. Furthermore, the contacts used in our samples are ohmic non-injecting contacts. Since the concentration of majority thermal carriers is negligible (due to the high resistivity), in the next chapter the physical quantities *n* and *p* will represent the densities of photo-generated electrons and holes.

CARRIERS' PHOTO-GENERATION AND PHOTO-CURRENT

The photon's absorption at x_0 depth in a semiconductor in which a bias is applied at the contacts in $x = 0$ *e* $x = L$, leads to the generation of a great number of electron-hole pairs. The application of a bias V leads electrons and holes to move to their respective electrode driven by the electric field $\vec{E}$ at different velocities because of their different mobilities.

In chapter 3 the topics about charge transport and photo-current will be widely explained.

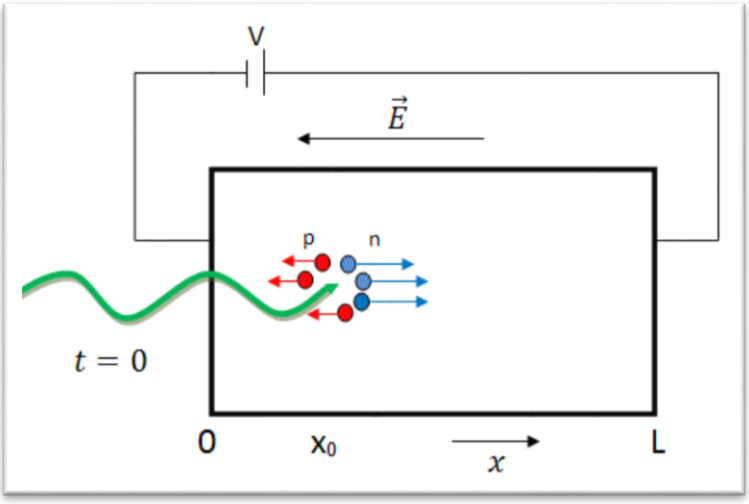

FIGURE 1.9. Photon's absorption with the consequent creation of electron-hole pairs separated by the electric field.

2 THE MATERIAL

The second chapter introduces the different materials studied for the detection of X and γ rays. In the paragraph 2.1 the properties of a great solid-state photodetector are investigated. The study of the detectors focused on the Tellurides $CdTe$ and $Cd_{1-x}Zn_xTe$, proposed as good candidates for the detection of high-energy photons at room temperature. The paragraph 2.4 shows the detectors' different configurations depending on the specific use, for example in the imaging systems in which the information is spectroscopic and also positional. This section introduces the importance of the geometry of the contacts, widely studied in Chapter 3.

Paragraph 2.5 explains instead the several methods employed in the growth of CdTe and CZT both for spectroscopic applications for the growth of substrates.

Defects and imperfections in $CdZnTe$ are examined in section 2.6. The chapter ends with the study of complex defects (A center) and auto-compensation process.

2.1 MATERIALS FOR DETECTORS OF X,γ RAYS

The last decade has seen a significant improvement in the ability to perform energy dispersive spectroscopy, both relatively to the detection of X and γ rays than to that of the particles. Many are the areas in which these technologies are used, medical diagnostics, astrophysics, monitoring of industrial processes, airport security, and environmental and food safety. Of fundamental importance in this process of "technology migration" from research laboratories to the most common commercial systems is the ability to make these spectroscopic devices operating at room temperature.

Semiconductors first used as active material in detectors of X and γ rays are silicon and germanium. Their success lies still in the ability to reduce sufficiently the level of impurities. For the germanium, the biggest limitation consists in the need for cooling to $77\ K$ to reduce leakage currents, which otherwise are generated due to the low bandgap of the semiconductor (0.67 eV at RT (*table* 2.1)). These difficulties are, however, matched by an excellent energy resolution spectroscopy relative to high photon energy. Because of its atomic number, the silicon manifests a reduced ability to absorb γ rays of about 50 times lower than the germanium; but for this reason it is even today widely used in the detectors of X-rays in low energy ranges, especially in situations in which it should measure X and γ rays simultaneously. These rays in fact would cross the silicon and then potentially be subsequently detected by other detectors. Favorable characteristic of silicon is its great bandgap (1.12 $eV\ at\ RT$) compared to the germanium, which allows then lower leakage currents.

If trapping events are reduced, the resolution is better than in germanium.

The great popularity of detectors based on Silicon or Germanium is due to their excellent charge transport properties, but the need for the continuous maintenance of the low temperature has prompted interest into new materials' research.

FIGURE 2.1 Silicon ingots Germanium ingot

Among these we mention HgI_2 that, with its 2.13 eV bandgap, allows the use at room temperature. Furthermore, this material is attracting attention because of its high average atomic weight, which allows to absorb the radiation in the vicinity of the surface and thus significantly reducing the problems related to the low mobility of carriers. At present, degradation of surfaces, a certain tendency to polarization and a still low mobility of holes, however, limit its applicability [4]

A composite semiconductor which on the contrary is already widely used is the CdTe. It has a good average atomic number and a bandgap of 1.52 eV, which allows its use at room temperature with reduced leakage currents (even if a cooling to $-40\ °C$ leads to an increase in the energy resolution). Just the Z allows a greater probability of photoelectric absorption $4-5$ times greater than the germanium and 100 times compared to silicon [4]. In view of these excellent characteristics, however, it presents the problem of internal polarization. This phenomenon is due to the capture of carriers by trapping centres such as impurities, point defects, plastic deformation, that induce an internal field to the material, in opposition to that applied. This electric field does not allow neither accurate collection nor a good control of the applied potential, leading overall to a significant deterioration of the intensity of the signal, of the counting rate and well then of the resolution. The major failing of CdTe detectors is finally the poor hole-transport properties. The low hole product $\mu_h\tau_h = 10^{-5} \div 10^{-4} cm^2/V$, compared to the electrons product $\mu_h\tau_h = 10^{-4} \div 10^{-3} cm^2/V$, increases the probability of recombination and trapping of the holes: only a fraction of the charge signal generated within the semiconductor is collected on the detector electrodes.

To overcome this drawback, it is possible to study an appropriate geometry of the electrodes which reduces the path of holes. It should however be remembered that in the case of highly energetic photons, since their interaction occurs in depth, such geometry loses much in effectiveness and therefore the reduced mobility of the holes becomes a highly limiting factor of the capacity of the detector itself. The evolution of CdTe has led to the synthesis of the cadmium zinc telluride CZT, which immediately has shown itself more performant for spectroscopic applications.

In the $Cd_{1-x}\ Zn_xTe$ for X-rays detection the fraction of zinc x varies from 0.02 to 0.2 [5]. The CZT bandgap has values in the range of $1.5 - 2.2\ eV$ that provides a leakage current low enough to work without the cryogenic systems and to allow portable and compact equipment. The energy gap, however, is low enough to permit the generation of a high number of electron-hole pairs by interaction with X and γ-rays and then allows to get good statistics. A great difference with the CdTe is the absence of polarization effects and therefore the chance to produce detectors with less electrical problems and best global efficiencies [6]. Another feature that makes better the use of CZT compared to CdTe is that it can easily reach resistivity of the order of 10^{10} Ω cm. Such resistivity allows the application of strong electric potential and thus increases the capacity of the detectors. The main objective in the growth of a material capable of detection is to obtain a high resistivity single crystal, free of extended defects and inclusions and precipitates that would to degrade the detector's response.

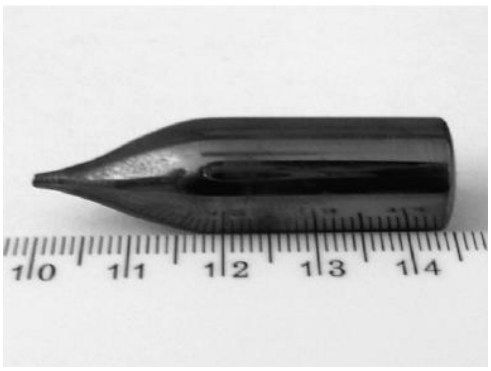

FIGURE 2.2. CZT ingot CdTe ingot

2.2 RADIATIONS DETECTOR'S PROPERTIES

A material can be effectively used as a detector for X and γ rays if it has the following characteristics [7]:

- high atomic number Z for an efficient interaction with the radiation. The photoelectric absorption capture cross section is proportional to Z^n, where $4 < n < 5$. CZT and CdTe have an atomic number close to 50; while $Z_{Si} = 12$ and $Z_{Ge} = 32$;

- a bandgap high enough to ensure high resistivity (> $10^9 \Omega \cdot cm$) and low dark current to ensure low noise in the devices;

- bandgap suitably low to have a small ionization energy for the electron-hole pairs (< $5eV$). There is no minimum value of the energy gap for this aim. Generally, values greater than 1.5 eV are necessary to ensure the control of currents generated thermally and therefore to limit the loss of energy resolution caused by the noise. The number of electron-hole pairs created is therefore reasonably high and a good statistic is ensured, which results in a greater signal-to-noise ratio. The energy gap in CZT results as a function of the x fraction of Zinc and the temperature T:

$$E_g(eV) = 1.606 + 0.38\,\mathrm{x} + 0.463\,\mathrm{x}^2 - 4.5 \cdot 10^{-4} \cdot \frac{\mathrm{T}^2}{264 + \mathrm{T}} \qquad (2.1)$$

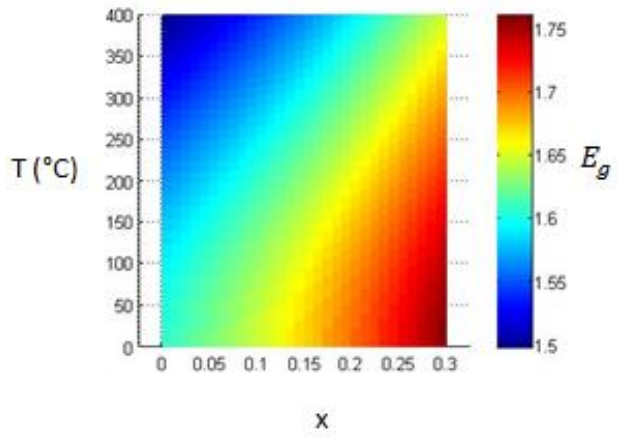

Figure 2.3. The energy gap in CZT as a function of x fraction of Zinc and temperature T. Energy gap increases at low values of the temperature and high values of the x fraction

The $Cd_{0.9}Zn_{0.1}Te$ at RT has an energy gap equal to 1.57 eV.

- high product value $\mu\tau$. The mean free path of carriers is given by the $\mu\tau E$ product [8], where μ is the mobility of the carriers, τ the lifetime, and E the applied electric field. The charge collection is determined by the fraction of photogenerated electrons and holes that can cross the detector thickness, in the interval of time in which the charge is collected. In the ideal case, the mean free path of the carriers must be much greater than the thickness of the detector, so as to ensure the complete collection of the charge.

In many materials, including the CZT, this condition is generally satisfied for the electrons, while it is more difficult that this happens for the holes. Consequently, one of the problems related to the development of the devices is an incomplete holes' collection, which results in a lower total charge collection and a reduced current pulse. The spectrum that emerges is therefore less solved, especially for low currents, and the photopeak is widened.

- the material must be highly pure, homogeneous and, if possible, free of defects. The device must also have sufficiently large area and thickness: ideally an area of about $1\ cm^2$ and $2-10\ mm$ of thickness. The demand of a large volume of the detector is associated with better efficiency and sensitivity. The greatest possible number of incident photons must have the possibility to be collected by the device so that it is required the detector material has high density. In the case of solid state detectors this request is always satisfied, when compared for example with gas detectors. The homogeneity and the low concentration of defects are used to ensure good charge transport characteristics and low leakage currents. In many cases it is required that the detector is entirely composed of monocrystalline material, in order to avoid the negative effects on transport related to the presence of grain boundaries or other extended defects.

- electrodes that favor a good charge collection. The contacts must ensure that the field inside the device is as uniform as possible and free from polarization effects. Some processes, such as the formation of the charge drained areas, make the electric field locally non-uniform thus making variable the characteristics of the device. The best contacts, in this case, are those ohmic, because they are used for materials where the resistivity reaches $10^{11}\Omega \cdot cm$ and also their use prevents the formation of space charge and thus the distortion of the electric field inside the CZT.

- the material must have a high surface resistivity to ensure a low surface conduction, i.e. low surface leakage current. They must also remain stable over time so that the leakage current of the device is limited for a long time. It is also important that the electric field lines do not terminate on the free surface of the detector (far from the electrodes), so to avoid the formation of surface free charges. The $\mu\tau$ product still remains one of the parameters indicative of the quality of the material and therefore of the detector itself. However, for the realization of a good detector they are not sufficient the characteristics of the active material; great care should be devoted to the further processing of the grown material. Cutting, polishing, preparation of contacts and their geometry, and global electronics are fundamental.

Table of the properties of the main solid-state photo detectors

Material	***Si***	***Ge***	***CdTe***	***$Cd_{0.9}Zn_{0.1}Te$***	***HgI_2***
Atomic Number Z	14	32	48-52	48-30-52	80-53
Mean Atomic Number	14	32	50	49.1	62
Density at 300 °K (g/cm^3)	2.33	5.33	5.85	5.78	6.40
Bandgap at 300 °K (eV)	1.12	0.67	1.44	1.572	2.15
Ionization energy (eV)	3.62	2.96 $(77°K)$	4.43	4.64	4.20
Relative dielectric constant ϵ_r	11.7	16	11	10.9	8.8
Resisitivity $(\Omega \cdot cm)$	$<10^4$	50	10^9	3×10^{10}	10^{13}
$(\mu\tau)_{EL}$ (cm^2/V)	>1	>1	3.3×10^{-3}	$(3\text{-}5)\times10^{-3}$	10^{-4}
$(\mu\tau)_{HO}$ (cm^2/V)	≈1	>1	$2\ 10^{-4}$	5×10^{-5}	4×10^{-5}

Table 2.1 [9]

2.3 Crystalline Structure of the CZT

$Cd_{1-x}\,Zn_xTe$ is a complete substitutional solid solution. CZT results a substitutional material because the Zinc atoms are casually replaced to Cadmium in a fraction equal to x, while it is said complete because the CZT solid phase can be produced in the entire interval $0 < x < 1$. Both end-members (binary compounds), CdTe ($x = 0$) and ZnTe ($x = 1$) show zinc-blende structure. The different distance of CdTe and ZnTe show that such substitutions lead to a change of the size of the average unit cell.

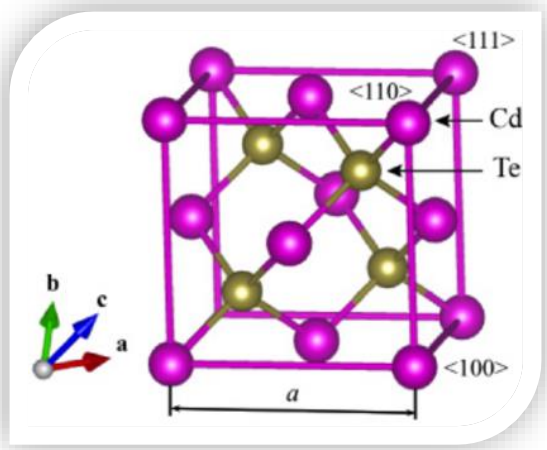

FIGURE 2.4 The unit cell of CdTe. The atomic structure is the Zinc-Blende structure. In CZT a x fraction of Cd is replaced by atoms of Zinc.

2.4 Devices

The detector for X and γ rays operating at room temperature can be used in different configurations depending on the specific use. The main used geometries are schematically shown in figure 2.5:

(a) simple planar device
(b) co-planar grids
(c) pixelated detector

Each of them can be used for applications [5] in which particular parameters must be optimized; for example, the geometries (a) and (b) are usually used for large single detector element. Simple planar geometries can be easily implemented in terms of the associated electronics, while the geometry with grids provides a higher spectral resolution (especially in the case of energy of γ rays, that is, above 200 keV).

As regards the geometry (c), in which each pixel provides an own signal, it is used in imaging systems in which it needs spectroscopic performance and positional resolution. The metal electrodes are applied to the semiconductor crystal through suitable lithographic processes which allow to obtain the required geometry.

The choice of the type of metal and the control of the deposition method greatly affect the overall quality of the detector. Under operating conditions, a very high voltage is applied between the device electrodes to reach an electric field of a few $kVolts/cm$.

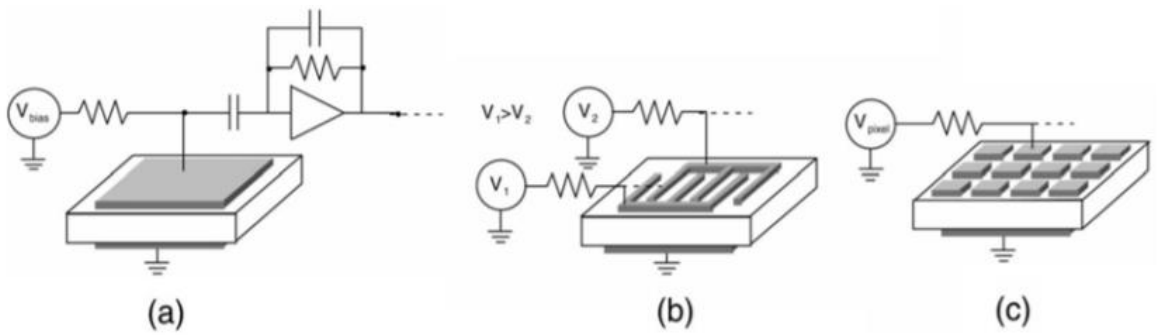

FIGURE 2.5 Device's geometries: simple planar (a), co-planar (b) and pixelated detector (c)

The photons X or γ absorbed by the device originate electron-hole pairs which induce a current in the external circuit. Through this electrical circuit the current is integrated over time by providing a signal proportional to the total charge produced which in turn is proportional to the energy of the incident photon. The geometry of the electrodes and the electronic readout determine the performance of the device; therefore, a material that has a low spectral response in a given geometric configuration with a given external circuit could be a detector if used in a different geometry or making use of more sophisticated electronics.

2.5 GROWTH OF CZT CRYSTALS

Several methods are currently employed with success in the growth of CdTe and CZT, both for spectroscopic applications and for substrates. For applications in *X* and γ rays detection the methods of growth that have found the best results are the Bridgman (with the respective variants) and the THM (traveling heater method). From the industrial point of view, the technique that has gained more support is the HPB method (high pressure Bridgman). Our detectors have been grown using the HPB method.

2.5.1 THE BRIDGMAN METHODS

Bridgman techniques start from the melt that reaches solidification at the solid-liquid interface by diffusion of latent heat. In general, the synthesis of the compound can be carried out "in situ" or "ex situ". It is possible to insert the individual elements in the bulb of growth precursors and to enter in the bulb the compound synthesized previously.

VERTICAL BRIDGMAN METHOD

A sealed ampoule containing the compound already synthesized is normally used. [10] This ampoule moves longitudinally in a furnace in which a special temperature profile is set (figure 2.6). To avoid interfacial instability, the heating rate must be sufficiently high in the vicinity of the melting temperature. Alternatively, it is possible to hold the ampoule and to move the oven. There are both the vertical configuration that the horizontal one. Inside the ampoule the material is contained in a specially shaped crucible to favor only one initial nucleation of solid phase and then the growth of a single crystal [12]. A further variation of the Bridgman technique is represented by the Vertical Gradient Freeze, where the thermal profile is electronically modified so that the transition is without mechanical movements of the crucible and the furnace [12]

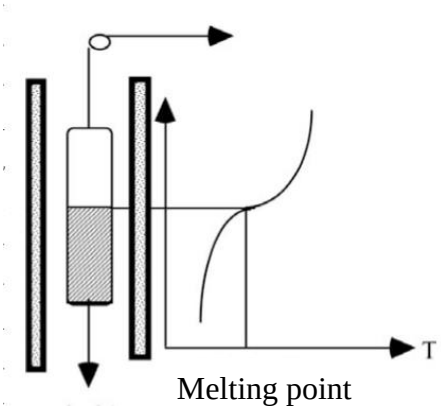

FIGURE 2.6. Vertical Bridgman method [11]

HIGH PRESSURE BRIDGMAN

The HPB method does not use a sealed ampoule, so to inhibit the decomposition of the components it is applied an overpressure of an inert gas, generally argon, the pressure of which varies commonly between 10 and 150 atmospheres [13]. The high pressure of the gas does not completely prevent leakage of material from the ampoule, but it slows down the process by decreasing the diffusion coefficient of Cd and Te vapours. At the melting temperature the evaporation is highly incongruent, so that the vapours are constituted for the most part by cadmium and in the crystal is then observes overabundance of tellurium.

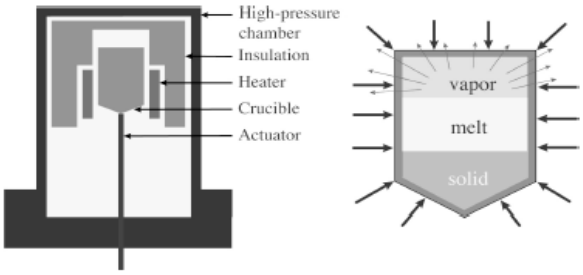

FIGURE 2.7: High Pressure Bridgman Method [8]

The fundamental components of a HPB plant (figure 2.7) are:

- Steel container inside which pressure is applied
- Heating elements for the control of the thermal gradient (typically graphite [11])
- Crucible and the mechanism which allows movement.

The choice of the crucible is a rather delicate process, since it may be contaminated, as happens for example in the case of quartz that releases oxygen at high temperature [13].

Quartz covered with graphite or graphite crucibles directly turn out to be excellent materials. The size can be up to eight inches in diameter. As regards the individual elements (Cd, Zn and Te), they are introduced already in the bulb in stoichiometric proportions and chosen with high purity levels. Before the beginning of growth, the charge is heated according to a precise temperature ramp up to about $1100\ °C$. During this process the synthesis of the compound occurs. The ampoule containing the melt is then subjected to a suitable vertical temperature gradient.

The crystallization of the material begins on the ampoule bottom and may be favoured by the addition of a crystalline seed. The speed of growth varies typically in the range $0.1 \div 1\ mm/h$. At the end of the process the crystal is then gradually brought to room temperature and pressure with a speed of a few $°C/h$ [5]. The entire growth process therefore has an average duration of about three or four weeks. With the HPB method it results very hard to obtain a single crystal and there are often grain boundaries, inclusions, precipitates of tellurium, and cracks.

LOW PRESSURE BRIDGMAN

In LPB growth occurs within the quartz ampoule in which the vacuum has been made and which is subsequently sealed. Even in this case, the oven can be both vertical and horizontal, but in LPB technique the vertical alignment is preferred [12]. In this case the speed of growth is about 1 mm/h [14]. The glass may also be coated by a thin layer of graphite to limit the contamination; however, the graphite cannot be sealed and the coating must therefore be limited to the lower part of the ampoule. The stoichiometry is much more assured than in HPB as the ampoule is sealed. However, a stoichiometric deviation in the crystal is always found, caused by poor control of the composition of the vapour phase in the ampoule.

The CdTe, as well as the CZT, has not congruent evaporation to the melting temperature, and then in the vapours is established a different stoichiometry with respect to the molten material, the vapours are rich in cadmium and consequently in the crystal an excess of Te is found that gives rise to inclusions and precipitates. For this reason, it is preferable the modified LPB in which it is a reserve of cadmium at one extremity.

MODIFIED LPB

This technique, as already mentioned, exploits a reserve of cadmium within the ampoule which is specially shaped (figure 2.8) so as to keep the Cd in an area of the thermal profile at a lower temperature than that of the growth. By acting on this temperature, it is possible to control the partial cadmium pressure in the vapors, which represents an additional degree of freedom in controlling the composition of the individual elements in the compound during growth. This possibility of management of the single crystal stoichiometry distinguishes itself from the classical technique. The extremity with the cadmium is typically maintained at a temperature of $825°C$ (to maintain the pressure of Cd of around 2 bar). The whole system is then brought above the melting point and finally the growth can start.

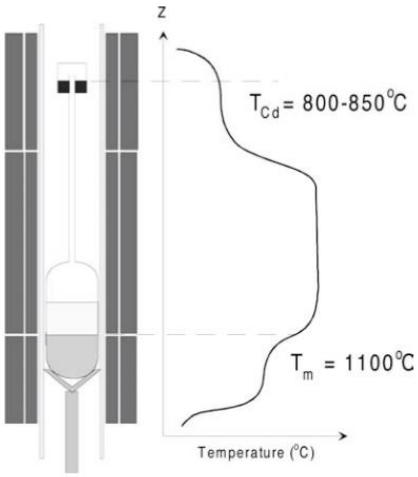

FIGURE 2.8 Method modified low pressure Bridgman [15]

The Cd excess condenses separately and crystallizes in the coldest part of ampoule. To reduce stress and achieve a higher quality, the crystal is often subjected to an annealing treatment at $600°C$. A CZT compound of high stoichiometric quality can be obtained. The stoichiometry of the grown crystal is not only more accurate, but also more uniform [16]. The dislocation density in LPB is less of an order of magnitude than the traditional one due to its minor stoichiometric deviations during growth.

TRAVELLING HEATER METHOD

The Bridgman techniques involve inherent drawbacks such as high temperatures (with relative increase in contamination), the risk of explosion due to the pressure of Cd and possible accumulations of Cd itself. For this reason, industry research is moving towards other methods such as the travelling heater method (THM). The components of the charge, already synthesized, are placed inside an open ampoule in which Te is added in excess.

The ampoule is then placed within a furnace in which the thermal gradient can be set and modified. Once heated, the tellurium in considerable excess liquefies, bringing in solution the CZT polycrystalline at temperatures of about $800\ °C$, smaller than those needed in fusion. The subsequent handling of such liquid zone (using the thermal gradient) involves the dissolution of the charge in the upper part and the crystal deposition in the lower part of the area [17].

THM is therefore a method of growth from solution. The latent heat is easily disposed of but there are several problems in the diffusion of the various elements within the solution to achieve the growth interface. The THM growth is slow and thus the growth rate amounted to about $1-2\ mm/day$. Also the growth of Te from solution highly facilitates the formation of inclusions and precipitates of tellurium in the crystal.

THE ZINC'S SEGREGATION

Among the most important aspects in the growth of CZT ingots, the main purpose is to maintain the desired stoichiometry uniformly throughout the crystal. This aspect is made difficult because of the progressive variation of Zinc concentration along the growth axis, generated by its segregation coefficient K. The latter is defined as the ratio between the concentration in solid phase C_S compared to that in the liquid phase C_L.

$$K = \frac{C_S}{C_L} \tag{2.2}$$

Zinc has a segregation coefficient value $K_{Zn} = 1.35$, which means a higher concentration in solid phase compared to the molten material : this aspect causes a continuous variation of the concentration of Zinc within the part of growing ingot. This problem is intrinsic in all melt-growth techniques and therefore it cannot be eliminated.

The control of the amount of zinc is very important: the local variation of the fraction of Zinc change the bandgap of the material and worsens the spectroscopic properties of the CZT. In the main growth's techniques, a strict control over the partial pressures of Cd and Zn is made, such as the HPB technique. [18]

2.6 Defects and Imperfections in CdZnTe

Impurities hold a key role in charge transport: they operate both as scattering centers, by changing its mobility and generating shallow and deep levels, and capture centers by reducing its lifetime.

In a perfect crystal, the only charge carriers present are the electrons and holes that belong to the crystal atoms. The electrons and holes determine the occupation of the energy levels, but does not introduce new levels.

Additional energy levels are associated with the presence of structural crystal defects such as vacancies, interstitial defects, atoms in antisite position and dislocations. Wherever the periodicity of the perfect crystal's structure is disturbed, it becomes possible for an electron to take energies that are prohibited in the perfect crystal. The presence of a structural defect may introduce one or more additional energy levels in the energy gap between the valence and the conduction bands. Unlike the bands that extend through the entire crystal, such additional energy levels are localized to the defect site.

A classification of imperfections in the crystals was given by Seitz [19] and includes nine different types of imperfections. We limit here considering only those imperfections that are relevant for understanding the electrical properties and their relationship with the defect of stoichiometry.

Such imperfections are:

- Point defects such as vacancies, interstitial defects, Te antisites and their associates;
- Dopant atoms different from the crystal's constituents;
- Associations between impurities and point defects;
- Dislocations

POINT DEFECTS

The main point defects in the undoped material are Frenkel defects, consisting of vacancies and Cadmium interstitial atoms:

• ionized cadmium vacancies V_{CD} can generate two different acceptor centers V_{Cd}^{-} and V_{Cd}^{2-}, with localized energy levels in the forbidden energy gap. The largest concentration of these defects makes the CZT material p-doped;

• similarly, Cadmium interstitial atoms form two donor levels Cd^{+} and Cd^{2+};

• another very important defect for the electrical properties is Te_{Cd}: the Tellurium atoms occupy sites of the sub-lattice of Cadmium. This kind of defect introduce a level approximately located in the midgap that acts as a trap level.

DOPANTS

These impurities, like the structural defects, introduce localized levels in the forbidden gap:

• chlorine (Group VII) can replace tellurium (Group VI) creating the donor level Cl_{Te} that if ionized, can donate an electron according to the reaction $Cl_{Te} \rightarrow e^{-} + Cl_{Te}^{+}$;

• indium (Group III) replaces Cadmium generating the donor level In_{Cd};

• sodium (Group I) replaces the Cadmium generating the acceptor level Na_{Cd} that can take an electron according to the reaction: $Na_{Cd} + e^{-} \rightarrow Na_{Cd}^{-}$;

ASSOCIATIONS BETWEEN POINT DEFECTS AND DOPANTS

A third way to generate localized levels is finally given by associations of structural defects between them or with impurities. Complexes are of fundamental importance as regards the electrical properties of the material and the good quality of a radiation detector: the dark currents must be the lowest possible and then material's resistivity request must be greater than $10^9\ \Omega \cdot cm$.

$CdZnTe$ with resistivity of the order of $10^{10}\ \Omega \cdot cm$ can be obtained through the doping with suitable elements such as chlorine and Indium [20], through the self-compensation mechanism.

DISLOCATIONS

The dislocations act as a pole of attraction of the point defects. In this way the action of the dislocations is deleterious for the material. Furthermore, the presence of a system of dislocations running through the whole thickness can create percolation paths that may short-circuit the two electrodes. Figure 2.9 shows a measure of etch pit density (EPD) made on oriented $CdZnTe$ (111) using the method of Nakagawa [21], using $HF, H_2O_2, and\ H_2O$.

This method allows to reveal dislocations after etching (white dots in the figure 2.9).

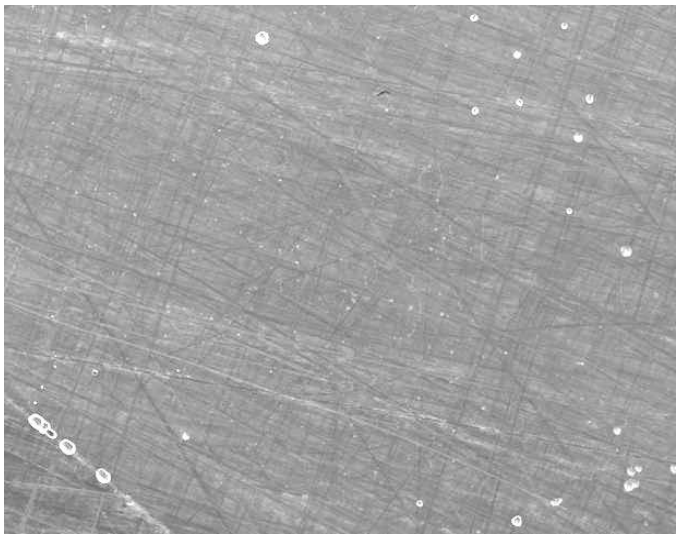

FIGURE 2.9. Dislocations in CZT.
Image's height: $= 1mm$.
Etch pit density $= 1.5 \cdot 10^{-3}\ cm^{-2}$

Impurities in CZT and their relationships with the transport properties are of great interest and they have been studied in detail. The largest contribution comes from Aluminum which acts as a dopant, followed by Iron. The other elements have lower concentrations of one part in a million (Table 2.2) The aluminum in the undoped materials appears in concentrations close to one part in a million [5]

GDMS analysis of a first-to-freeze segment of HPB grown $Cd_{1-x}Zn_xTe$

Element	ppmw	Element	ppmw	Element	ppmw
Li	0.010	Ca	0.041	Ga	0.42
B	0.004	Ti	0.002	As	0.005
Na	0.16	V	0.0003	Se	0.69
Mg	0.47	Cr	0.021	Ag	<0.05
Al	450	Mn	0.088	In	<0.1
Si	0.020	Fe	1.0	Sn	<0.03
P	0.10	Co	0.004	Sb	<0.03
S	0.84	Ni	0.047	Pb	<0.005
K	0.005	Cu	0.036	Bi	<0.005

TABLE 2.2 Impurities in CZT in *ppmw*

The point defects in CZT caused by many impurities are shallow levels. The CZT constituents belong to II and VI groups. Then the elements of I, III, IV, V and VII groups can act as dopants (Table 2.3). The elements of the V group act as acceptors. The elements of Group III and VII are instead donor. The elements of group I are amphoteric: act as donors if they are located in the interstitial sites, and as acceptors if they replace the cation. [5]

Ionization energies of groups I, III, IV, V, and VII elements

Element	Photoionization, E (meV)	Thermal ionization, E (meV)	Method
Li	Acceptor: 58.0		PL
Na	Acceptor: 58.7		PL
N	Acceptor: 56.0		PL
P	Acceptor: 68.2		PL
As	Acceptor: 92.0		PL
Cl	Donor: 14		
Cl	Donor: 14.48		PL
Cl–V_{Cd}	Acceptor: 120		PL, ODMR
Cl DX1		Donor: 220	Theory
Cl DX2		Donor: 470	Theory
Cl DX3		Donor: 210	Theory
Al	Donor: 14.05		PL
F	Donor: 13.71		PL
Ga	Donor: 13.83		PL
In	Donor: 14.08		PL
In DX		Donor: 300	Theory for $Cd_{0.8}Zn_{0.2}Te$
Ge	Donor: 950	Acceptor: 730	Photo-EPR
Sn	Donor: 850		Photo-EPR
Sn	Donor: 900		DLTS
Sn	Donor: 890, 430		QTS
Pb	Donor: 1280		Photo-EPR

TABLE 2.3 Acceptors and donors in CZT

The transition metals can act both as donor and as acceptor. (Table 2.4) The importance of the 3d transition metals, with the shell partially filled 3d lies in the fact that these atoms can create deep energy levels increasing the resistivity of CZT (improving the radiation detector's quality). A recent study showed that the doping of CZT with concentrations $10^{18} - 10^{19}\ cm^{-3}$ of Vanadium brings the CZT resistivity to $10^{9} - 10^{10}\ \Omega \cdot cm$ [5]

Ionization energies of transition metal elements

Element	Thermal ionization, E (eV)	Photoionization, E (eV)	Method
Sc		Donor: 0.0105	PL
Ti	Donor: 0.73	Donor: 0.008	PL, TDH
Ti		Donor: 0.83	DLTS, photo-DLTS
V		Donor: 0.67	Photo-EPR
V	Donor: 0.95		DLTS, photo-DLTS
V	Acceptor: 0.74		Theory
V	Acceptor: 0.51		TSC
Cr		Acceptor: 1.34	EPR, ODMR, PL
Mn	Donor: 0.05, 0.73		Hall
Fe		Donor: 1.45	Photo-EPR
Fe		Acceptor: 0.35	EPR, ODMR, PL
Fe	Acceptor: 0.43		TSC
Fe		Acceptor: 0.15	SPS
Fe		Acceptor: 0.2	CPM
Co		Acceptor: 1.25	EPR, ODMR, PL
Ni		Acceptor: 0.92	EPR, ODMR, PL
Ni		Donor: 0.76	CPM
Cu		Acceptor: 0.36; unknown: 0.6	PICT
Cu	Acceptor: 0.146		PL
Cu		Acceptor: 0.37	PICT
Ag		Acceptor: 0.1075	PL
Au		Acceptor: 0.263	PL

TABLE 2.4 Transition metals in CZT

Also the native defects in CZT can be donor and acceptor. (Table 2.5). Cadmium and Tellurium vacancies are found in concentrations less than $10^{16}\ cm^{-3}$. [5]

Ionization energies of native defects

Defect	Thermal ionization, E (eV)	Photoionization, E (eV)	Method
V_{Cd}	Acceptor: <0.47		Photo-EPR
V_{Cd}		Acceptor: 0.78	PICTS
V_{Cd}	Acceptor: 0.2, 0.8		Theory
V_{Cd}	Acceptor: 0.1, 0.4, 0.76		DLTS, PICT
V_{Cd}	Acceptor: 0.1		Theory
V_{Cd}	Acceptor: 0.43		TEES
V_{Cd}	Acceptor: 0.21; Donor: 0.73		TEES
Te_{Cd}	Donor: 0, 0.4		Theory
Te_{I}	Donor		Theory
Te_{Cd}–V_{Cd}	Neutral		Theory
V_{Te}		Donor: 1.4	Photo-EPR
V_{Te}	Donor: 1.1		DLTS, PICT
V_{Te}	Donor: 0.4, 0.5		Theory
Cd_{I}	Donor: 0.64		DLTS, PICT
Cd_{I}	Donor: 0.54		PICT
Cd_{I}	Donor: 0.5		Theory
Cd_{I}	Donor: 0, 0.2		Theory

TABLE 2.5 Native Defects in CZT

Figure 2.10 shows the levels' pattern in the band-gap presented in the Szeles' work [22]

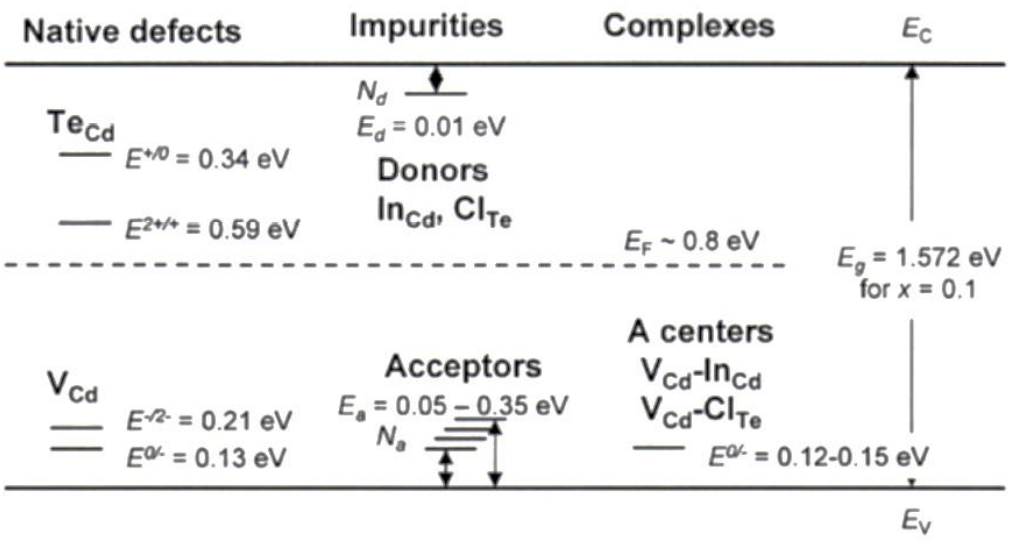

FIGURE 2.10. Energy levels in the band-gap due to defects (native, impurities and centers)

2.7 AUTO-COMPENSATION PROCESS & A CENTER

The introduction of impurities in the crystal leads to the formation of defects electrically active and centers that contribute to the compensation of the material. The main dopants used for the CdTe and CZT are Indium and halogens such as Chlorine.

The auto-compensation model proposes, for the formation of semi-insulating CdTe and CZT, the following mechanism: the concentration of the impurity ionized X^+ must be equal to that of cadmium vacancy ionized V_{Cd}^- and of the complex formed by a cadmium vacancy doubly ionized and the ionized donor: $(V_{Cd}^{2-}, X^+)^-$.

This complex is named "A center". This equality is very difficult to obtain: the concentrations should differ by less than one part in 10^{11}, taking into account that the free carriers are about 10^5 and an average dopant concentration level is 10^{16}. This model can work only if a deep level that pins the Fermi level to mid-gap, is present.

THE TELLURIUM'S DEEP LEVEL

From the auto-compensation model it is obtained that, by varying the dopant concentration in any case, an excess of acceptor levels is present. This excess can be compensated only by a deep donor level, which has the same concentration of the acceptor.

The origin of this level can be attributed to the intrinsic defects. Being sure the Tellurium excess, candidates to form the deep level are the interstitial (Te_i) and Tellurium antisite Te_{Cd}. In the crystal, the presence of tellurium in the precipitates' form is often observed, which would suggest that the interstitial Te have the time to join in the precipitates [23-24]. The deep level can be attributed to Te_{Cd}. [25]

TELLURIUM INCLUSIONS AND PRECIPITATES

The excess of Te within the CZT crystals has another consequence: Tellurium inclusions and precipitates originated by condensation of intrinsic point defects such as interstitial Cd and Te are always present. Their size may be less than one micrometer, but they can reach 100 μm size with important consequences on device performance [26]. They operate as traps for charge carriers and deform the ideal crystalline lattice in their proximity degrading the local transport properties of the detector.

It is assumed that the occurrence of inclusions is attributable to the morphological instability present at the interface of solid-liquid growth. During the growth, tellurium droplets from the molten Cd-Te (Te-rich) are formed at the interface. These Te micro drops tend to move in the crystal and, once the crystal cooled, the drops combine with each other creating the Te inclusions [27].

Therefore, the mechanism that generates the presence of such inclusions is closely correlated with the speed of growth and with the temperature gradient at the solid-liquid interface.

Through a systematic study carried out on samples of CdTe and CZT grown by the Bridgman THM, it was discovered that the dominant contribution to the distribution of inclusions ($\geq$ 95%) is given by inclusions with diameters between 1 and 4 microns with a maximum around the 2.5 μm.

They are distributed homogeneously in the space [28].

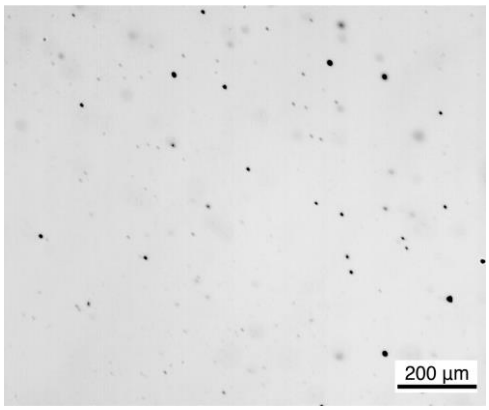

FIGURE 2.11 Tellurium inclusions in CZT [29]

3 MODELING

In this chapter, the modelling of the transport processes in bulk semiconductors is presented. Two different new models, suitable to determine the transport parameters of both charge carriers together with the spatial profile of the electric field, and a new model for the diffusion process are introduced. All the models are based on the analysis of current transients induced by laser-beam, as in the well-known time-of-flight experiment.

As both electrons and holes contribute to the electric currents, it needs to separate the two contributions with an appropriate experimental setup. In a sandwich configuration with the electrodes deposited on two opposite faces of a parallelepiped, if the collecting electrode is set at zero voltage (ground), the illuminated electrode is set at a positive voltage to study the transport of holes while it is set to a negative voltage to study the electronic transport. Moreover, a laser-beam with a wavelength equal to 532 nm is used, which corresponds to a photon energy equal to 2.33 eV and then higher than the energy gap of $CdZnTe\ and\ CdTe$. This value of energy allows the creation of only one electron-hole pair for each photon and the radiation is absorbed within a few micrometers of material under the illuminated electrode. In this way, we can easy decouple the electronic signal from the lacunar contribution.

If we set a negative bias on the illuminated electrode, a number N_0 of electron-hole pairs in proximity of the same electrode is generated. The charges of opposite sign move in opposite directions as effect of the presence of the electric field. The electrons will travel towards the illuminated electrode (at a positive voltage) covering a distance ideally equal to zero, while the holes will have to run right across the whole sample's thickness up to the collecting electrode, using a time equal to the flight time. In summary, the application of a positive or negative voltage on the electrode illuminated allows the analysis of contribution of holes or of electrons, respectively.

Assuming that the sample be uniform and isotropic, the study of charge's transport can take place for all models with a one-dimensional approach, along the x direction joining the two electrodes.

.

3.1 General Phenomenology

PHYSICAL QUANTITIES:

• Q_0	Initial Charge photo-generated	$[C]$
• $\rho(\vec{r},t)$	Free charge density	$[C/cm^3]$
• $\rho_T\ (\vec{r},t)$	Trapped charge density	$[C/cm^3]$
• τ_D	Detrapping time	$[s]$
• τ	Trapping time (carriers lifetime)	$[s]$
• μ	Mobility	$[cm^2/(Vs)]$
• D	Diffusion coefficient	$[cm^2/s]$
• s	1 for holes, -1 for electrons	

During the flight time the charges experience different physical phenomena:

- Photo-generation
- Electric drift
- Diffusion drift
- Trapping
- Detrapping
- Recombination

Charge Photo-Generation

The internal photoelectric effect, as a consequence of the absorption of an optical photon, leads to the creation of a free electron-hole pair. The rate of generation G for the free charges induced by the laser-beam at time $t = 0$ in the point (0,0,0) immediately underneath the illuminated electrode, is equal to:

$$G_{PH} = Q_0\ \delta(t)\ \delta(x)\ \delta(y)\ \delta(z) \tag{3.1}$$

ELECTRIC DRIFT

The charges drift towards the collecting electrode with a velocity proportional to the electric field and to the mobility:

$$\overrightarrow{v}_{DRIFT} = \frac{d\vec{x}}{dt} = s\,\mu\,\vec{E} \tag{3.2}$$

The value of s justifies the fact that the electrons move in the opposite direction to the electric field, while holes move in the same direction.

The direction of the electric field is however different in the two different setups, because the electric field is directed always toward the electrode at lower potential. In summary:

$$\overrightarrow{E} = s\,E\,\hat{x} \tag{3.3}$$

- $s = 1$ for holes and $s = -1$ for electrons
- $E = |\vec{E}|$ is the magnitude of the electric field

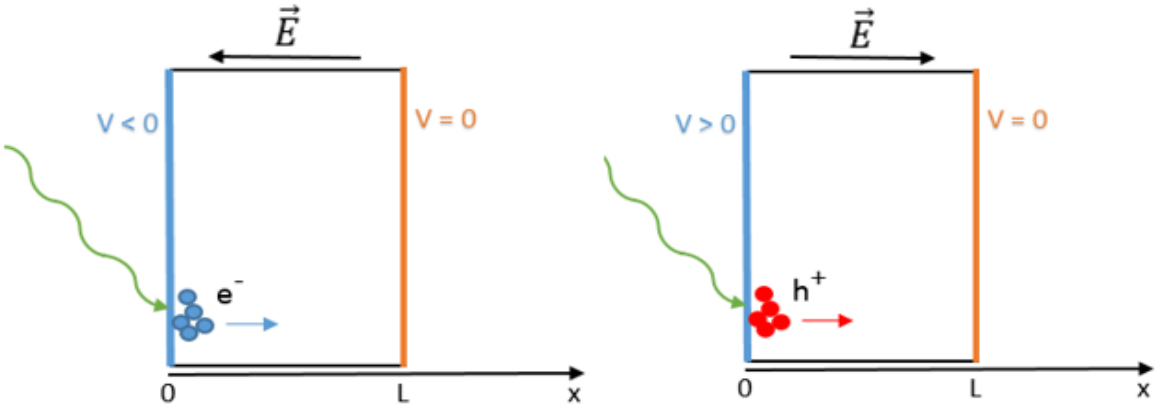

ONLY ELECTRONS
$s = -1$

ONLY HOLES
$s = 1$

FIGURE 3.1 The radiation in the visible range is absorbed in a few micrometers. The application of a negative potential (left) on the illuminated electrode pushes the electrons to the collection electrode, fixed at zero voltage, instead a positive potential (right) leads the holes to travel along the sample always toward the electrode of collection

DIFFUSION DRIFT

The carriers diffuse thermally decreasing the gradient of the concentration of the free charge density. The diffusion velocity is then proportional to this gradient and to the diffusion coefficient D:

$$\vec{v}_{DIFF} = -D\frac{\vec{\nabla}\rho}{\rho}$$

In this case both electrons that holes move in the same direction with the same form of the free charge density: if the charge density is increasing in a certain direction, and then the gradient is positive, the carriers will move in the opposite direction, because the diffusion tends to flatten spatially the charge density profile.

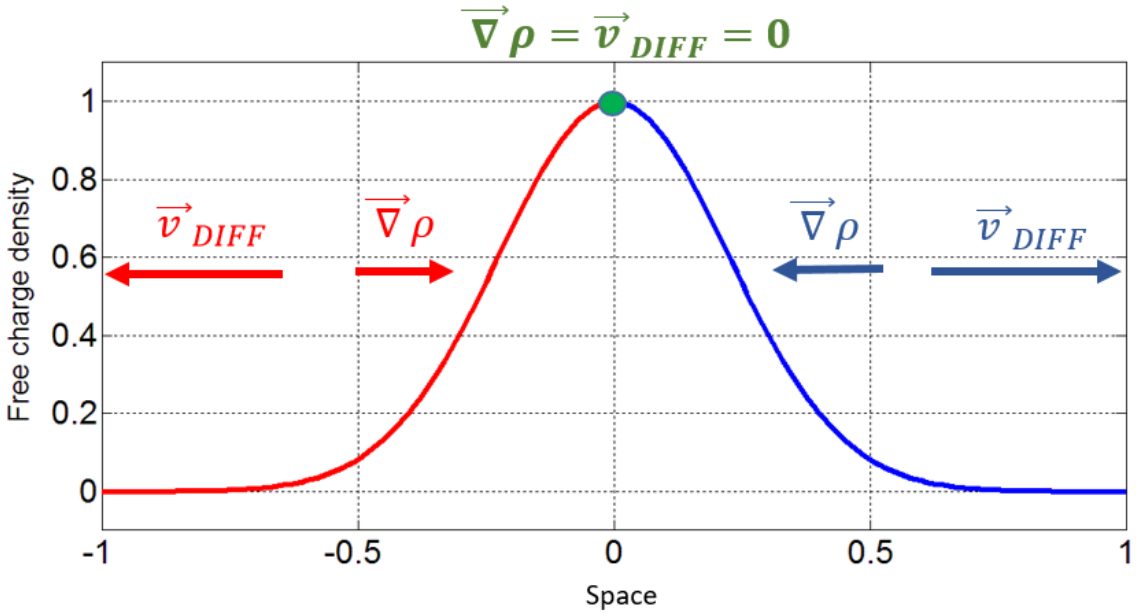

FIGURE 3.2 Charge density spatially profile. The green point indicates the barycenter position, the unique point that is not affected by diffusion. Instead to the left (red) and to the right(blue) of the barycenter the charges move away from it at a velocity proportional to the gradient of the free charge

CHARGE DESTRUCTION (TRAPPING)

The charges are trapped during the flight with a rate of entrapment:

$$U_\tau = \frac{\rho}{\tau} \tag{3.4}$$

This phenomenon is due to the presence of traps within the material. The probability of entrapment is in fact proportional to this traps density. The term *U* is a destruction rate because it cuts down the number of charge carriers in time.

DETRAPPING

The trapped charge can escape from the trap and return to drift to the electrode collection. The detrapping rate is in effect a generation rate of free charges:

$$G_D = \frac{\rho_T}{\tau_D} \tag{3.5}$$

Detrapping rate is proportional to trapped charge density. Detrapping time depends on temperature and density traps. In fact, carrier must overcome thermally an energy barrier to be able to escape from the trap.

RECOMBINATION

Electrons and holes, during the flight, could recombine with the creation of a photon, just as happens for example in a LED. This phenomenon is however inhibited in this experiment because electrons and holes are "separated at their birth" by the electric field and they move in opposite directions during their flight.

3.2 The Continuity Equation

Both the free density than that trapped must obey the equation of continuity, relating to the conservation of the total charge itself:

$$\frac{\partial \rho}{\partial t} + \vec{\nabla} \cdot (\rho \, \vec{v}_{TOT}) = G_{TOT} - U_{TOT} \tag{3.6}$$

where:

- ρ represents the charge density (free or trapped);
- $\vec{v}_{TOT}$ is the velocity of the charge density;
- G_{TOT} is the sum of all the generation contributions;
- U_{TOT} is the sum of all the destruction contributions;

Taking into account all the physical phenomena described above, the two continuity equations become:

$$\begin{cases} \dfrac{\partial \rho}{\partial t} + \vec{\nabla} \cdot (\rho \, \vec{v}_{\mathrm{TOT}}) = G_{PH} + \dfrac{\rho_T}{\tau_D} - \dfrac{\rho}{\tau} \\ \dfrac{\partial \rho_T}{\partial t} = -\dfrac{\rho_T}{\tau_D} + \dfrac{\rho}{\tau} \end{cases} \tag{3.7}$$

where:

- $\vec{v}_{\mathrm{TOT}}$ is the velocity of free charge because the velocity of the trapped charge is obviously equal to zero. The velocity is the sum of drift velocity, due to electric field and to diffusive velocity.

$$\vec{v}_{TOT} = \vec{v}_{DRIFT} + \vec{v}_{DIFF} = s\mu\vec{E} - D\frac{\vec{\nabla}\rho}{\rho} \tag{3.8}$$

- $\vec{\nabla} \cdot (\rho\, \vec{v}_{TOT})$ takes into account the spatial variation of the free charge density due to the electrical movement and diffusion of carriers (3.3; 3.8)

$$\vec{\nabla} \cdot (\rho \vec{v}_{TOT}) = \vec{\nabla} \cdot \left(s\mu\rho\vec{E} - D\rho \frac{\vec{\nabla}\rho}{\rho} \right) = \vec{\nabla} \cdot \left(s^2 \mu\rho E\vec{x} - D\vec{\nabla}\rho \right) =$$

$$= \frac{d}{dx} (\, \mu\, \rho\, E\,) - D\, \nabla^2 \rho \tag{3.9}$$

The scalar term $\nabla^2\rho$ is the Laplacian of the free charge density, the term s disappears because s^2 is equal to one. In this way the partial differential equations takes into account generation of charge, entrapment, detrapping, diffusion and electric drift for both free charges both for the trapped charges:

$$\begin{cases} \dfrac{\partial \rho}{\partial t} = G_{PH} - \dfrac{d}{dx} (\, \mu\, \rho\, E\,) + D\, \nabla^2 \rho + \dfrac{\rho_T}{\tau_D} - \dfrac{\rho}{\tau} \\ \dfrac{\partial \rho_T}{\partial t} = - \dfrac{\rho_T}{\tau_D} + \dfrac{\rho}{\tau} \end{cases} \tag{3.10}$$

THE TOTAL CHARGE

An important quantity for the subsequent results is the total charge density ρ_{TOT}:

$$\rho_{TOT}(\vec{r}, t) = \rho_T(\vec{r}, t) + \rho(\vec{r}, t) \tag{3.11}$$

That remains constant in time:

$$\frac{d}{dt} \left(\rho_{TOT}(\vec{r}, t) \right) = 0 \tag{3.12}$$

The integral of total charge density over the whole volume is the total charge:

$$\int \rho_{TOT}\, (\vec{r}, t)\, d\vec{r} = Q_0 \tag{3.13}$$

The term Q_0 takes into account also of the carriers thermally generated, that could create a current which contributes to an increase in noise. Anyway the high resistivity of CZT inhibits the presence of this charge thermally promoted.

3.3 THE CURRENT SIGNAL

The solution of the equations of continuity system described just above allows to obtain the current profile in the time induced on the collection electrode, which in effect is the electrical signal acquired experimentally.

The Ramo–Shockley theorem [30, 31] (Section 3.6.1) states that the induced charge $Q(t)$ is in fact the integral over the whole volume of the total charge density

$$Q(t) = \iiint \rho_{TOT}\,(\vec{r},t)\,V_w(\vec{r})\,d\vec{r} \tag{3.14}$$

Where $V_w(\vec{r})$ is the weighting potential in the material. The weighting field $\overrightarrow{W}(\vec{r})$ is defined as the negative gradient of the weighting potential:

$$\overrightarrow{W}(\vec{r}) = -\overrightarrow{\nabla}\,V_W(\vec{r}) \tag{3.15}$$

The current signal $I(t)$ obtained experimentally is the change in time of induced charge (using 3.12, 3.14 and 3.15)

$$I(t) = \frac{d}{dt}\,Q(t) = -\frac{d}{dt}\iiint \rho_{TOT}\,(\vec{r},t)\,V_w(\vec{r})\,d\vec{r} =$$

$$= -\iiint \frac{d}{dt}\left(\rho_{TOT}(\vec{r},t)\,V_w(\vec{r})\right)d\vec{r} = -\iiint \rho_{TOT}(\vec{r},t)\frac{d}{dt}\left(V_w(\vec{r})\right)d\vec{r} =$$

$$= -\iiint \rho_{TOT}(\vec{r},t)\,\frac{d\vec{r}}{dt}\cdot\overrightarrow{\nabla}\left(V_w(\vec{r})\right)d\vec{r} =$$

$$= \iiint \rho_{TOT}(\vec{r},t)\,\vec{v}_{TOT}(\vec{r})\cdot\overrightarrow{W}(\vec{r})\,d\vec{r} \tag{3.16}$$

The weighting potential and the weighting field come from the Ramo-Shockley theorem and depend only on the contact geometry. These geometric quantities are largely explained by the mathematical point of view even with simulations in section 4.3. The current depends on only free charge because the charge trapped has no velocity and does not contribute to the electric current. The current results the coupling between velocity, proportional to electric field and weighting field. This coupling is then weighed by free charge density and integrated over the entire volume.

3.4 THE MODELS

The general analytical solution of the equations of continuity does not exist for every electric field profile. Different simplifications with suitable assumptions are used to study the photocurrent transient profile [32, 33]. In this thesis three different models are presented, by which it becomes possible to obtain information about transport properties of the material:

MODEL	*Trapping*	*Detrapping*	*Diffusion*	*Weighting Field*	*Electric Field*
2 τ	YES	NO	NO	UNIFORM	ANY
1 τ	YES	NO	NO	ANY	ANY
DIFFUSIVE	YES	NO	YES	ANY	UNIFORM, LINEAR

Table 3.1 Transport models and the assumptions made to obtain transport parameters and electric field

3.4.1 THE 1-2τ MODELS : THE SAME DENSITY SOLUTION

The 1τ model concerns the presence of a non-uniform field weighting, while the 2τ model takes into account of a uniform spatially profile of the weighting field.

The analytical form of the charge density in the 1τ and 2τ models is the same. In this two models the diffusion and detrapping phenomena are assumed as negligible.

Under these assumptions, the charge is subject to:

- generation in the proximity of the illuminated electrode.
- drift toward the collecting contact with a speed proportional to the electric field: $v\,(x) = \mu\, E(x)$.
- trapping with a rate proportional to the inverse of the lifetime τ of carriers.

The two continuity equations are also decoupled because of the absence of detrapping: the carriers, once trapped, cannot return to give contributions to the free charge density.

$$\begin{cases} \dfrac{\partial \rho}{\partial t} = G_{PH} - \dfrac{d}{dx}(\mu\, \rho\, E) - \dfrac{\rho}{\tau} \\ \dfrac{\partial \rho_T}{\partial t} = \dfrac{\rho}{\tau} \end{cases} \tag{3.17}$$

The solutions of the two differential equations are:

$$\rho(\vec{r},t) = Q_0\, e^{-\frac{t}{\tau}}\, \delta\big(x - x(t)\big)\, \delta(y)\, \delta(z) \tag{3.18}$$

$$\rho_T(\vec{r},t) = \frac{1}{\tau}\int_0^t \rho(\vec{r},t')dt' = \frac{1}{\tau}\int_0^t Q_0\, e^{-\frac{t'}{\tau}}\, \delta\big(x - x(t')\big)\, \delta(y)\delta(z)\, dt' =$$

$$\frac{Q_0\delta(y)\delta(z)}{\tau}\int_0^t e^{-\frac{t'}{\tau}}\frac{dt(x)}{dx}\delta\big(t' - t(x)\big) = \frac{Q_0\delta(y)\delta(z)}{\tau\, v(x)}\int_0^t e^{-\frac{t'}{\tau}}\delta\big(t' - t(x)\big)dt'$$

$$\frac{Q_0}{\mu E(x)} e^{-\frac{t(x)}{\tau}}\, H(t - t(x))\, \delta(y)\, \delta(z) \tag{3.19}$$

The shape of the charge density (3.18) is obviously a Dirac delta of space-time $\delta(x - x\,(t))$: the free charge density is created as a Dirac delta and travels compact toward the collecting electrode. This density is not subject to those phenomena like diffusion and detrapping which could spatially enlarge the free charge density. The number of the carriers, at $t = 0$, is equal to the photo-charge generated initial Q_0. Then the carriers' number decreases over time with an exponential law with a characteristic time equal to the carriers' lifetime τ.

Carriers travel through the material with a law of motion $x(t)$ imposed by the electric field. Since the electric field is directed only along the x direction, also the charges drift in this direction.

The trapped charge density instead has a spatiotemporal Heaviside profile. The Heaviside function in (3.19) states that the charge density is equal to zero for times lower than the term $t(x)$ (3.21). In the next section this term will be shown as essential to the clarity of the whole thesis. The meaning of the Heaviside function is clear: at the time t the free charge density is located in the position $x = x(t)$, the trapping has had effect only in $0 \leq x \leq x(t)$

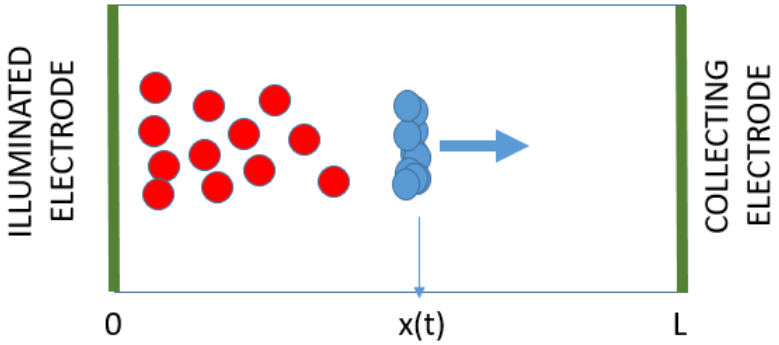

FIGURE 3.3 The free carriers (blue) follow the law of motion $x(t)$. Trapped charges (red) are distributed in all positions less than the free charges position.

3.4.2 The Current Signal In 1-2τ models

From the space-time profile of the free charge density (3.18) the induced current signal (3.16) on the electrode collection becomes:

$$I(t) = Q_0\, e^{-\frac{t}{\tau}}\, W\big(x(t)\big)\, \mu E\big(x(t)\big) \tag{3.20}$$

The current signal results proportional to the product between electric and weighting fields and to the decreasing exponential term due to trapping.

The $x(t)$ and $t(x)$ Terms

The carriers move within the material following a precise law of motion. The charge movement is only due to the electric field because in this two models the diffusion phenomenon is neglected.

The charge travels towards the collection electrode with a non-uniform velocity proportional to the electric field and to the mobility (3.2)

The differential equation has the following integral solution:

$$t(x) = \int_0^x \frac{dx'}{\mu E(x)} \tag{3.21}$$

The function $t(x)$ indicates how long the charge takes to reach the position x. The term T_R, equal to the time taken to cross the entire sample of thickness L correspond to the flight time:

$$T_R = t(L) = \int_0^L \frac{dx}{\mu E(x)} \tag{3.22}$$

So the flight time can be calculated knowing the electric field spatial profile and the mobility.

The law of motion $x(t)$, which indicates the charge's position at the time t, now can be calculated by the function $t(x)$:

$$x(t) = t^{-1}(x) \tag{3.23}$$

THE $E(x(t))$ AND $W(x(t))$ TERMS

The current signal (3.20) is proportional to the terms $E(x(t))$ and $W(x(t))$: the law of motion of the carriers becomes an important quantity to find transport information.

The charge, after having traveled for a time t inside of the material, will be in position $x = x(t)$.

Here the electric and weighting fields are equal to:

$$\text{At the time } t \rightarrow \begin{cases} E = E\big(x = x(t)\big) \\ W = W\big(x = x(t)\big) \end{cases}$$

These two fields are not directly functions of time. In fact, in a fixed position, the E and W values do not change in time and their partial derivative in time is zero:

$$\frac{\partial E}{\partial t} = \frac{\partial W}{\partial t} = 0 \tag{3.24}$$

Indeed, the physical quantity that changes in time is the position of the charge.

Carriers, during flight, experience different field values because they change position; then the term $E(x(t))$ indicates the electric field value probed by the carrier in the position $x(t)$ after travelling for the time *t*. Since the signal is proportional to the velocity, and then to the electric field, the charge carrier acts as probe of electric field during their flight. In this way the electric spatial profile can be reconstructed. The functions $E(x(t))$ and $W(x(t))$ can be calculated once mobility and field spatial profile are known:

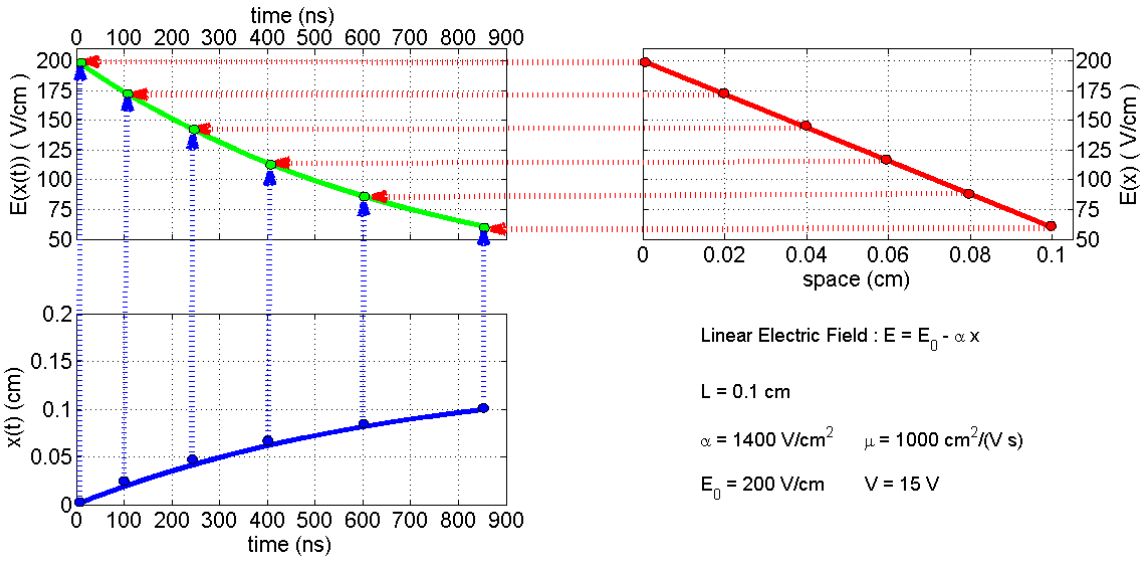

FIGURE 3.4. Calculation of the electric field $E(x(t))$ probed in time by carriers starting from the knowledge of the spatial electric field.

Starting from the value of the spatial electric field is in fact possible to obtain the term $t(x)$ (3.21) and then the law of motion $x(t)$. Now we have to correlate each position with the relative value of electric field $E(x)$ and time $t(x)$. In this way it becomes possible to link a value of time with the relative value of the electric field, generating the function $E(x(t))$. For example, in figure 3.4, in position $x = 0.08$ cm the electric field is equal to $88\ V/cm$. Now, starting from the law of motion, the time at which the carriers are in position $x = 0.88$ cm has to be calculated. This time results $t = 600\ ns$. Then, after a flight of $600\ ns$ the electric field probed by carriers is equal to $88\ V/cm$. The spatial and temporal profile of the field can be a different form: for example, a spatial linear profile becomes a temporal exponential profile. In fact, since the electric field is proportional to the velocity, the link between $E(x)$ and $E(x(t))$ passes through the solution of a differential equation (3.2) and a function's inversion (3.23)

3.4.3 CURRENT WITH UNIFORM/LINEAR ELECTRIC FIELD

In this section the analytical results are shown. This chapter explains how the time of flight, the law of motion and the electric field, probed in time by carriers, depend only on the electric field and not on the weighting field profile.

The spatial profiles of the electric field chosen for an analytical approach are:

1) Uniform profile: $E = E_0$
2) Linear profile: $E = E_0 - ax$

The uniform field (in literature [35], [36]) results as a special case of the linear field with the slope term $a = 0$.

This section will be accompanied with a simulation to introduce the physical quantities that will be presented. In this simulation the parameters for the calculation are:

- $Thickness\ \ L = 0.1\ cm$
- $Voltages\ \ V = 10, 30, 50, 70, 90\ Volts$
- $Mobility\ \ \mu = 1000\ cm^2/(V \cdot s)$
- $Lifetime\ \ \tau = 1\ \mu s$
- Uniform Weighting field $W = 1/L$
- $Slope\ \ \alpha = 5000\ cm^2/V$ (in case of linear electric field profile)

UNIFORM ELECTRIC FIELD PROFILE

The application of a potential difference V across the two electrodes, imagined as two flat and parallel planes, in which the edge effects are ignored and where the absence of localised charge within the material is assumed, leads to a uniform electric field profile equal to:

$$E(x) = E_0 = \frac{V}{L} \tag{3.25}$$

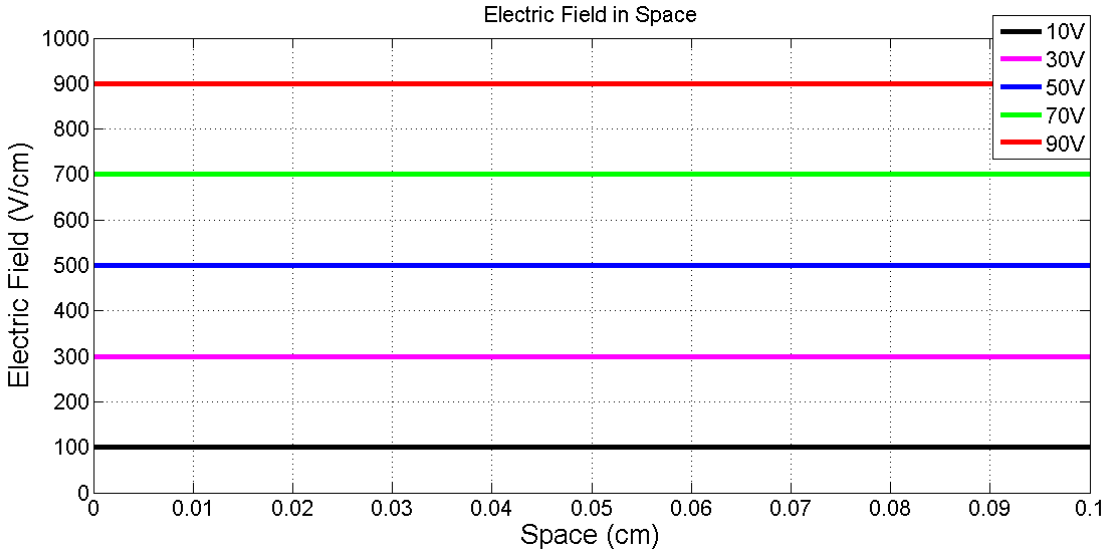

FIGURE 3.5 Spatial electric field profiles for different voltage values

The term $t(x)$, that is the time used by the carriers to reach the x position, corresponds to:

$$t(x) = \frac{x}{\mu E_o} = \frac{xL}{\mu V} \tag{3.26}$$

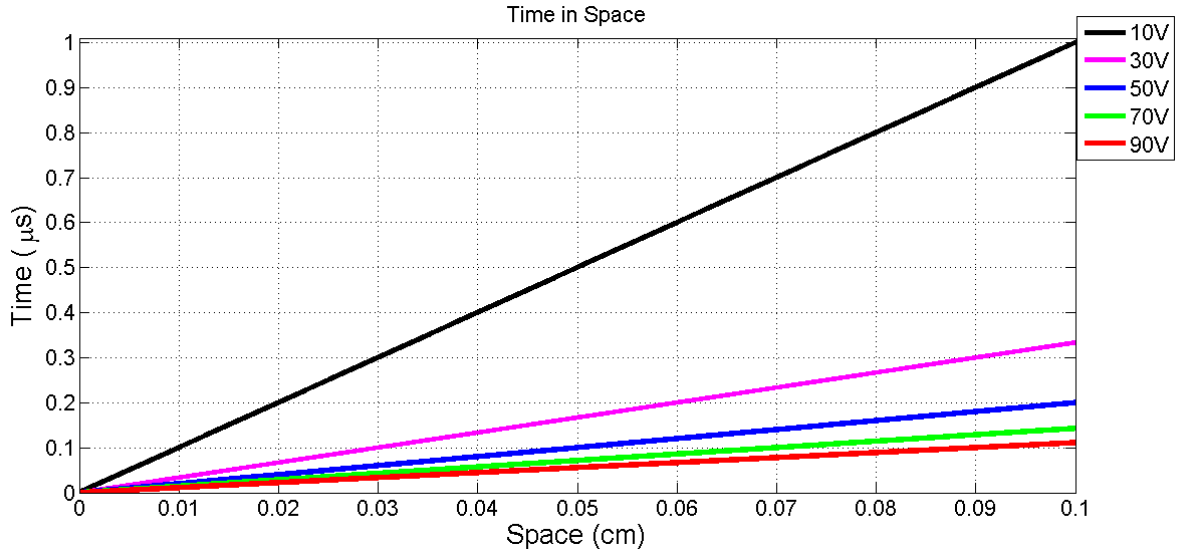

FIGURE 3.6 Time $t(x)$ used by the carrier to reach the x position

The flight time T_R becomes:

$$T_R = t(L) = \frac{L^2}{\mu V} \tag{3.27}$$

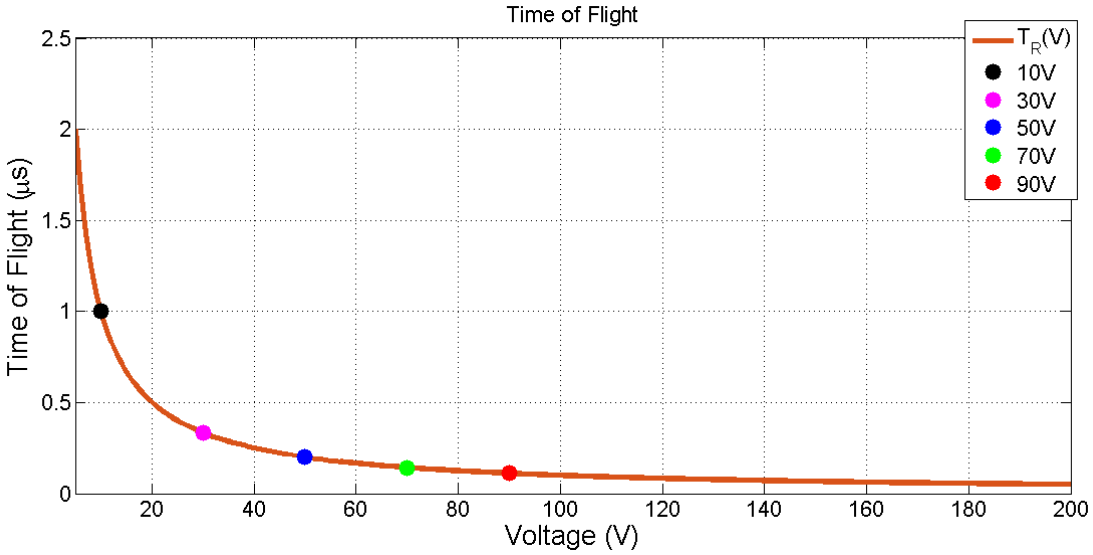

FIGURE 3.7 Flight times as a function of the applied bias V

The law of motion $x(t)$ is obtained by the inversion of $x(t)$

$$x(t) = \mu \frac{V}{L} t \tag{3.28}$$

Carriers, travelling in a uniform field, experience a constant velocity. The law of motion represents a uniform linear motion.

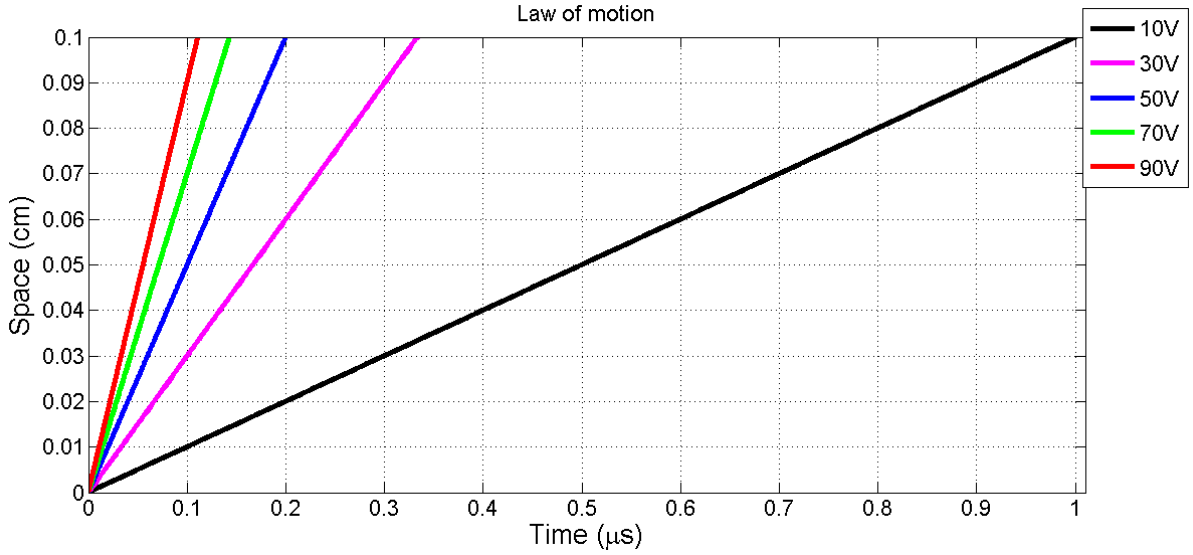

FIGURE 3.8 Law of motion as a function of time

The electric field probed in time by the carrier doesn't change because of its spatially uniformity:

$$E\big(x(t)\big) = E_0 = \frac{V}{L} \qquad 0 < t < T_R \tag{3.29}$$

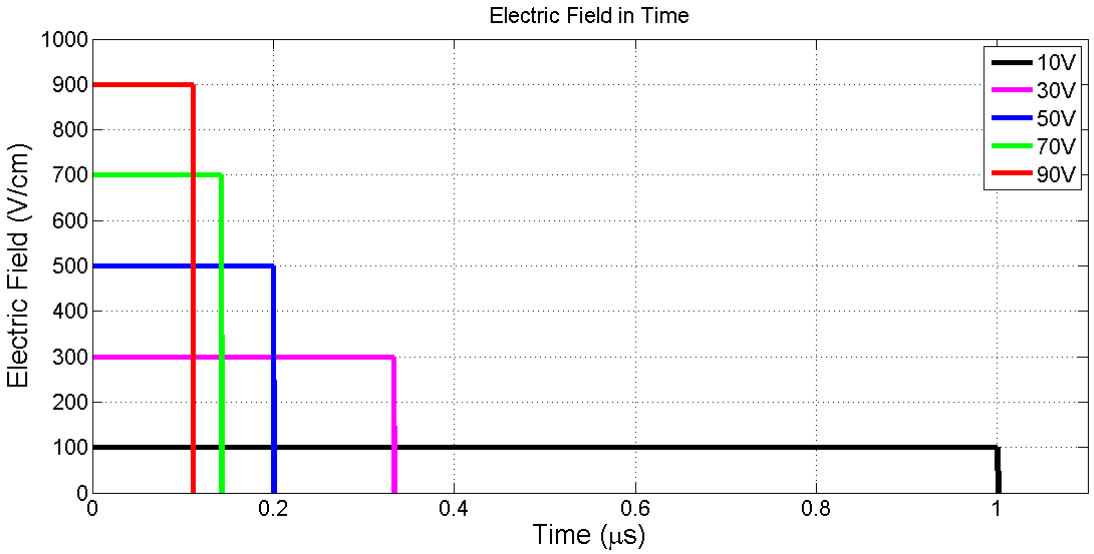

FIGURE 3.9 Electric field $E(x(t))$ probed in time by the charge carrier

The Current signal becomes:

$$I(t) = \frac{\mu V}{L} Q_0 \, e^{-\frac{t}{\tau}} W_x \, (x(t)) \qquad 0 < t < T_R \tag{3.30}$$

Under uniform weigthing field assumption the transient results:

$$I(t) = \frac{\mu V}{L^2} \, Q_0 \, e^{-\frac{t}{\tau}} \qquad 0 < t < T_R \tag{3.31}$$

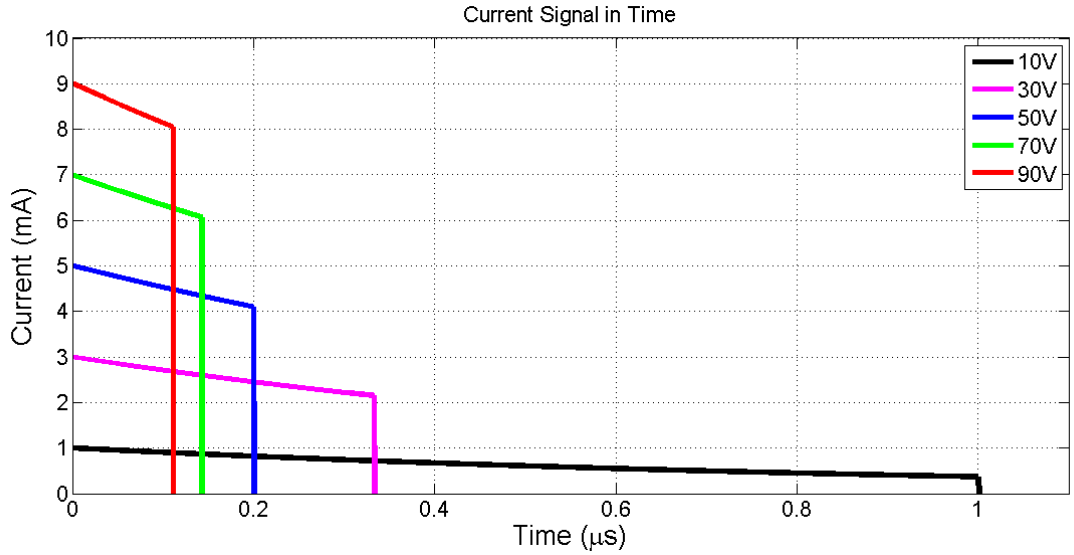

FIGURE 3.10 Current transient signals. The signal's decay in time is due only to trapping

SPATIAL LINEAR ELECTRIC FIELD PROFILE

The presence of a fixed localised charge density ρ within the material changes the spatial profile of the electric field: the first Maxwell equation explains how charge density causes distortion of the electric field from the uniform profile:

$$\overrightarrow{\nabla} \cdot \vec{E} = \frac{\rho}{\epsilon} \tag{3.32}$$

where ϵ is the absolute dielectric constant of the material.

A uniform spatial charge distribution leads to a linear profile of the electric field:

$$\rho(x) = \rho_0 \rightarrow E(x) = E_0 - \alpha x \quad with\ \alpha = -\frac{\rho_0}{\epsilon} \tag{3.33}$$

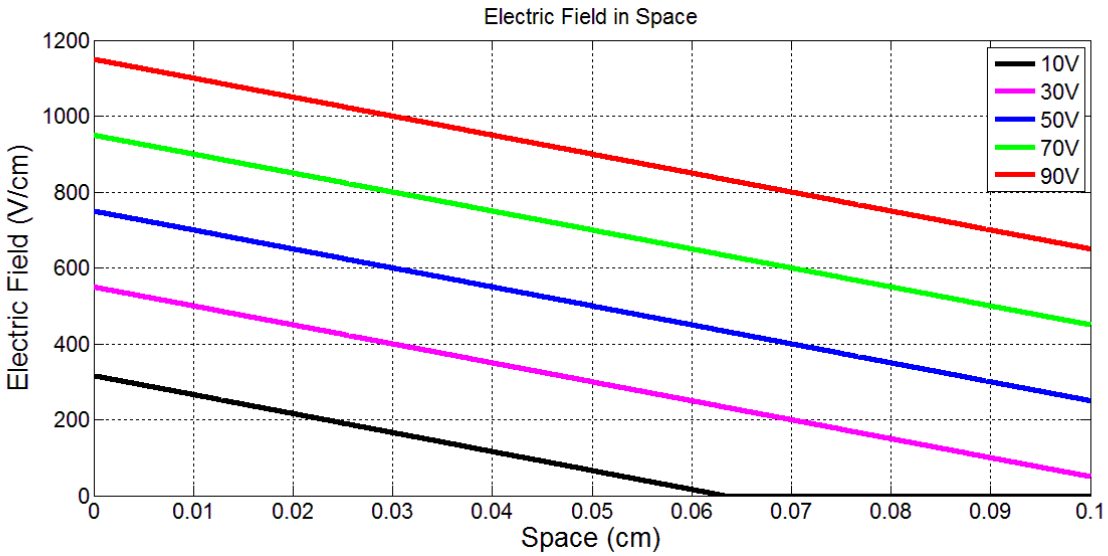

FIGURE 3.11 Linear Electric fields as a function of the detector's depth.

Electric field can drop to zero inside the material for voltages

$$V \leq \frac{1}{2}\,\alpha L^2 = V_T \tag{3.34}$$

The term $E_0 = E(0)$ represents the value of electric field in proximity of illuminated electrode:

$$E_0 = \begin{cases} \sqrt{2\alpha V} & V \leq \dfrac{1}{2}\,\alpha L^2 \\ \dfrac{V}{L} + \dfrac{\alpha L}{2} & V > \dfrac{1}{2}\alpha L^2 \end{cases} \tag{3.35}$$

The time $t(x)$ required to reach the general position x results:

$$t(x) = \frac{1}{\mu\alpha} \ln \left| 1 - \frac{\alpha}{E_0} x \right| \tag{3.36}$$

If the voltage is less than the threshold voltage V_T, the electric field vanishes inside the material. In this case the carriers probe a zero field while they are approaching in the x_n position: charges employ an infinite time to arrive in x_n position.

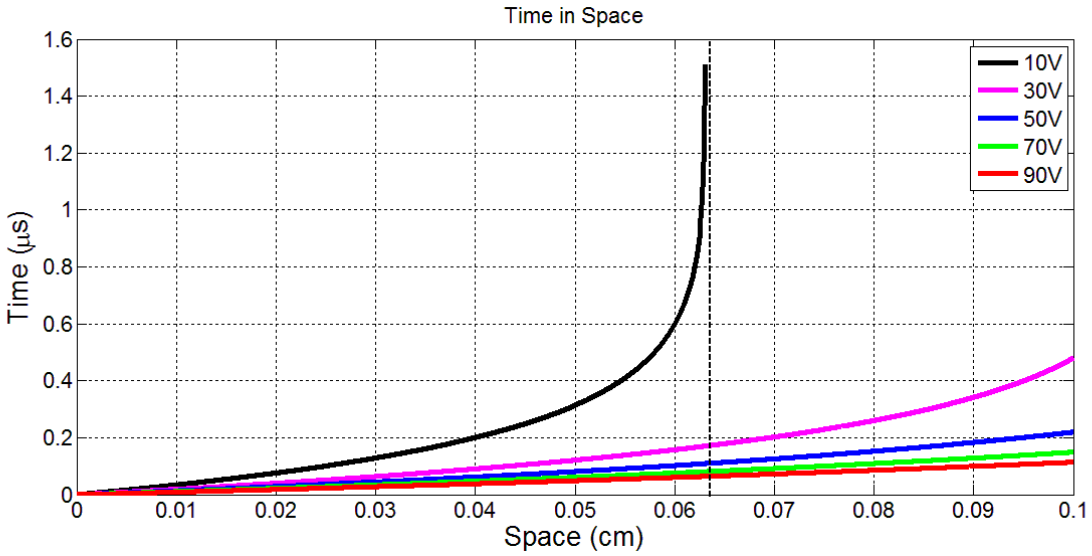

FIGURE 3.12 Time $t(x)$ request to reach the x position. For the value of voltage equal to 10 Volt, lower than the threshold voltage value ($V_T = 25\ V$), carriers can't reach the collecting electrode.

The flight time $T_R = t(L)$ becomes:

$$T_R = \frac{1}{\mu\alpha} \ln \left| \frac{V - \frac{\alpha L^2}{2}}{V + \frac{\alpha L^2}{2}} \right| \tag{3.37}$$

The flight time in the presence of decreasing linear field can therefore diverge if the voltage reaches the threshold value V_T :

$$\lim_{V \to V_T^+} T_R = +\infty \qquad if\ V \leq \frac{\alpha L^2}{2}$$

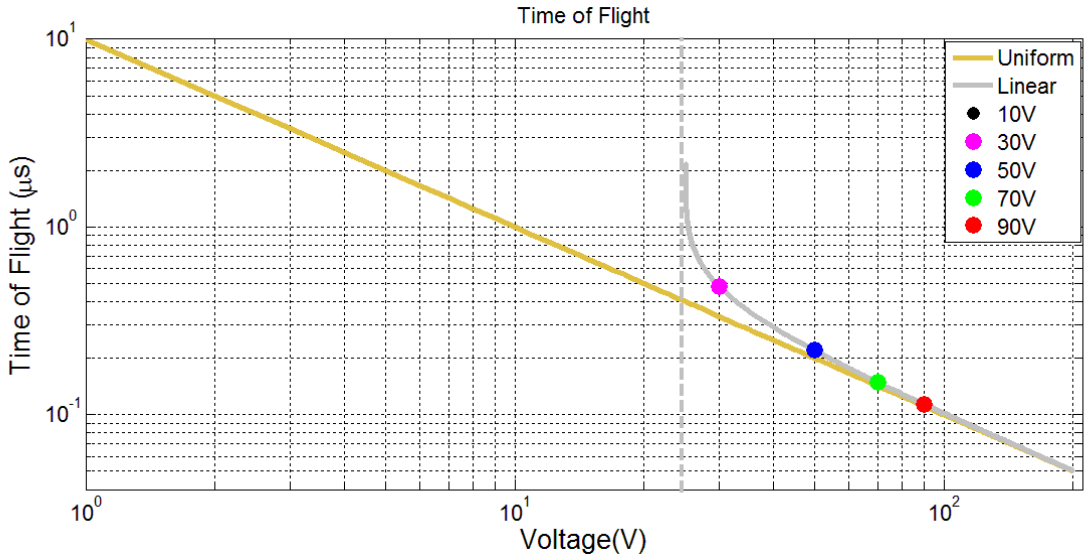

FIGURE 3.13 Flight times as a function of the applied voltages in the case of linear electric fields (grey) compared to the flight times in presence of uniform fields (orange). The discrepancy between them becomes evident near the threshold voltage.

From an experimental point of view, this means that the induced current on the collecting contact continues to give signal for a very long time, despite no charge can never arrive at the electrode. In this case, measurements are not of interest since it is impossible to establish a flight-time because the hypothesis that carriers travel for a space equal to the sample thickness falls.

This condition is more general than the single case of linear field and it occurs whenever that the electric field collapses to zero in a point inside the material.

In these cases an infinite flight time is observed and the carriers come closer indefinitely to x_n position for which $E(x_n) = 0$. The mathematical explanation is provided by the relation (3.22)

The presence of points in which the electric field vanishes, causes the divergence of the time of flight.

The inversion of the function $t(x)$ leads to the writing of the law of motion $x(t)$:

$$x(t) = \frac{E_0}{\alpha}(1 - e^{-\mu\alpha t}) \tag{3.38}$$

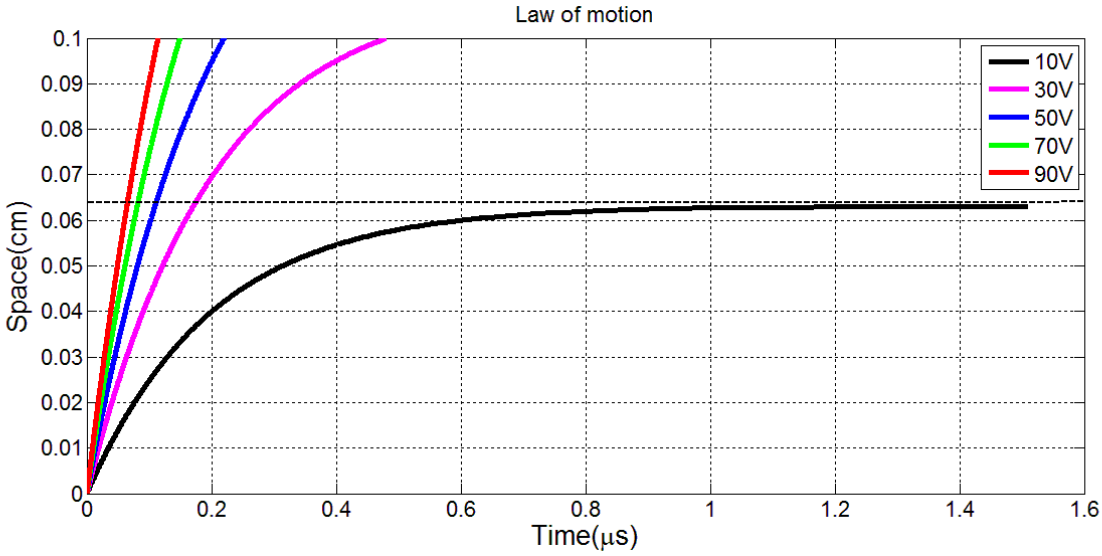

FIGURE 3.14 Laws of motion as a function of the time.

In the case when the voltage V is less than threshold value V_n, carriers come close to x_n and the charge will not reach the collecting electrode.

$$x_n = \frac{E_0}{\alpha} \tag{3.39}$$

The electric field probed in time by the charge carriers is a function of time with an exponential law:

$$E\big(x = x(t)\big) = E_0\, e^{-\mu\alpha t} \tag{3.40}$$

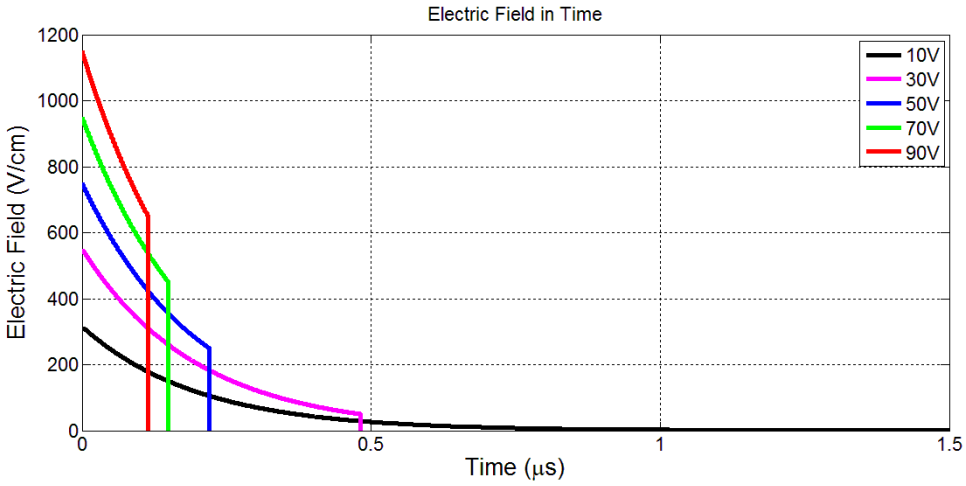

FIGURE 3.15. Electric field probed in time. The decay is due to the fact that the carrier's velocity is changing during the flight

The temporal profile of the current signal in the presence of an electric field which spatially linear profile can be obtained:

$$I(t) = Q_0\,\mu E_0\, e^{-t\left(\mu\alpha+\frac{1}{\tau}\right)}\, W_x\,(x(t)) \qquad 0 < t < T_R \tag{3.41}$$

In presence of a uniform field weighting the signal becomes [37]:

$$I(t) = Q_0 \frac{\mu E_0}{L} e^{-t\left(\mu\alpha+\frac{1}{\tau}\right)} \qquad 0 < t < T_R \tag{3.42}$$

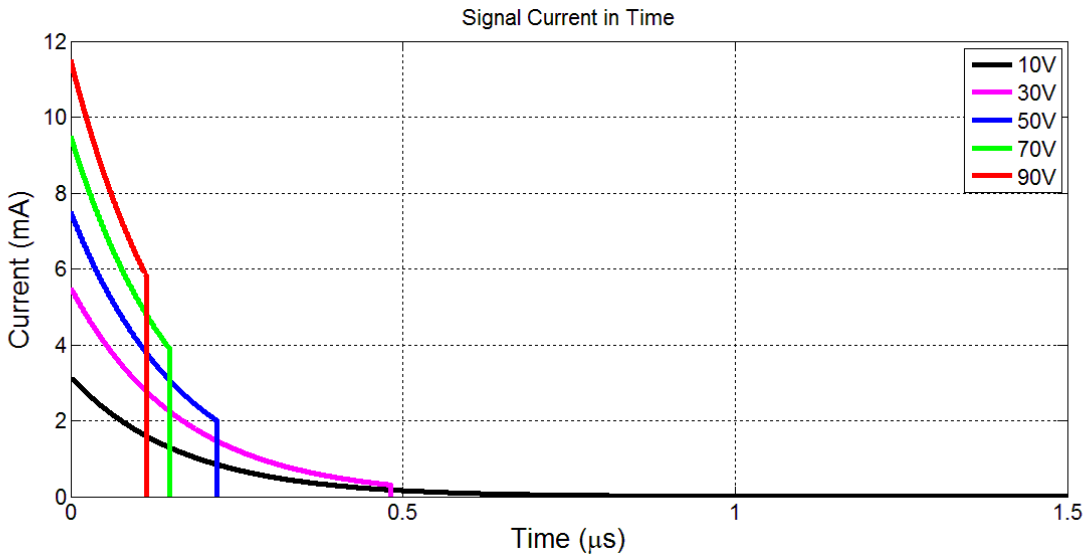

FIGURE 3.16 Current transient signals with linear electric field profile

The current transients show a temporal decay due to the trapping, to the mobility but also to the electric field slope. In fact, the effective characteristic time of decay is:

$$\frac{1}{\tau_{EFF}} = \mu\alpha + \frac{1}{\tau} \tag{3.43}$$

For voltages lower that the threshold voltage the transient exhibit a signal with no finite flight time.

3.4.4 Analysis of Current Signals

The analysis of the current transients allows to get information about the transport properties of the studied sample. In the past works, it was possible to obtain these values by selecting the electric field profile, uniform [36] or linear [32]. In fact, knowing the electric field profile (analytical function or experimental behavior) becomes possible to obtain the law of motion, the time of flight as a function of the applied voltage, and the value of the electric field probed in time $E\big(x(t)\big)$ and then the time profile of the current $I(t)$.

Uniform electric field

In the case of uniform electric field's assumption [35, 36] it becomes very simple to derive the lifetime and the mobility, in fact:

1. The value of the life time is obtained from the slope of the fitted straight line of the logarithm of current signal as a function of time:

$$\ln\big(I(t)\big) = \ln\left(\frac{\mu V Q_0}{L^2}\right) - t/\tau$$

2. The value of mobility is obtained instead from the slope of the straight line interpolating the different flight times as a function of the inverse of the applied voltages:

$$T_R\ (V) = \frac{L^2}{\mu V}$$

Once the mobility is known also the value of Q_0 can be found by the first term of the logarithm of the signal $I(t)$.

LINEAR ELECTRIC FIELD HYPOTHESIS

In the presence of a linear field [32, 33] is still possible to obtain the values of the mobility, the life time and the slope of the field, assuming that this value does not change at different voltages.

1. From the logarithm of the current signal the characteristic time $\tau_f = \left(\mu\alpha + \frac{1}{\tau}\right)^{-1}$ with which the signal decreases exponentially in time is obtained.

2. From the relation (3.36) instead the values of μα and α are found. Since in this case the field may drop to zero within the material, measurements at voltages higher than the threshold voltage have to be done. This value, however, is unknown at the beginning as it depends on the α field slope. The measures are valid until, lowering the voltage, it is possible to observe the time of flight.

Combining all these experimental results, the lifetime, the mobility, the slope of the electric field, and the value of the photo-generated charge can be obtained.

PROBLEMS REGARDING THE ELECTRIC FIELD PROFILE

In the previous paragraphs, it has been shown that the electric field spatial profile modifies the profile and the duration of the current signal. For this reason, the hypothesis of a certain electric field profile can lead to a disastrous consequence about the right calculation of mobility and lifetime values. For example, for both uniform and linear electric fields, the profile of the current follows a decreasing exponential function of time. If we assume a uniform electric field profile, we obtain directly carrier lifetime, while in the case of a linear profile hypothesis we find an artificial lifetime that depends on the lifetime, mobility, and field bending. In addition, the approach with a linear electric field hypothesis implies that the bending of the electric field does not depend on the voltage applied. The question is: if the electric field profile is different from a linear or a uniform trend?

Under a wrong hypothesis about the electric field spatial profile, we could obtain erroneous mobility and lifetime values, obtained by forcing the carriers to follow an electric field profile different from that they really probe in that position. One of the greatest novelty of this work is that the electric field spatial profile is not selected at the beginning, indeed it is obtained as an output function of the model.

3.5 2τ MODEL

A general model [34] has been developed in the first instance assuming a uniform weighting field with which it becomes possible to obtain information on both the material transport properties and the shape of the electric field.

3.5.1 ASSUMPTIONS IN 2τ MODEL

2τ model's assumptions are:

- **The transport properties do not change with the applied voltage.**

  The relationship between the carrier saturation velocity and the electric field is the carrier mobility, normally assumed as independent on the applied electric field. This relation loses validity for a saturation velocity higher than $v_s = 1.5 \cdot 10^7\ cm/s$.

  This condition of nonlinearity between field and velocity is reached when the field becomes greater than $E_s = 1\ Kv/mm$.

- **The carriers are generated under the illuminated contact**

  A high energy incident radiation is absorbed as a result of the photoelectric effect inside the material and creates a lot of electron-hole pairs that give an electrical signal. In this way the carriers cover a distance shorter than the thickness of the material so that the information regarding electrons and holes are mixed and it is impossible to evaluate the transport properties for each kind of charge carrier. Furthermore, the radiation must have a photon energy at least equal to the energy necessary to create the electron-hole pair. The visible radiation has been chosen as the best candidate for the current transient experiment: the visible photon is absorbed near the surface, within a few wavelengths (μm). The photon has an energy ranging from 1.75 to 3.1 eV for red and violet radiation, respectively. In particular, our experiment was carried out using a pulsed laser that shoots photons of $\lambda = 532\ nm$ and energy $E = 2.33\ eV$.

- **The electric field does not vanish inside the material**

  This assumption is critical for the use of the model. The current signal can be taken even at low voltages, but until the signal collapses to zero.

- **Diffusion phenomena and detrapping are neglected**

  The diffusion has the direct consequence of a broadening of the charge density. This leads to a drastic change, from an analytical point of view, in the mathematical analysis of the current signal. Despite the diffusion is a phenomenon always present, it is neglected here, as well as for analytical reasons, also because the final spatial spread of the charge package is much less of the thickness of the sample. For example, the application of 100 V on a sample with thickness equal to 1mm would lead to a spatial spread of the charge density equal to about 15 micrometers. We can therefore establish, with good approximation, that the charge density package travels inside the material as a space-time Dirac delta function. Furthermore, the detrapping phenomena are negligible since the characteristic times are greater than $100\ \mu s \div 1ms$,values $100 \div 1000$ times greater than typical times of flight in our experiments, so only an infinitesimal fraction of carriers trapped becomes able to escape from the traps and to take part in the signal.

- **The weighting field is uniform (valid for full-area samples)**

  The weighting field depends only from the contact geometry. Paragraph (3.6) shows how to get the weighting field profile in according to the electrode geometry. If contacts are approximated as two equal parallel planes deposited on the opposite sides of a parallelepiped and having negligible edge effects, the density of the electric field lines is uniform and hence the weighting field is equal to the inverse of the thickness of sample:

$$W(x) = \frac{1}{L}$$

  While the 2τ model is valid for those full area contacts of the samples in which the weighting field is nearly uniform, 1τ model has a more general applicability when the weighting field can be calculated starting from any geometry of the contacts.

- **The initial charge photo-generated is independent of the applied voltage.**

  The number of generated carriers does not depend on the voltage if the laser intensity has a good stability in time and if the set of measurements at different voltages can be carried out at a fixed beam energy. If at low voltages the intensity is increased to obtain a better signal-to-noise ratio, the laser energy for subsequent acquisitions cannot be changed.

In a classic experiment of current transients, the photo-generated charge and the voltage application generate a current signal. Furthermore, different current profiles for *N* voltage values are acquired. The physical quantities known before experiment are:

- The sample thickness *L*
- *N* values of the applied voltage $V_i \;\; i = 1{:}\,N$
- Uniform profile of weighting field $W(x) = 1/L$

At first, after the acquisition of the temporal profiles of the current transients, it's possible to measure:

- *N* time profiles of the current transients $I_i(t)$
- *N* flight time values (the choice of the flight times is explained in Section 3.7.4)

The quantities that remains unknown are:

- Mobility μ
- Life-time τ
- Photo-generated charge Q_0
- Spatial profile of the electric field $E_i(x)$

A semi-analytical model has been developed able to obtain all this information.

The charge generation in a few micrometers below the illuminated electrode has two important consequences:

- only a kind of carrier (electron or hole) produces signal; for example, if an electron is immediately collected by the anode, it does not travel and the time of flight is zero, whole the hole travels along the thickness of sample in a time equal to the time of time and it is collected by the cathode [40]
- as a consequence, only a kind of carrier crosses the entire thickness of the sample to reach the collecting electrode and gives an electric signal.

THE CONSTRAINTS IN 2τ MODEL

Choosing the charge sign according to the sign of the voltage V_i applied to the illuminated electrode (the collecting electrode is at ground as convention), the charge covers the sample's thickness in a time of flight so that:

$$L = \int_0^{T_{Ri}} v\big(x_i(t)\big)\, dt \tag{3.44}$$

Furthermore, whatever the form of the electric field in the sample, its integral over space must be equal to the applied voltage V_i:

$$V_i = \int_0^{L} E_i(x)\, dx = \int_0^{T_{Ri}} E_i\big(x(t)\big)\, v\big(x_i(t)\big) dt = \mu \int_0^{T_{Ri}} E_i\big(x(t)\big)^2 dt \tag{3.45}$$

Recalling the formula (3.20) of the current transient $I(t)$, the two constraints (3.44) (3.45), written as integrals over time, become

$$\begin{cases} Q_0 = \int_0^{T_{Ri}} I_i(t)\, e^{+\frac{t}{\tau}}\, dt \\ \mu Q_0^2 = \frac{L^2}{V_i} \int_0^{T_{Ri}} \left(I_i(t)\, e^{+\frac{t}{\tau}} \right)^2 dt \end{cases} \tag{3.46}$$

Although it seems that the number of the unknown quantities (Q_0, μ, τ and the $E_i(x)$ functions) is excessive compared to the constraints number, with the last form of the two constraints it is possible to observe that:

- quantities on the left (Q_0 *and* μQ_0^2), although they are unknowns, are constants because they not depend on the voltage applied.
- on the right the only unknown quantity is the life-time τ

The quantity on the left are not indexed, unlike those on the right. Then, for the right value of the life-time also the right sides of the equation should not depend from the index and should converge simultaneously at the same value. The question is: how is it possible to find the right value of the lifetime? Varying the lifetime, spanning a wide appropriate range of values (from 10 ns *to* 100 μs) we can calculate $Q_0(\tau)$ and $\mu Q_0^2(\tau)$. If exists a certain value of $\tau = \tau_{BEST}$, the quantities $Q_{0_i}(\tau_{BEST})$ converge to the same value and τ_{BEST} becomes the correct value of lifetime. The same procedure can be used for the quantity $\mu Q_0^2(\tau)$.

THE PROCEDURE IN 2τ MODEL

The 2τ model process consist of two phases:

1. Determination of the transport parameters and the photo-generated charge
2. Reconstruction of the electric field spatial profile

Current transients can be simulated to clarify the steps of the algorithm used. The physical quantities chosen for this example represent plausible values of our experiment:

- Linear electric field $E(x) = E_0 - \alpha x$
- Sample's thickness $L = 0.257\ cm$
- Mobility $\mu = 1100\ \mathrm{cm}^2/(V\ s)$
- Lifetime $\tau = 400\ ns$
- Photo-generated $Q_0 = 1\ pC$
- Electric field's slope $\alpha = 500\ V/cm^2$
- Voltages $V = from\ 30\ V\ to\ 90V\ with\ step\ of\ 10V$

The model, starting from the knowledge of thickness of sample, applied voltages and measured current profiles, allows to find all of the remaining amount, i.e. the transport parameters and the electric field profile. The simulated transients present the following profiles:

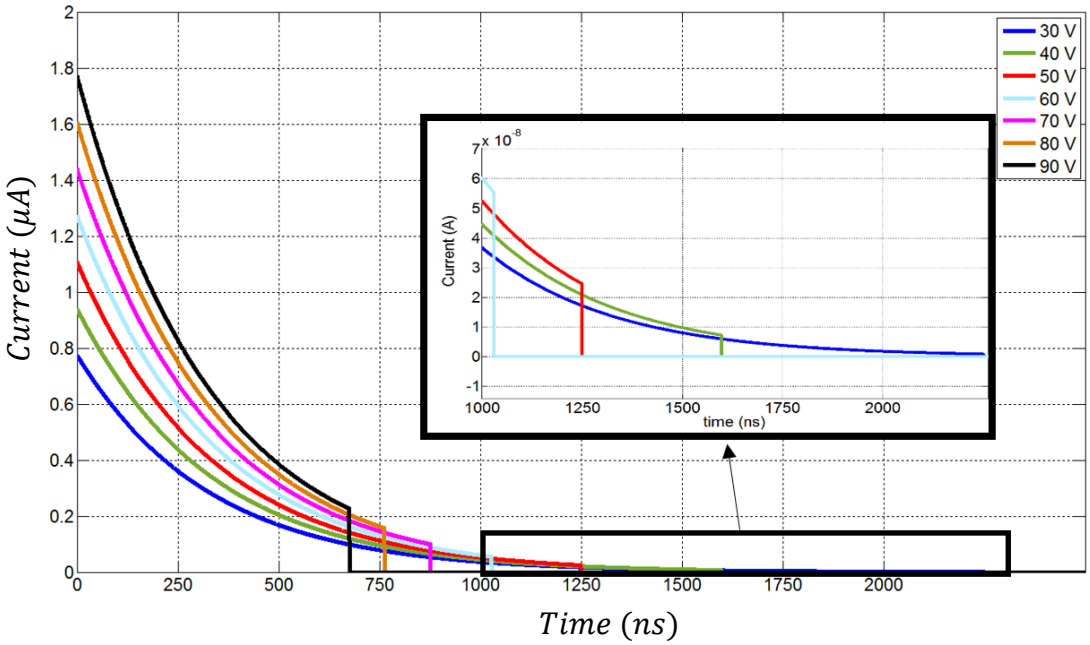

FIGURE 3.17 Simulated transients for model's explanation

The current transients show an exponential drop with a characteristic time which depends both on the life time both from bending α of the electric field (3.43). Signals collapse to zero after a time equal to the flight time of the carriers.

TRANSPORT PARAMETERS AND PHOTO-GENERATED CHARGE

First, the algorithm allows to derive the values of mobility, lifetime, and photo-generated charge. The first quantity calculated is the collected charge.

The integral of the current transient represents the charge induced on the electrode, equal to the charge amount that actually has covered the entire sample's thickness. The low-voltage measurements show obviously a greater time of flight, as the charge crosses the sample with a low velocity. Therefore, the carriers have a higher probability to be trapped, especially when the time of flight increases so much to reach the carriers' lifetime. During high voltage measurements, charges travel very fast and only a few charges are trapped: the collected charge becomes comparable to the total photo-generated charge Q_0.

$$Q_{i_{coll}}(V) = \int_0^{T_{R_i}} I_i(t)\, dt \tag{3.47}$$

The next figure shows the charge collection for the different voltage values, starting from transient simulated in the previous figure 3.17.

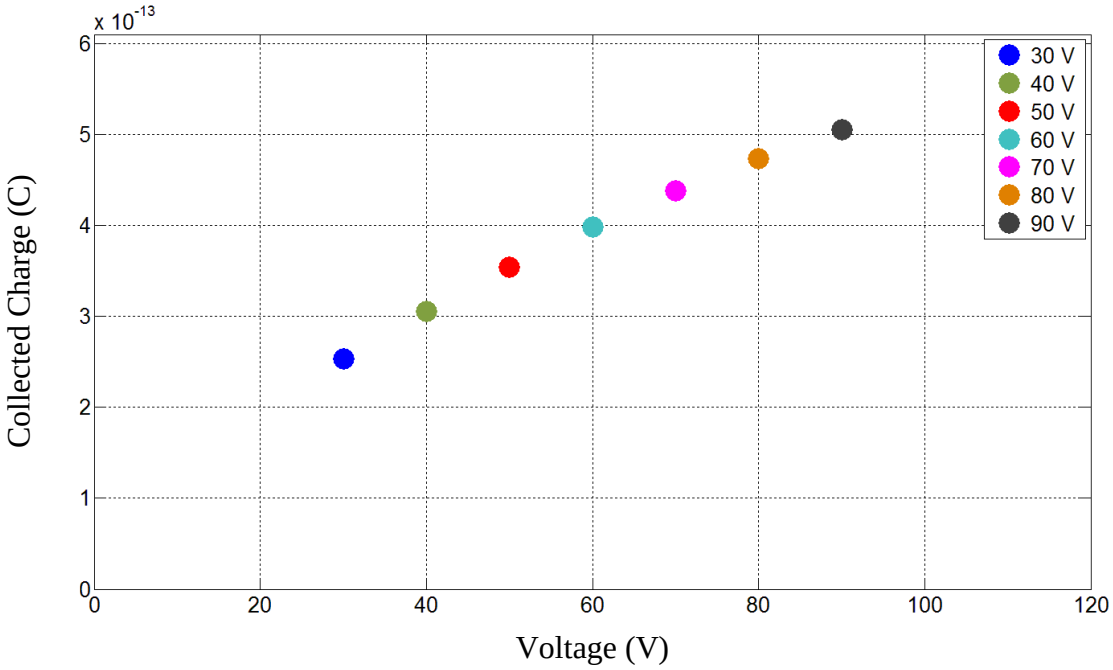

Figure 3.18 Collected charge as a function of voltage

The collected charges are obviously a fraction of the photo-generated charge Q_0. The measurements at lowest and highest voltage respectively show a partial collection of charge equal to 25.3% and 50.5%. The reason for which at low voltages the charge collection is low is due to charge trapping.

If we take into account the trapping, we can write the first model's constraint

$$Q_{0_i}(\tau) = \int_0^{T_{Ri}} I_i(t)\, e^{+\frac{t}{\tau}}\, dt \tag{3.48}$$

The product between the current signal and the $e^{\frac{t}{\tau_C}}$ factor, with the correct value of lifetime τ_C , produces an artificial rise of the number of carriers whenever they are trapped so that, for each voltage, the integral of the current coincides with the total charge Q_0.

$$Q_{0_i}(\tau_C) = Q_0 \;\; \forall i \tag{3.49}$$

A possible way to find the correct lifetime is to create a fairly wide range of possible lifetime values, including τ_C, for which the previous relation results valid.

Obviously, since in our case the transients are simulated, we know beforehand that the value of τ_C is equal to $400\, ns$, as it has been previously set. This example is useful to show how the algorithm works and how we can re-extract the correct lifetime value.

The τ_C value can be found by trying a set of possible candidates:

- $\tau = \infty$ An infinite lifetime corresponds to a value of the term $e^{+\frac{t}{\tau}}$ equal to one.
- $\tau > \tau_c$ In the case of a finite lifetime higher than the correct value (for example in this case $\tau = 500\, ns$) the term $e^{+\frac{t}{\tau}}$ has the effect to downsize the trapping effect and thus the value of the "artificial" collected charge increases.
- $\tau = \tau_c$ The correct life time course allows the exact reconstruction of the photo-generated charge since the "artificial" charges go close to the same value, which coincides with $Q_0 = 1\, pC$
- $\tau < \tau_c$ With a shorter time than τ_c the term $e^{+\frac{t}{\tau}}$ becomes very huge : at very low voltages, where the time of flight is very high, the effect of the integration of the current creates a huge artificial collected charge, even greater than those collected. This phenomenon is physically impossible.

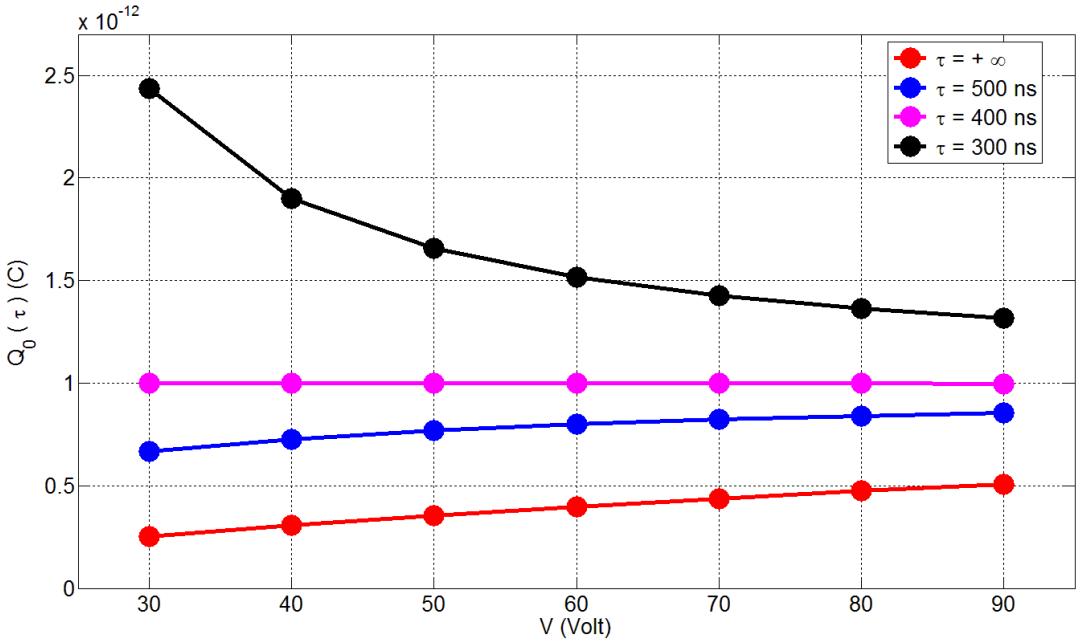

Figure 3.19 Collected charge as a function of voltage for different τ candidates. For the correct value of τ (400 ns) the total charge does not depend on the voltage

The main problem is to get good measurements of transient (good signal-to-noise ratio) at low voltage, where the flight times becomes at least comparable to the carrier lifetime. In fact, if the measurements are carried out only at high voltages, where the flight time is a small fraction of the lifetime, the measure becomes insensitive to the trapping phenomenon and the τ_C value cannot be obtained, finding only the lowest possible value for lifetime, equal to the time of flight of the lower voltage.

The figure 3.19 shows a way to find the correct lifetime, but this method is unsuitable due to the huge number of lifetime values that must be tried before obtaining the correct value.

Instead, it is preferred to calculate at fixed voltage V_j the values of the charges $Q_{0_j}(\tau)$ as a function of the lifetime. A number of curves *N*, equal to the number of the measurements as a function of voltage, are obtained. Each curve represents the "artificial" charge collection at a fixed voltage as a function of τ.

Figure 3.20 shows the results for the seven transient simulated above:

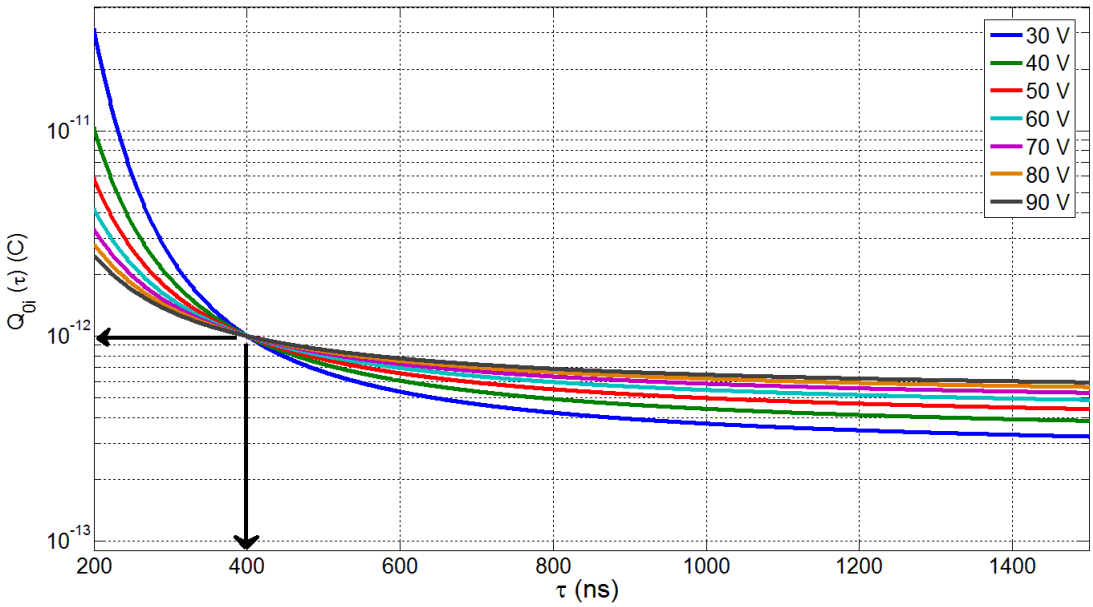

Figure 3.20 Collected charge as a function of the τ candidates for different values of the applied voltage

Spanning the lifetime in a range between $200 \div 1500\ ns$, the correct lifetime and the photogenerated charge are obtained as the crossing of the curves at different voltages. Despite the clarity of the figure, we have not yet reached the correct way to find the lifetime in a real experiment. Unlike a simulated experiment in fact, the *N* different curves will never meet exactly in a single point, but they will cross each other in a cloud of points very close together, indicating a convergence towards a value of Q_0. The quantity that measures the relative deviation between the *N* curves for each value of the lifetime is the variance of $Q_{0_i}(\tau)$:

$$Var_{(Q_0)}(\tau) = \log\left[\frac{1}{N}\sum_{i=1}^{N}\left(Q_{0_i}(\tau) - \overline{Q_{0_i}}(\tau)\right)^2\right] \tag{3.50}$$

where $\overline{Q_{0_i}}(\tau)$ is the mean value calculated over all voltages at fixed τ.

$$\overline{Q_{0_i}}(\tau) = \frac{1}{N}\sum_{i=1}^{N} Q_{0_i}(\tau) \tag{3.51}$$

The quantity of interest is, however, the logarithm of the variance because of the different order of magnitude caused by the term $e^{\frac{t}{\tau}}$.

In an equivalent way, the quantity μQ_0^2 introduced by the second constraint allows to obtain another value of the lifetime. In fact, even in this constraint the only variable factor in the second member is again the lifetime. The same procedure used for the first constraint is applied: the variance of the quantities $\mu Q_{0_i}^2$ must be calculated for each voltage:

$$Var_{(\mu Q_0^2)}(\tau) = log\left[\frac{1}{N}\sum_{i=1}^{N}\left(\mu {Q_0}_i^2(\tau) - \overline{\mu {Q_0}_i^2}(\tau)\right)^2\right] \tag{3.52}$$

The two variances can be drawn as a function of τ. In figure 3.21 the two minimum of the two variances is equal to $\tau_c = 400\, ns$.

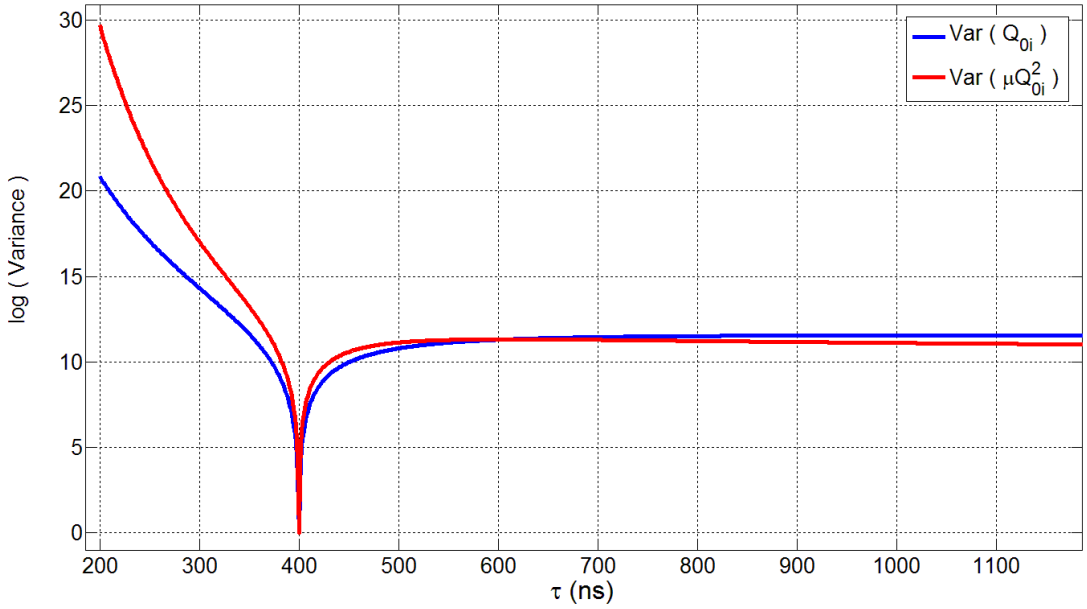

Figure 3.21 Variance curves of the term Q_0 and μQ_0^2 for the determination of the lifetime

The quantities present in the first members of the following equations can be evaluated:

$$Q_{0_i}(\tau) = \int_0^{T_{Ri}} I_i(t)\, e^{+\frac{t}{\tau}}\, dt \tag{3.53}$$

$$\mu Q_{0_i}^2 = \frac{L^2}{V_i}\int_0^{T_{Ri}} \left(I_i(t)\, e^{+\frac{t}{\tau}}\right)^2 dt \tag{3.54}$$

The Q_0 and μQ_0^2 values, that in reality do not depend on the applied voltage, are obtained as mean value over all the voltages: at this point it becomes possible to calculate the mobility.

ELECTRIC FIELD RECONSTRUCTION

The knowledge of transport parameters and photo-generated allows, starting from the relation 3.20 to obtain the quantity $E_i(x(t))$, so the electric field for each voltage V_i probed in time by the carriers during their flight is:

$$E\left(x_i(t)\right) = \frac{L}{\mu Q_0} I_i(t)\, e^{+\frac{t}{\tau}} \tag{3.55}$$

The laws of motion can be calculated:

$$x_i(t) = \int_0^t v_i(t')\, dt' = \mu \int_0^t E(x_i(t'))\, dt' \tag{3.56}$$

For each instant $\bar{t}$ the terms $E\left(x_i(\bar{t})\right)$ and the law of motion $x_i(\bar{t})$ are calculated; in this way it is possible to correlate each position with its relative value of the electric field and then to reconstruct the electric field $E(x)$

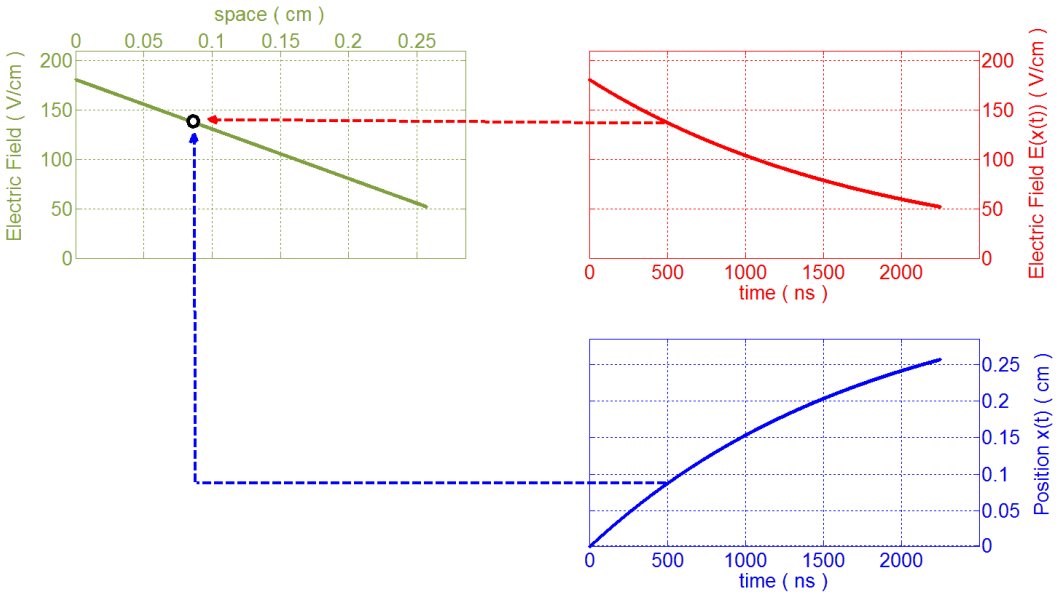

FIGURE 3.22 Electric field spatial profile reconstruction

In synthesis, this method allows to obtain the transport parameters, the photo-generated charge and the spatial electric field profile, with the assumption of uniform weighting field. The lifetime can be found only if the voltages are low enough to have flight time comparable to the lifetime itself.

3.6 1τ MODEL

The previous model can successfully get mobility values, life time and electric field with the hypothesis that the contacts deposited on the samples are both full contact area.

Recently, complex geometries such as pixelated detectors and strip detectors [38,39] have focused attention to couple a good spectroscopic performance to a good spatial resolution. In this way, a single device can identify the photon interaction position together with its energy.

3.6.1 THE RAMO-SHOCKLEY THEOREM

A different geometry, however, entails complications from the point of view of the calculation of the current signal. The Ramo-Shockley theorem [40] explains how the charge motion in a semiconductor creates instantaneously (at the speed of light) an induced signal at the collecting electrode (CE).
For example, a charge q in the position $\overrightarrow{r_q}$ at the time t, that moves with a velocity $\vec{v}(\vec{r}_q)$; induces the movement of a Q_{IND} image charge through the collecting electrode CE equal to:

$$Q_{IND} = -qV_W\left(\overrightarrow{r_q}\right) \tag{3.57}$$

Where $V_W(\vec{r})$ is the weighting potential, a geometric scalar quantity that is obtained:

- Removing the charge q
- Fixing the CE potential equal to one ($V_{W_{CE}} = 1$)
- Fixing all others electrodes at zero voltage. ($V_{W_{NO_{CE}}} = 0$)
- Solving the Laplace equation , $\Delta\left(V_W\left(\vec{r}\right)\right) = 0$ with the correct boundary conditions.

Starting from this assumption, it is possible to obtain the weighting potential $V_W(\vec{r})$. Furhermore, the negative gradient of V_W results the geometrical vector quantity called “weighting field” $\overrightarrow{W}(\vec{r})$.

The weighting field is then subject to the constraint:

$$\int_{NO-CE}^{PIXEL} \overrightarrow{W}(\vec{r}) \cdot d\vec{r} = V_W(PIXEL) = 1 \tag{3.58}$$

Where NO-CE stands for a point of one of the no collecting electrodes.

Then in case of uniformity of the weighting field (full area electrodes) it results equal to the inverse of the thickness, along the x direction:

$$W_{UNIF} = 1/L \ \hat{x} \tag{3.59}$$

The weighting potential is different from the electric potential due to the assumption of the R.S. theorem: other electrodes, different from the collecting electrode, are at weighting potential equal to zero.

For example, in a pixelated detector the electric field could remain uniform with the application of the same bias between the guard ring (no collecting electrode) and the pixel (collecting electrode). In this way, in absence of fixed charge and neglecting the small gap between the guard ring and the pixel, generally a small fraction of the pixel size (100 μm), the uniformity of the electric field is insured. The weighting field instead does not show a uniform profile because, for the weighting potential calculation, the guard ring potential is set to zero, since it is not a collecting electrode.

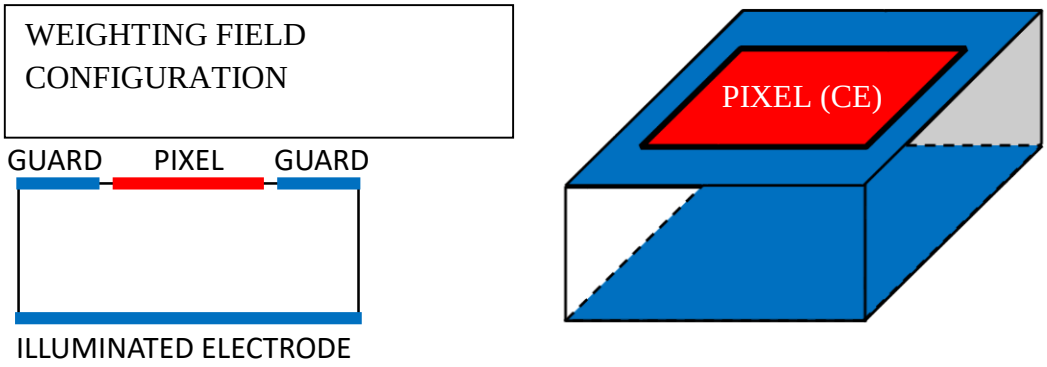

FIGURE 3.23 For the calculation of the weighting potential the illuminated electrode and the guard ring (non collecting electrodes) are set at zero weighting potential, while the pixel is set at one. Illuminated electrode and guard have the same weighting potential.

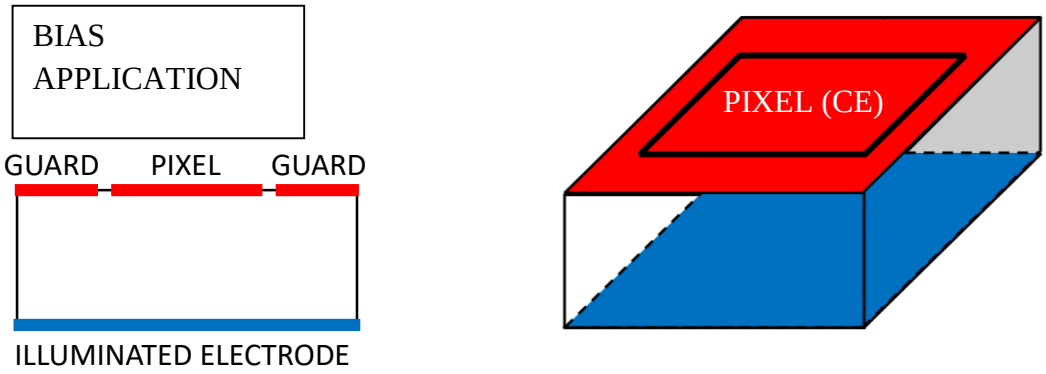

FIGURE 3.24 The application of the same voltage on guard ring and pixel guaranties the ideal uniformity of the electric field. Pixel and guard ring have the same electric potential.

While the electric field determines the charge trajectory and velocity, the weighting field depends only on geometry and determines how charge motion couples to a specific electrode.
Only in 2-electrode configurations, i.e. planar configuration, the electric field and the weighting field have the same form.

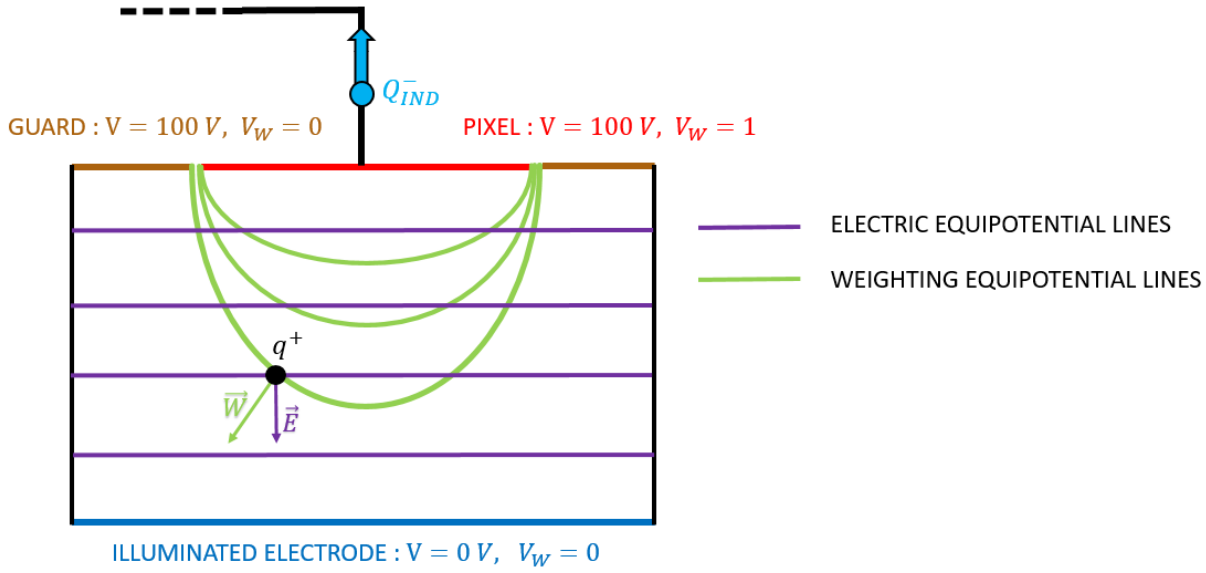

FIGURE 3.25 Generation of the induced charge Q_{IND} at the collecting electrode (PIXEL) due to the movement of the charge q in the material.

The figure 3.25 shows how the motion of a positive charge towards the lower potential electrode leads the creation of an induced negative charge (3.57) that is responsible for the current transient signal. The time derivative of the induced charge, the induced current, is proportional to the coupling between the velocity, and then to the electric field, and the weighting field:

$$\frac{d}{dt}Q_{IND} = I_{IND} = q\,\vec{v}(\vec{r})\cdot\vec{W}(\vec{r}) = q\,\mu\vec{E}(\vec{r})\cdot\vec{W}(\vec{r}) \tag{3.60}$$

The planar geometry and the assumption of uniformity inside the material lead the creation of an electric field along the only x direction. The current signal becomes:

$$I_{IND} = q\,\mu E\,W_x \tag{3.61}$$

Then, starting from the electrodes' geometry it is possible to obtain the weighting potential, the weighting field and its W_x component.

The presence of pixels is responsible for the non-uniformity of weighting field along the electric field direction. The weighting potential lines are indeed concentrated near the pixel, so on the collecting electrode the weighting field results to be higher than that on the illuminated one (figure 3.26)

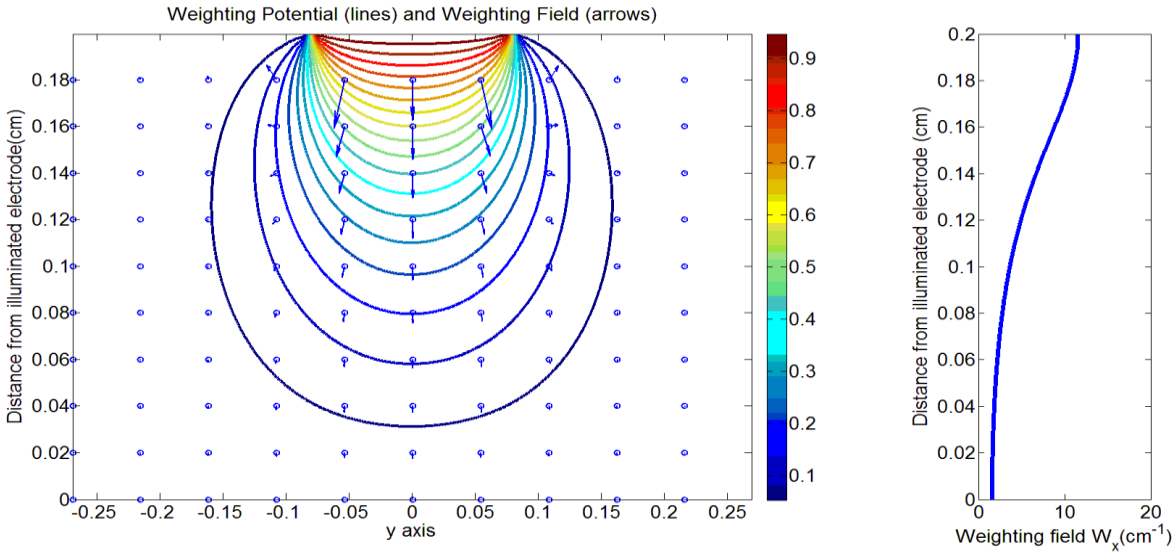

Figure 3.26. Sample (5 x 5 x 2) mm^3. The pixel size is equal to 1.5 mm. On the left the distribution of the weighting potential and weighting field. On the right the component along the electric field direction of the weighting field as a function of the distance from the illuminated electrode (x direction).

The profile of the weighting field modifies the temporal profile of the transient current : this field in fact is so-named because it weighs differently the induced charge Q_{IND} (and induced current) based on the position of the charge q inside the material.

The component of the weighting field required for the calculation procedure is the component parallel to the direction of motion of the charges, that is, the direction of the electric field. (x direction) Weighting field is not uniform, however, for the sections along planes parallel to the directions perpendicular to the motion (y and z directions).

Then a diffuse illumination of the entire electrode leads the carriers to probe very different weighting fields. There are also areas where the weighting field should be antiparallel to the electric field, leading to a reversal of the sign of the current. Lighting should be conducted within a minimum space and at the exact center of the contact, so that all carriers probe the same weighting field and also they reach the collecting pixels, not the guard ring. Then, observing the figure 3.26, the useful component of the weighting field W_x is the one along x direction at $y = 0$

3.6.2 THE PIXEL EFFECT

Then current in a pixelated detector differs from that in a full-area detector, even if the transport parameters, the thickness, the voltage, and the electric field profile are exactly the same. In presence of a pixel as collecting electrode, the current shows the "pixel effect", a final spike due to the weighting fields increase. This effect increases with decreasing the size of pixel.

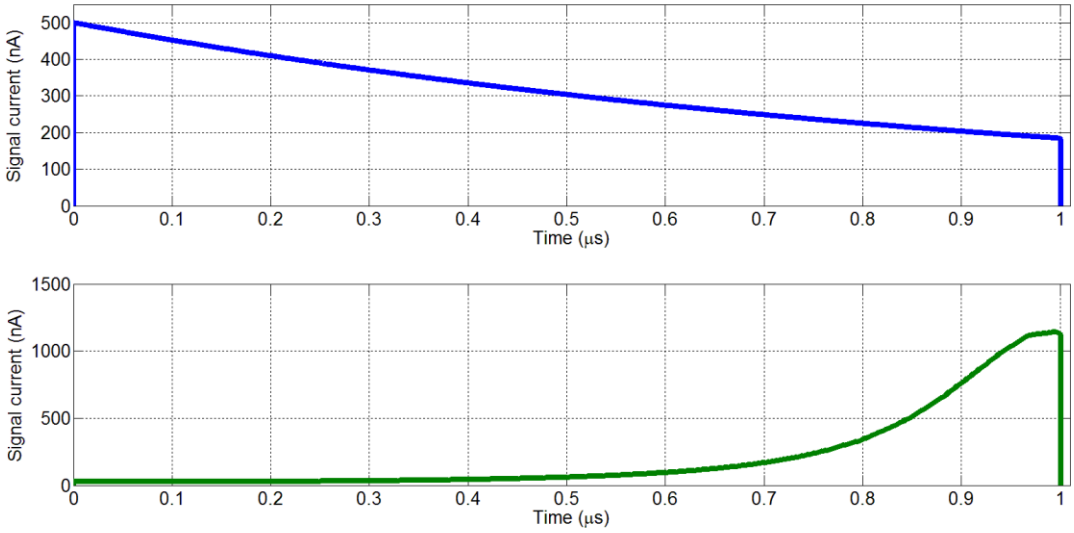

FIGURE 3.27 Simulated current transient on full-area electrodes detector (blue line), and pixelated detector (green line).Values: $Q_0 = 500\ fC; Thickness = 2mm, \mu = 10^3 \frac{cm^2}{Vs}$, $\tau = 1\mu s$, $V = 100\ V$, $Uniform\ E$, $L_{ILL-EL} = 5\ mm$, $L_{PIXEL} = 1.5\ mm$

The pixel effect increases the temporal final part of the current because, at the end of the flight, the no-trapped carriers are located at points where the weighting field is very high. In this case anyway the charge collection result lower then that with full area contacts: the signal current decreases at the beginning more than increases at the end. In other words, the induced charge in the pixelated detector results lower than the total charge that crosses the pixel at the flight time.

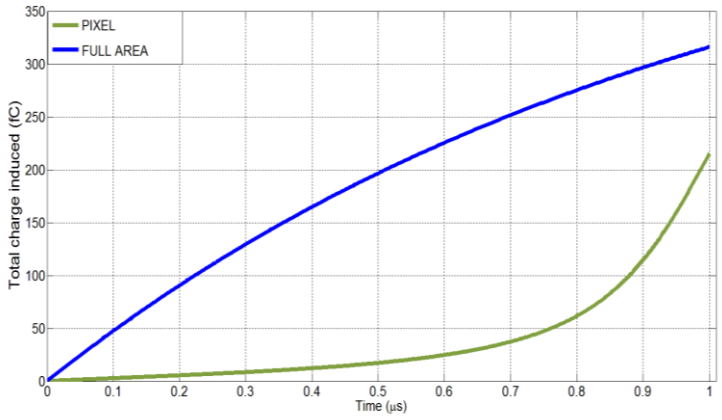

FIGURE 3.28 Collected charge in pixel (green line) and in full-area detectors (blue line). This curves represent the integral over time of the currents showed in figure 3.27

3.6.3 THE PROCEDURE IN 1τ MODEL

The 1τ model proposes a method to find the transport parameters and the spatial electric field profile taking into account a non-uniform weighting field. The transient current depends strongly on this geometrical field:

$$I(t) = Q_0\, \mu E\big(x(t)\big)\, W\big(x(t)\big)\, e^{-\frac{t}{\tau}} \tag{3.62}$$

Then the current profile is subject to change in time because the carriers:

- Probe a different electric field during the flight
- Probe a different weighting field
- Decrease due to trapping

The difficulty lies in the fact that the term $W(x(t))$ is unknown at the beginning as the law of motion $x(t)$. The low of motion, in fact, depends on the electric field profile, that it is initially unknown.
The model's assumptions are the same as those presented in the previous section (3.5.1) for the 2τ model, with the only difference that here the weighting field is not assumed as uniform, because of the different geometry of the electrodes. In the previous paragraph it's widely explained as the presence of a pixel as collection electrode modifies this weighting field.

The model consists of three main steps:

1. Geometric
2. Experimental
3. Analytical

GEOMETRIC STEP

Starting from the contacts' geometry (thickness L, size of the illuminated electrode and pixel) the spatial weighting field $W(x)$ is calculated using the Laplace equation. (using Matlab or Comsol) (figure 3.26).

EXPERIMENTAL STEP

The acquisition of the current transient signals $I_i(t)$ is performed for N different voltages V_i. Afterwards the flight times T_{R_i} are measured for each transient. The experimental setup is shown in section 4.1.

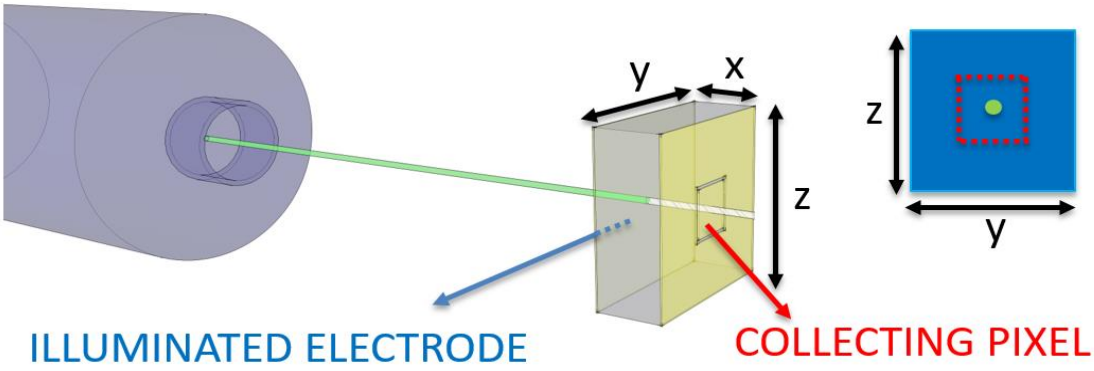

FIGURE 3.29 Laser beam through the optical fiber, comes exactly at the contact center. The knowledge of the position of the generated charge is essential for the success of the procedure of the 1τ model.

ANALYTICAL STEP

After the geometric and the experimental acquisition of data it is possible to obtain in order:

a. The lifetime τ and the photo-generated charge Q_0
b. The laws of motion $x_i(t)$
c. The mobility μ
d. The spatial electric fields $E_i(x)$

a. The weighting field must respect the constraint:

$$\int_0^L W(x)\,dx = 1 \tag{3.63}$$

Using the current's definition (3.20), this constraint becomes:

$$Q_0 = \int_0^{T_{Ri}} I_i(t)\, e^{+\frac{t}{\tau}}\, dt \tag{3.64}$$

It can be observed that this relation is exactly the same found for the 2τ *model*, that allowed through a minimization procedure, to find just τ and Q_0, assuming that the latter and the transport parameters do not depend on the applied voltage.

b. The law of motion $x_i(t)$ is the indefinite integral over time of the velocity $v_i(t)$:

$$x_i(t) = \int_0^t v_i(t)\, dt = \int_0^t \mu E_i\big(x(t)\big)\, dt \tag{3.65}$$

Then using the (3.62), this relation becomes:

$$x_i(t) = \int_0^t \frac{I_i(t)\, e^{+\frac{t}{\tau}}}{Q_0\, W\big(x_i(t)\big)} dt \tag{3.66}$$

The only unknown quantity is the law of motion, present in the first member and also in the second one as argument of the weighting field. It is impossible then to obtain it with an analytical process. The only way is to perform a self-consistent iterative process:

$$x_{NEW}(t) = \int_0^t \frac{I_i(t)\, e^{+\frac{t}{\tau}}}{Q_0\, W\big(x_{PREV}(t)\big)} dt \tag{3.67}$$

Initially the unknown electric field profile is assumed as uniform. Then the initial law of motion is:

$$x_{PREV}(t) = v \cdot t = \mu E_i t = \frac{\mu\, V\, t}{L} \tag{3.68}$$

Now the quantity $W\big(x = x_{PREV}(t)\big)$ can be calculated, as the entire second member of the equation (3.67), that results equal to the recalculated law of motion $x_{NEW}(t)$.

If the two law of motions are significantly different, the uniform electric field assumption was not adhering to the physical reality, and the law $x_{PREV}(t)$ becomes the new one $x_{PREV}(t)$, which will generate a new motion's law and so on, until reaching a convergence.

When the two motions' law differ less than a tolerance, the correct time law $x_i(t)$, unless the same tolerance, is found. This procedure must be performed for each transient $I_i(t)$ at different voltages, obtaining N different laws of motion.

c. The knowledge of the law of motion allows to obtain the velocity as a function of the time:

$$v_i(t) = \mu E\big(x(t)\big) = \frac{dx_i(t)}{dt}$$

Now, starting from the same integral, it is possible to obtain two different result:

$$\int_0^L v(x)\,dx = \begin{cases} \int_0^L \mu E_i(x)\,dx = \mu V_i & using \int_0^L E_i(x) = V_i \\ \int_0^{T_{Ri}} \big[v\big(x(t)\big)\big]^2 dt & using\ dx = v\big(x(t)\big)dt \end{cases} \tag{3.69}$$

Then the mobility can be finally obtained:

$$\mu_i = \frac{1}{V_i} \int_0^{T_{Ri}} \big[v\big(x_i(t)\big)\big]^2 dt$$

The value of mobility, as for hypothesis does not depend on the applied voltage, it is obtained by averaging the N values obtained.

d. The electric field probe in time can be now calculated:

$$E_i\big(x(t)\big) = \frac{1}{\mu}\, v_i\big(x(t)\big)$$

Then the spatial electric field profile can be reconstructed in the same way as presented for $2\tau\ model$. (section 3.5)

3.7 THE DIFFUSION MODEL

The current transients contain a lot of information about the transport properties of the sample. We have shown previously as the mobility and lifetime of charge carriers can be found and furthermore as the profile of electric field can be reconstructed, as long as detrapping and diffusion phenomena are neglected in the transport model.

This assumption is reasonable since the detrapping time ($100\mu s - 10ms$ in these materials) is in fact much greater than the typical times of flight and then the probability that a carrier, once trapped, manage to escape from the trap is very low.

The thermal diffusion is usually neglected since its only effect is to spread the spatial carrier distribution during the flight. As will be seen later, the barycenter of carriers' cloud follows the law of motion while carriers move away from it with a thermic velocity proportional to the diffusion coefficient. This phenomenon does not change the acquisition of the times of flight times and, as a consequence, it does not modify the procedure used to deduce the mobility and lifetime values.

Diffusion instead affects heavily the electric field reconstruction because the final part of the signal is affected by the current due to those carriers that are collected after the arrival of the barycenter due to the spread of charge. This effect can alter the electric field reconstruction. In this paragraph, it is proposed a new method to evaluate the diffusion coefficient from the current transients and jointly to obtain a different way to find the value of carriers' mobility. The Einstein–Smoluchwoski relation [46] shows as the diffusion coefficient *D* depends on the mobility of carrier:

$$D = \mu \frac{K_B T}{e} = \mu V_{TH} \tag{3.70}$$

Where V_{TH} is the thermal voltage equal to 26 mV at room temperature. For example, for a mobility value of electrons in CZT equal to 1000 $\mathrm{cm}^2/(Vs)$, the coefficient diffusion results $D = 26\ \mathrm{cm}^2/s$.

3.7.1 THE CHARGE DENSITY WITH DIFFUSION

The transient signal is due to the motion of the charge carriers. Electrons or holes are drifted by the potential gradient towards the collecting electrode traveling across the entire detector following the law of motion imposed by the electric field.

The total current is the sum of a drift motion, due to the electric field $\vec{E}$, and a diffusive contribution, due to a possible concentration gradient $\vec{\nabla}\rho$:

$$\vec{J} = \vec{J}_{DRIFT} + \vec{J}_{DIFFUSION} = s\mu\vec{E}\rho - D\,\vec{\nabla}\rho \tag{3.71}$$

where:

- $\vec{J}$ is the current density $[C/(s \cdot cm^2)]$
- μ is the carrier mobility $[cm^2/(V \cdot s)]$
- D is the diffusion coefficient $[cm^2/s]$
- $\rho(x,t)$ is the charge density $[C/cm^3]$
- $s = 1$ for holes and $s = -1$ for electrons
- $\vec{E} = s|\vec{E}|\hat{x}$ is the stationary electric field

If we rewrite the equation (3.71) we obtain:

$$\vec{J} = \left(s\mu\vec{E} - D\frac{\vec{\nabla}\rho}{\rho}\right)\rho \tag{3.72}$$

$$\vec{v} = \left(s\mu\vec{E} - D\frac{\vec{\nabla}\rho}{\rho}\right) \tag{3.73}$$

We can observe that the carriers experience a drift and a diffusive velocity:

$$\vec{v}_{DRIFT} = su\vec{E} \qquad \vec{v}_{DIFF} = -D\,\vec{\nabla}\rho/\rho$$

The maximum number of carriers is localized in the charge barycenter and this is the only point where $v_{DIFF} = 0$ because $\vec{\nabla}\rho = 0$. The barycenter is the unique point that moves following only the law of motion imposed by the electric field. All other carriers depart instead relatively to the barycenter during flight, leading to a continuous enlargement of the package carriers.

3.7.2 THE CONTINUITY EQUATION

The charge density is the solution of differential equation of continuity:

$$\begin{cases} \dfrac{\partial \rho}{\partial t} = -\vec{\nabla} \cdot \vec{J} + G - U = -\vec{\nabla}\left(s\mu\vec{E}\rho \right) + D\,\Delta\rho + G - U \\ G(x,t) = Q_0\,\delta(\vec{r})\delta(t) \\ U(x,t) = \dfrac{\rho}{\tau} \end{cases} \tag{3.74}$$

The term G is the generation rate: at $(x = 0, t = 0)$ the initial charge Q_0 is the photogenerated charge. The term U is the destruction rate due to the trapping. Lifetimes of electrons and holes are in general different values with relation to the presence of traps (defects) within the detector. The value of lifetime has a great importance in X-γ ray detectors: the carriers with a small lifetime, once trapped, do not give contribution to the electrical signal and causes the detection of an outwardly lower energy of the incident photon.

The bias application in the x direction leads to the creation of an electric field in the same direction. The uniformity within the material suggests that the electric field $\vec{E}$ can be written:

$$\vec{E}(x,y,z) = s\,E\,\hat{x} \qquad\qquad E(x) = |\vec{E}|$$

The x direction of the electric field leads the differential equation to assume this form:

$$\begin{cases} \dfrac{\partial \rho}{\partial t} = -\dfrac{\partial}{\partial x}(\,\mu E \rho) + D\left(\dfrac{\partial^2}{\partial \mathrm{x}^2} + \dfrac{\partial^2}{\partial \mathrm{y}^2} + \dfrac{\partial^2}{\partial \mathrm{z}^2} \right)\rho - \dfrac{\rho}{\tau} \\ \rho\,(\vec{r}, t = 0\,) = Q_0\,\delta(\vec{r})\,\delta(t) \end{cases} \tag{3.75}$$

The general solution can be factored and written as the product of three functions respectively of x, y and z:

$$\rho(\vec{r}, t) = Q_0 \, e^{-t/\tau} \rho_x(x,t) \cdot \rho_y(y,t) \cdot \rho_z(z,t) \tag{3.76}$$

Along the y and z directions there is there is no voltage gradient: charges can't be drifted towards this direction by electric field. Electrons and holes can move along y and z because of the diffusion.
The densities $\rho_y(y,t)$, $\rho_z(z,t)$ are solutions of a typical diffusion differential equation:

$$\frac{\partial \rho}{\partial t} = D \frac{\partial^2}{\partial y^2} \rho \qquad \rho = \rho\,(y,t) \tag{3.77}$$

The charge density undergoes a change in time due to a diffusive term. The solution of this equation is a space-time Gaussian:

$$\rho(y,t) = G_y[\,\bar{y}(t); \sigma^2\,(t)] = \frac{1}{\sqrt{2\,\pi\,\sigma^2}}\, exp\left[\frac{(y-\bar{y})^2}{2\,\sigma^2}\right] \tag{3.78}$$

The charge generation (at $t = 0$) lies at $y = 0$.
The term $\bar{y}$ represents the mean value of y. This value can change in time if a force is applied along the same direction. In our case, the charge movement is due only to the diffusion and to the spread of the charge density along the y direction around the initial position: $\bar{y}$ remains equal to zero during the flight of charge. The charge spreads into the sample and its spatial distribution increases over time. The variance σ^2 is proportional to the diffusion coefficient *D* and increases linearly with the time through the following relation:

$$\sigma^2 = 2Dt \tag{3.79}$$

The charge densities along y and z directions can be therefore written as:

$$\rho_{y,z} = G_{y,z}\,[\,0;\; 4Dt\,] \tag{3.80}$$

Along the x direction instead the differential equation is generally impossible to solve for a generic spatial profile of the electric field, but it admits solution in a few cases.
The electric field term causes the charge drift in the x direction. The mean value of x position of the charge depends on the law of motion $x(t)$ imposed by electric field .
The partial differential equation has solution if the electric shows a linear profile:

$$E(x) = E_0 - \alpha x = \left(\frac{V}{L} + \frac{\alpha L}{2}\right) - \alpha x \tag{3.81}$$

The uniform profile is a particular linear profile with electric slope α equal to zero.

It is noteworthy that in a time of flight measurement the electric field must not vanish: if the electric field becomes equal to zero the carrier experiences a velocity that drop to zero, while the time of flight diverges. The α value, which represents the bending of the field, must therefore be smaller than the maximum value α_{MAX}:

$$\alpha_{MAX} = \frac{2V}{L^2} \tag{3.82}$$

Under these assumptions, it becomes possible to solve the equation and obtain the charge density:

$$\rho(x,t) = G_x\,[x(t); \sigma_x^2(\mathrm{t})] \exp(-\mu\alpha t) \tag{3.83}$$

The charge density shows a Gaussian shape, depending on the spatial coordinate and on the time, which decays in time due to the bending α of the electric field. The law of motion x(t) is the solution of the differential equation (3.2) and represents the barycenter position as a function of time, starting from the generation time t = 0.

$$x(t) = \frac{E_0}{\alpha}\,(1 - \exp(-\mu\alpha t)) \xrightarrow{\alpha=0} \mu E_0 t \tag{3.84}$$

In the case of a uniform electric field, the law of motion is a linear function of the time.

The variance of the charge density increases in time as in a typical diffusion process. In the case of a uniform electric field, the well-known result, in which the standard deviation is proportional to the diffusion coefficient and the time, is obtained. [46]

$$\sigma_x^2(t) = \frac{D(1 - exp(-2\mu\alpha t))}{\mu\alpha} \xrightarrow{\alpha=0} 2Dt \tag{3.85}$$

In the linear case the variance increases more slowly: with increasing time the variance converges to the value

$$\lim_{t\to\infty} \sigma_x^2(t) = \frac{D}{\mu\alpha} \tag{3.86}$$

The solution of the general differential equation of drift-diffusion with an electric field along x direction with a linear profile is a space-time 3D charge density written as the product of three Gaussian curves:

$$\rho(\vec{r}, t) = Q_0\, e^{-t/\tau} \cdot G_x[x(t);\ \sigma_x^2] \cdot G_y\,[0;\ 2Dt] \cdot G_z[0;\ 2Dt] \tag{3.87}$$

3.7.3 THE DIFFUSION SIMULATION

The charge density is obtained by using a simulation with the typical physical values of our experiments. Simulation values:

$V = 10\,Volt$ $L = 0.1\,cm$ $Q_0 = 1\ \mathrm{pC}$ $\mu = 10^3\ \mathrm{cm}^2/(\mathrm{V}\cdot\mathrm{s})$

$\tau = 1\,\mu s$ $D = 26\ \mathrm{cm}^2/s$ $\alpha_{MAX} = 2000\ \mathrm{V/cm}^2$

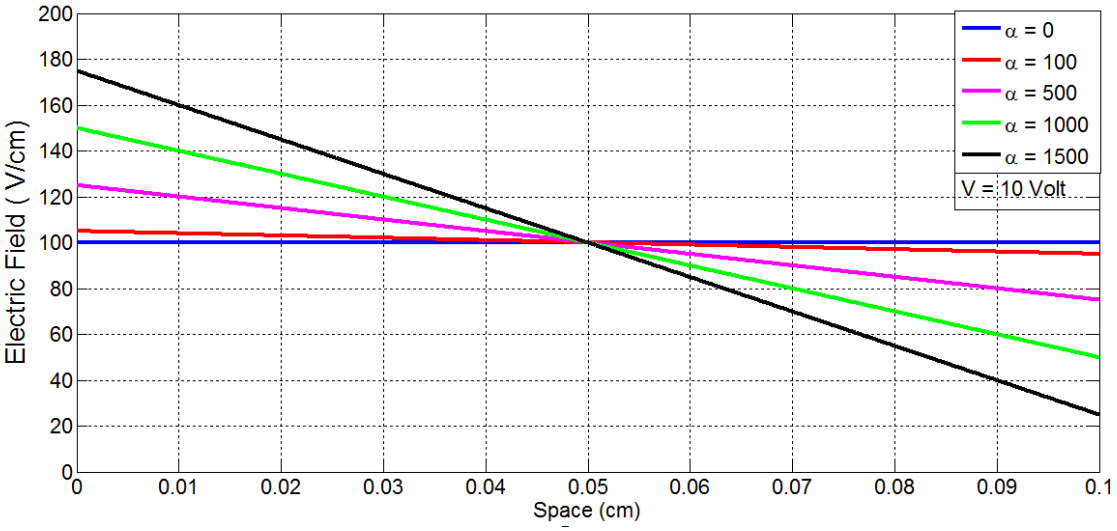

FIGURE 3.30 Electric field profiles at the same voltage $V = 10$ with different slope $\alpha = 0, 100, 500, 1000, 1500\ \mathrm{V/cm}^2$

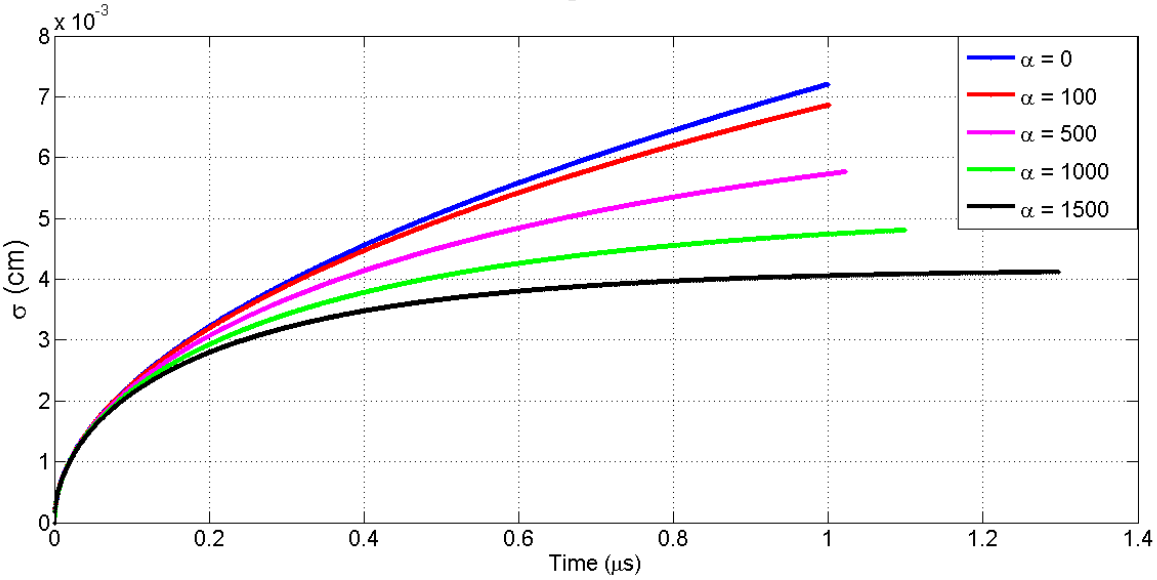

FIGURE 3.31 Standard deviations along electric field direction as a function of time for different values of the electric slope $\alpha = 0, 100, 500, 1000, 1500\ V/cm^2$

Electric field with a linear profile cause instead the flight time increase, for the same voltage. From the figure we can observe that the carriers, despite traveling inside the detector for a longer time, show a lower standard deviation and then a lower diffusion. In fact the variance converges to the $D/(\mu\alpha)$ value.

In the case the field falls to zero within the material in position x_0 the charge density come close indefinitely to this position using an infinite time to reach it. Despite the flow of time the variance would stand on a steady value. The charge density therefore would not move and does not spread more, but would continue to decrease because of trapping.

THE CHARGE DENSITY IN 4D

The charge density is a 4D quantity, as it evolves in space and time. Since the charge density fills completely the space, 3D isosurfaces are represented at different time values. The values for the parameters used in the simulation are the same as presented in the previous section. The values of the slope of the electric and the relative time of flight are:

$$\alpha = 950\frac{V}{cm^2} \qquad T_R = 1\ \mu s$$

Figure 3.32 shows the charge density for the following times: $t = (0.01, 0.1, 0.3, 0.5, 0.7, 0.9, 1)\ \mu s$ In this way the charge density is shown from the time of generation to the collecting time through seven different snapshots

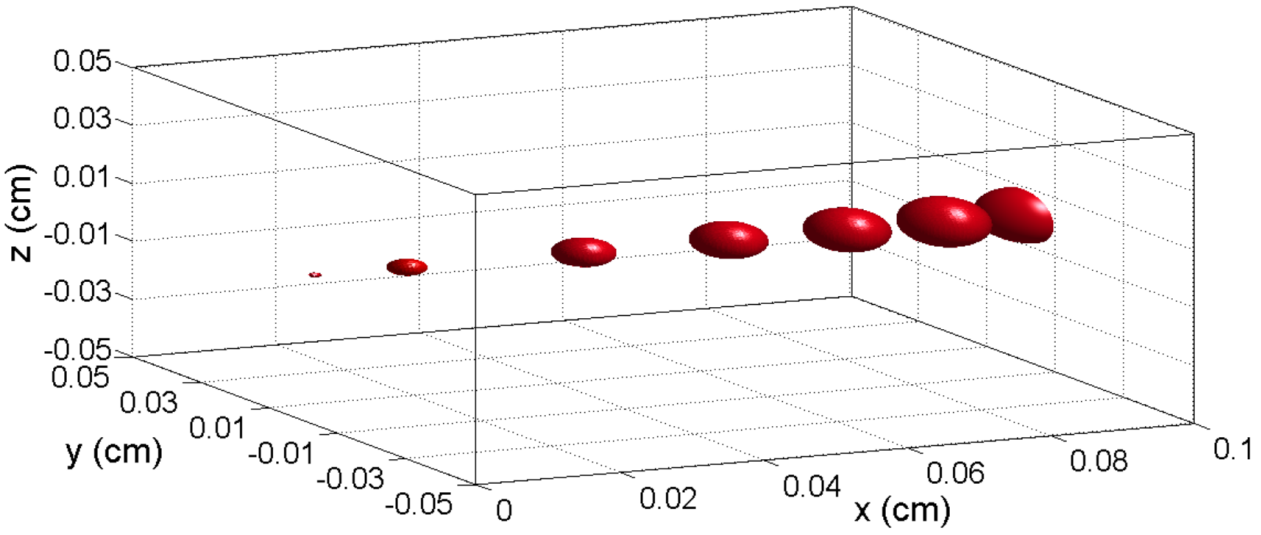

FIGURE 3.32 Isosurfaces at 1σ of the charge density for different times

The density evolves in time widening as a spheroid, where the semi-axes (equals along y and z) represent the standard deviation of the respective densities G_x, G_y and G_z.

THE CHARGE COLLECTION ALONG Y AND Z DIRECTIONS.

The expansion along the y and z directions, as we shall see, has no effect on the current profile, if the weighting field is assumed uniform. In this way a charge that moves along a direction orthogonal to the x axis, brings no contribution to the current signal because this purely diffusive current has zero coupling with the weighting field. Anyway, the standard deviations of these Gaussians must therefore be much smaller than the size of the contact itself. For example, in this simulations the value of the standard deviations at the flight time is equal to 100 μm, while the contact side is usually equal to 5 mm. Then the free charge that moves along directions perpendicular to the electric field direction is totally collected and does not change the current profile.

$$\iint G_y \, G_z \, dy \, dz = 1 \quad \forall t \tag{3.88}$$

The contact collects, instant by instant, the current density over the whole volume. Some charge takes a shorter time to the flight time to traverse the entire thickness because it is pushed forward by both the electric field (which defines the time of flight value) and by the diffusion phenomenon. (figure 3.2). All charges on the right of the barycenter is pushed forward, while all charges on the left are pushed back, and braked by diffusion. Essentially only the charges that are located in the barycenter take a time equal to the time of flight to cross the sample. At the instant in which the barycenter passes through the contact, (figure 3.32) half of the charge is still inside the material, so the contact is able to integrate only half of the total current.

$$0 \leq \int_0^L G_x \, dx \leq 1 \tag{3.89}$$

The importance of this model is in fact twofold: on the one hand it is able to get the value of the diffusion coefficient, on the other hand it allows to find a way to measure the time of flight correctly, understanding form the current profile at what time the barycenter crosses the collecting electrodes.

3.7.4 The Current Signal with Diffusion

The induced current signal depends essentially on the spatial integral of the coupling between the weighting field and current density, where the latter is the product between the carriers' velocity and the charge density.

The charge density $\rho(\vec{r},t)$ (3.87),with the constraint (3.88), that moves with a drift-diffusive velocity (3.8), induces on the collecting electrode a current signal (3.16).

If we assume a uniform weighting (3.59) (planar full area detector) and a linear electric field along x direction with α slope (3.33), the current transient becomes:

$$I(t) = \iiint \vec{v}_{TOT}(\vec{r}) \cdot \overrightarrow{W}(\vec{r})\, \rho(\vec{r},t)\, dV$$

$$= \frac{1}{L}\left(\mu \iiint E(x)\, \rho(\vec{r},t)\, dV - D \iiint \frac{\partial \rho(\vec{r},t)}{\partial x}\, dV\right) =$$

$$= \frac{Q_0\, e^{-t/\tau}}{L}\left[\mu\left(\int_0^L (E_0 - \alpha x) G_x(x,t)\, dx\right) - D\big(G_x(L,t) - G_x(0,t)\big)\right]$$

$$= \frac{Q_0}{L}\, \mathrm{e}^{-t/\tau}\, [\mu E_0 e^{-\mu\alpha t}\, \Delta_1(t) - D e^{-2\mu\alpha t} \Delta_2(t)] \qquad (3.90)$$

where:

- the term Δ_1 takes into account of the charge broadening and it's equal to the Heaviside function if $D = 0$, and change the current profile substantially in the proximity of the contacts (at $x = 0$ and $x = L$)

$$\Delta_1(t) = \frac{1}{2}\left[\mathrm{erf}\left(\frac{L - x(t)}{\sqrt{2}\sigma_x(t)}\right) + \mathrm{erf}\left(\frac{x(t)}{\sqrt{2}\sigma_x(t)}\right)\right] \qquad (3.91)$$

$$\lim_{D\to 0} \Delta_1 = \begin{cases} 1 & 0 \le x(t) \le L \\ 0 & otherwise \end{cases}$$

- the term Δ_2 instead represents two Gaussian function centered always in the proximity of the contacts and in diffusion absence Δ_2 represents two Delta-Dirac.

$$\Delta_2(t) = \frac{1}{\sqrt{2\pi}\sigma_x(t)}\left\{\exp\left[-\left(\frac{L-x(t)}{\sqrt{2}\sigma_x(t)}\right)^2\right] - \exp\left[-\left(\frac{x(t)}{\sqrt{2}\sigma_x(t)}\right)^2\right]\right\} \qquad (3.92)$$

$$\lim_{D\to 0} \Delta_2 = \delta[x(t)] + \delta[L-x(t)]$$

While the first current term $\mu E\big(x(t)\big)\,\Delta_1(t)$ results a zero-order diffusion process, the second term $De^{-2\mu\alpha t}\Delta_2(t)$ is a first-order diffusion process. Then, if the diffusion phenomenon is negligible compared to the charge drift, the second term would become negligible.

We can compare the mean drift velocity to the mean diffusion velocity:

- The mean drift velocity is equal to the ratio between the thickness and the time of flight.

$$\bar{v}_{DRIFT} = \frac{L}{T_R} = \frac{\mu V}{L}$$

- The mean diffusion velocity is the ratio between the broadening of the charge at the end of flight and the time of flight:

$$\bar{v}_{DIFF} = \frac{\sigma_X(T_R)}{T_R} = \frac{\sqrt{(\,2\,D\,T_R\,)}}{L} = \sqrt{\frac{2D}{\mu V}} \qquad (3.93)$$

The coefficient diffusion D is connected to the mobility from the relation (3.70)
The ratio between drift and diffusion velocities becomes:

$$\frac{\bar{v}_{DIFF}}{\bar{v}_{DRIFT}} = \sqrt{\frac{2V_{TH}}{V}} \qquad (3.94)$$

The diffusive term is then negligible until the applied bias results much higher than the thermal voltage. The main effect of the diffusion is visible in the current signal close to the time of flight. Without diffusion, all the free charges are collected at the same time, while the diffusion broadens the charge distribution: the density becomes more broadened as the diffusion coefficient increases.

Diffusion phenomenon causes two consequences: the current profiles are distorted by the diffusion and it is more complicated to obtain the time of flight.

3.7.5 The Time Derivative of the Current Signals

Any transients with different coefficient diffusion have a common point: the final flex point (Figure 3.34). This point represents the arrival of barycenter of charge at the collecting electrode and it is the correct point to evaluate the time of flight.

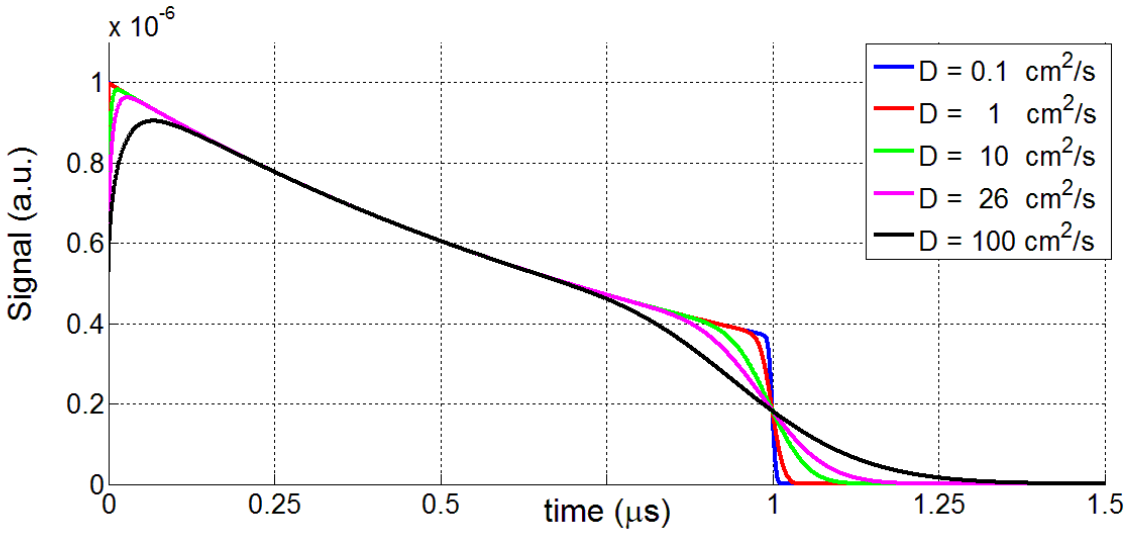

FIGURE 3.34 Current profiles for different values of coefficient diffusion $D = 0.1\,;\ 1\,;10\,;26\,;100\ cm^2/s$

The time at which the barycenter crosses the electrode is independent of diffusion because the barycenter is the only point which travels according to the law of motion and is subject only to the electric drift.

The signal is proportional to the term Δ_1, (3.91), giving when derived a temporal Gaussian centered at time in which the barycenter reaches the L spatial coordinate, that is exactly the time of flight.

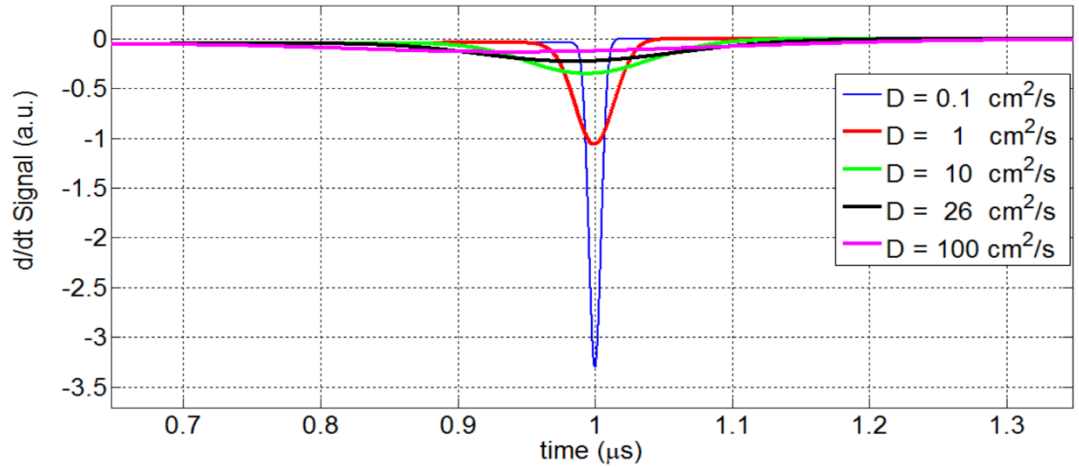

FIGURE 3.35 The figure shows the time derivatives of the current transients shown in Figure 3.34. The curves represent the temporal Gaussian curves centered on the time of flight with a width increasing with increasing diffusion coefficient.

The time derivative of the Δ_1 term actually has a more complicated shape: in the derivation process, we have to take into account that even the law of motion and the standard deviation are time-dependent. Furthermore the derivative of the current transient also implies the derivation of the term of trapping and of the drift term $E(x(t))$. As a consequence, the current gradient is not exactly a Gaussian, as can be seen from the next figure.

The purpose of this model is not in fact to get the exact analytical form of the derivative of the transient, but rather to find a relation between the Gaussian width and the diffusion coefficient.

This approximation remains valid until the time variations of the other quantities (trapping and electric field) are negligible during the passage of the charge density across the contact.

How much time does the charge density take to cross the contact?

The quantity of interest is the temporal full width at half maximum, $FWHM_T$. It is equal to $2\sqrt{2\ln(2)}\,\sigma \approx 2.335\,\sigma$ and represents the time required for a 76% of the charge amount around the barycenter to cross the contact. The $FWHM_T$ can be calculated easily from its definition.

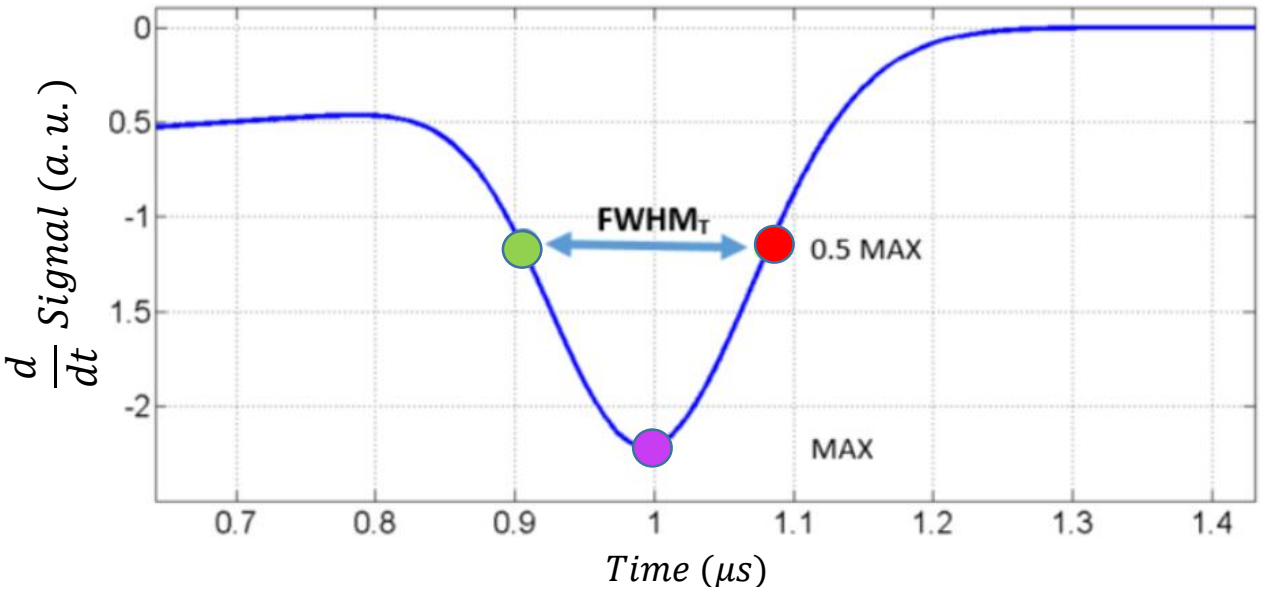

FIGURE 3.36 Current derivative in time, green and red point determine the $FWHM_T$. The purple point represents the time at which the barycenter reaches the contact

In figure 3.36 the green point represents the time $T_R^- = T_R - \frac{FWHM_T}{2}$ at which the charge that is located to the right of barycenter at a distance equal to half the spatial $FWHM_x$ crosses the contact. This charge portion employs a time shorter than the time of flight to reach the electrode as it has been accelerated by diffusion. At this time the 88% of the charge is still in the sample.

The purple point represents instead the contact crossing by the barycenter. This point is not affected by the diffusion and then takes a time equal to the time of flight to reach the contact. The 50% of the charge is still in the sample.

The red point represent instead the charge located to the left of barycenter at a distance equal to half the spatial FWHM. This charge takes a longer time than flight time $T_R{}^{+} = T_R + \frac{FWHM_T}{2}$ because it is slowed down by the diffusion. Only 12% of the charge is still in the sample.

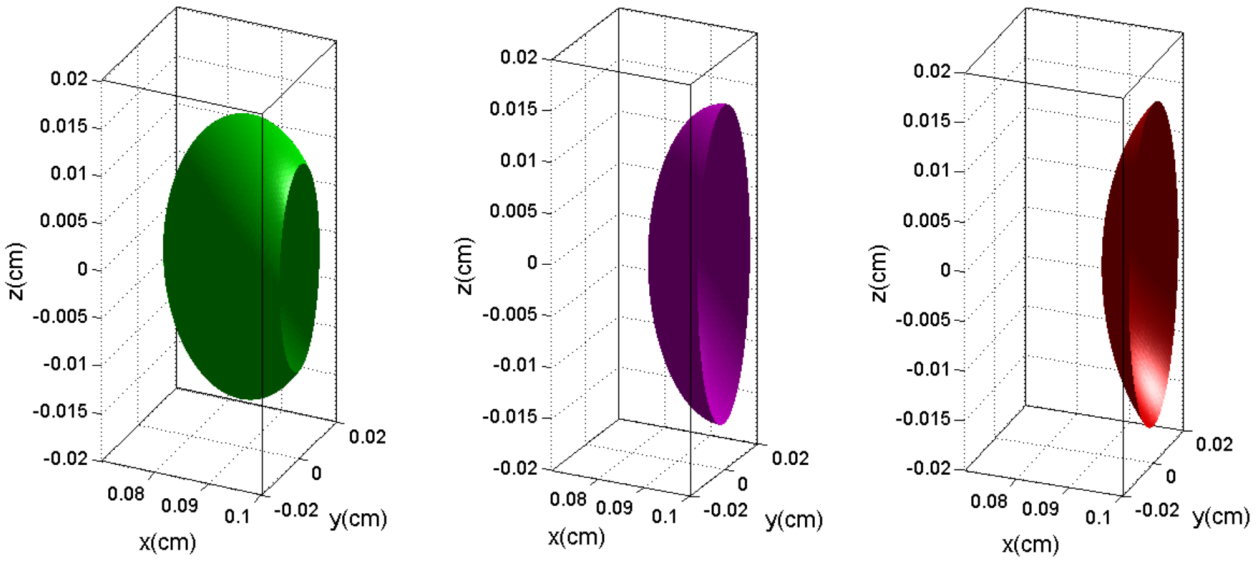

FIGURE 3.37 Three different frames of the charge density at times T_R^- , T_R , T_R^+. Charge is going through the contact ($x = L = 0.1\ cm$) (see figure 3.36)

The relation between $FWHM_X$ and $FWHM_T$ is very simple. The charge density, as it passes through the contact has a speed of drift (much greater than diffusion velocity) proportional to the electric field close to the contact. The charge portion which is within the $FWHM_X$ then employs a time equal to $FWHM_T$ to cross the contact, as a pure translational effect of the charge density.

$$(FWHM)_T = \frac{(FWHM)_X}{v(x = L)} = \frac{2\sqrt{(2\,ln(2))}\,\sigma_x(t = T_R)}{\mu E(L)} \tag{3.95}$$

For example, in presence of a uniform electric field (or for a weak linear profile) the $FWHM_T$ becomes:

$$(FWHM)_T = \sqrt{\frac{16\ln(2)\,DT_R^3}{L^2}} \tag{3.96}$$

During the data acquisition from the derivative in time of the signal we can obtain:

- the correct flight time T_R from the maximum of the derivative (the derivative in a downward inflection becomes a minimum);
- the quantity $FWHM_T$ taking the points at half height of the same Gaussian.

Finally, the diffusion coefficient *D* can be obtained by linear interpolation by applying the logarithm to both sides of the equation (3.97):

$$ln\ (FWHM_T) = 0.5\ ln\left(\frac{16ln(2)D}{L^2}\right) + 1.5\ ln\ (T_R) \tag{3.97}$$

The measurements carried out at different voltages V_i allow the acquisition of different times of flight T_{R_i} and different values of $FWHM_{T_i}$. Linear interpolation allows to determine:

- the effectiveness of the model from the slope. In fact, the model predicts (for the uniform electric field) a slope equal to 1.5;
- the coefficient diffusion from the *y*-intercept. From the D values becomes possible to calculate the carrier mobility.

From further simulations, it has been observed that the validity of this approach is good for weak slopes of a linear field. In fact, for a slope equal to 10% of the maximum slope α_{MAX} (3.82) the relative error with which the diffusion coefficient is determined is equal to the one per cent. It must be remembered that this model is valid only for full planar detector area, where the weighting field is uniform.

3.8 CHARGE COLLECTION EFFICIENCY

The Charge Collection Efficiency (CCE) measurement is an alternative technique to obtain information about transport properties. In this case the photon excitation is continuous (DC) and it is conducted with a $250\ W$ lamp that emits white light. A monochromator is used to set the radiation's wavelength.

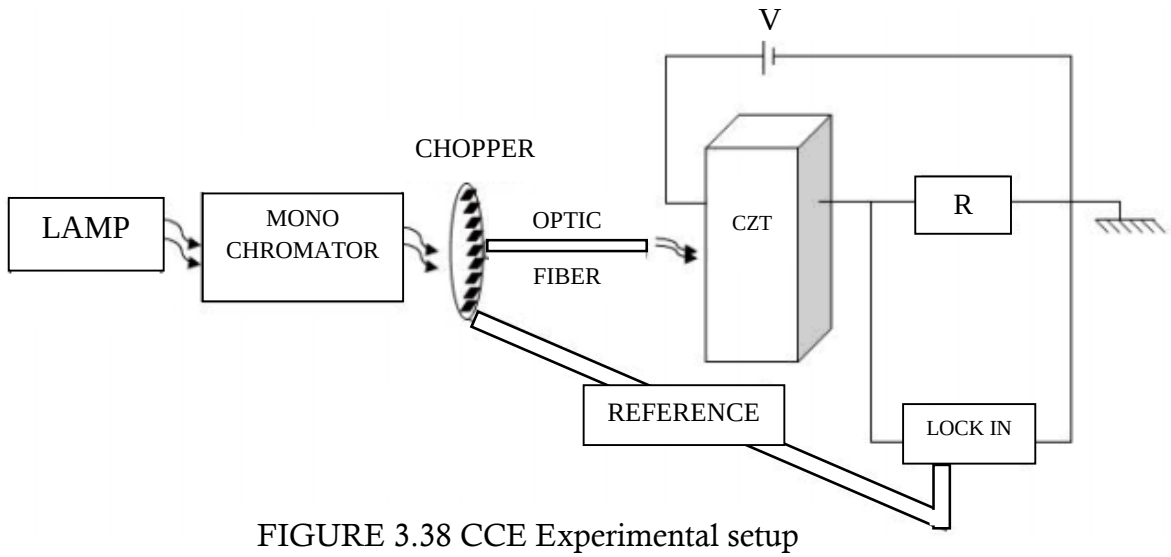

FIGURE 3.38 CCE Experimental setup

The signal is the voltage drop on a load resistance R (Figure 3.38), reading by a lock-in amplifier. The reference signal of the lock-in is provided by an optical chopper that works at $220\ Hz$. Despite the light arrives on the sample intermittently, the frequency is so low to consider the excitation as continuous compared to the time characteristic of the material response. The measurement is performed for different voltages applied to the sample.

If the applied bias is low, the carriers' time of flight results high and then the charge collection will be modest, while for high voltages the photo-generated charge will be collected almost completely. The charge collection efficiency is defined as the ratio between the collected charge at the electrodes and the photo-generated charge Q_0:

$$\eta(V) = \frac{Q_{COLL}(V)}{Q_0} = \frac{1}{Q_0}\int_0^{T_R(V)} I_V(t)\,dt \tag{3.98}$$

After a few steps, using the formula (3.20) of the current signal, the efficiency (3.98) can be written as:

$$\eta(V) = \int_0^{T_R(V)} Q_0 e^{-\frac{t}{\tau}} W\big(x(t)\big)\, \mu E_V\big(x(t)\big) dt =$$

$$= \int_0^{\min(L, x_n)} \mathrm{e}^{-\frac{\mathrm{t(x)}}{\tau}} \mu E_V(x) W(x) \frac{dx}{v(x)} = \int_0^{\min(L, x_n)} \mathrm{e}^{-\frac{\mathrm{t(x)}}{\tau}} W(x)\, dx$$

$$= \int_0^{\min(L, x_n)} W(x)\, e^{-\int_0^x \frac{dx'}{\mu\tau E(x')}} dx \qquad (3.99)$$

where x_n is the position in which the electric field could vanish within the sample.

This relation shows that:

- from the knowledge of the electric field profile the efficiency $\eta(V)$ can be obtained;
- it is impossible to separate the mobility to the lifetime for anyway electric field profile. Then in a CCE measurement it is possible to obtain only the $\mu\tau$ product.

The experimental $\eta(V)$ curves are analysed using theoretical models. Assuming uniform both electric and weighting fields, Hecht [41] and Many [42], provide two analytical curves that allow to fit the experimental curves and to find the $\mu\tau$ value.

$$\eta_{Hecht}(V) = \frac{\mu\tau V}{L^2}\left(1 - e^{-\frac{L^2}{\mu\tau V}}\right) \qquad (3.100)$$

$$\eta_{Many}(V) = \frac{\mu\tau V}{L^2}\left(1 - e^{-\frac{L^2}{\mu\tau V}}\right)\left(1 + \frac{sL}{\mu V}\right)^{-1} \qquad (3.101)$$

where the term s is the surface recombination velocity.

The collection efficiency in the case of linear field profile with a α slope becomes: (ModHecht and ModMany models [37]),with a uniform weighting field:

$$\eta_{MH} = \begin{cases} \sqrt{\frac{2V}{\alpha L^2}}\left(\frac{\mu\alpha\tau}{\mu\alpha\tau+1}\right) & |V| \le \frac{|\alpha|L^2}{2} \\ \left(\frac{V}{\alpha L^2}+\frac{1}{2}\right)\left(\frac{\mu\alpha\tau}{\mu\alpha\tau+1}\right)\left[1-\left(1-\frac{1}{\frac{V}{\alpha L^2}+\frac{1}{2}}\right)^{\frac{\mu\alpha\tau+1}{\mu\alpha\tau}}\right] & |V| > \frac{|\alpha|L^2}{2} \end{cases} \quad (3.102)$$

$$\eta_{MM} = \left(1+\frac{sL}{\mu V}\right)^{-1}\eta_{MH} \quad (3.103)$$

The figure 3.39 shows several collection charge efficiencies a functions of voltage for different values of the product $\mu\tau$ in the case of uniform field. The CCE increase at fixed voltage with increasing $\mu\tau$ product and at fixed $\mu\tau$ value the efficiency increase with increasing the voltage because charge has less probability to be trapped.

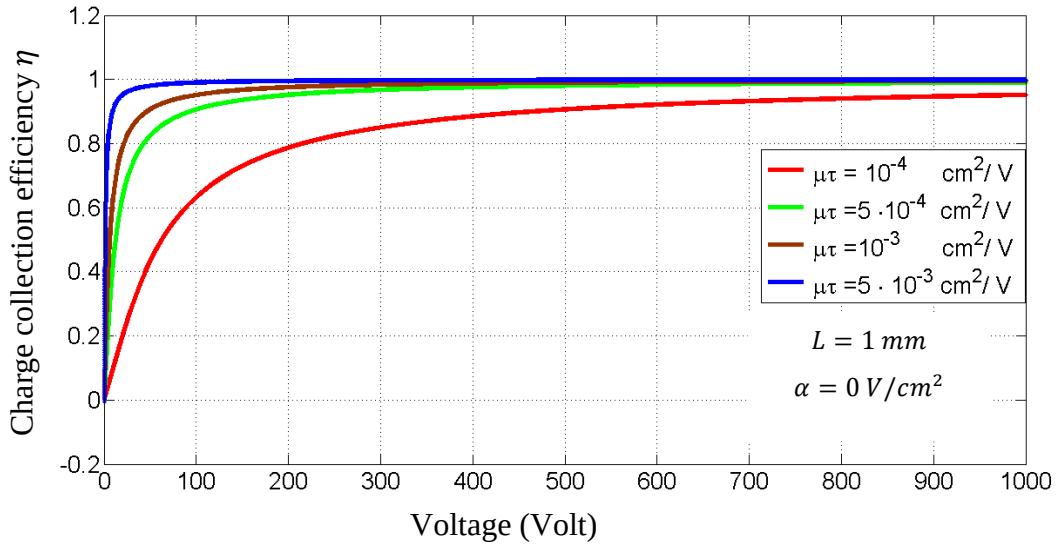

FIGURE 3.39 Charge collection efficiency in the case of a uniform electric field for different values of $\mu\tau$.

In figure 3.40 the efficiencies in the case of a linear electric field result lower than that calculated with a uniform electric field if the voltages are lower than the threshold voltage, with the same transport parameters. In the case the electric field drops to zero, no one carrier reaches the electrode and the collected charge becomes very low: i.e. the blue line in the figure above represents a low CCE due to the high electric field slope.

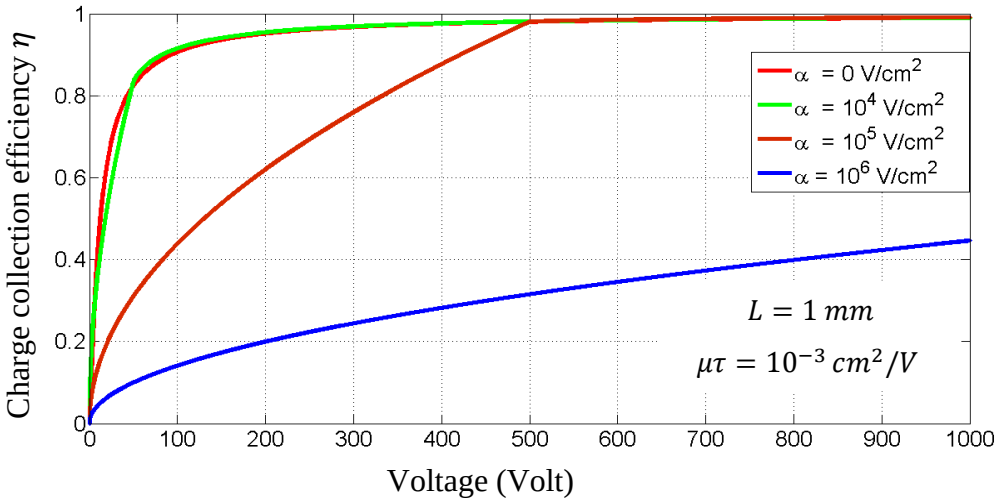

FIGURE 3.40 Charge collection efficiency in presence of linear electric field profile [37]

4 MEASUREMENTS

Measurements are carried out on solid-state detectors based on $CdTe\ and\ CdZnTe$. Analysis of experimental results by means of suitable transport models allows to obtain a carefully characterization of the charge collection processes.

The samples studied differ for:

- Type of material $(CdTe;\ CdZnTe)$
- Growth technique and provider $(REDLEN;\ IMEM)$
- Geometry of metal contacts $(FULL-AREA;\ PIXEL)$
- Thickness $(from\ 500\ \mu m\ to\ 4\ mm)$
- Metal for the electrodes $(Gold;\ Platinum)$

Measurement on full area detectors have been analysed by using the 2τ model whereas the 1τ model has been applied to pixelated detectors. The technique developed in order to obtain information about the transport properties and the electric field inside the material called Laser Excited-Transient Current Technique: (LE-TCT) [43]

4.1 EXPERIMENTAL SETUP

The laser used in the experiment is the $Polaris\ II\ Nd{:}Yag$. The wavelength of the first harmonic is $\lambda = 1064\ nm$, in the infrared region. Since the energy gap of the CZT is about 1.57 eV, corresponding to the energy of a photon with $\lambda = 800\ nm$, the 2° harmonic at $\lambda = 532\ nm$ is able to promote electrons from the valence to the conduction band. The laser pulse has a maximum energy equal to 30 mJ for pulse, a beam diameter $d = 2.75\ mm$ and a time pulse duration $\Delta t = 10 \div 20 ns$. The pulse energy and voltage of the flash-lamp (PFN) can be modified by the user to change the laser beam intensity.

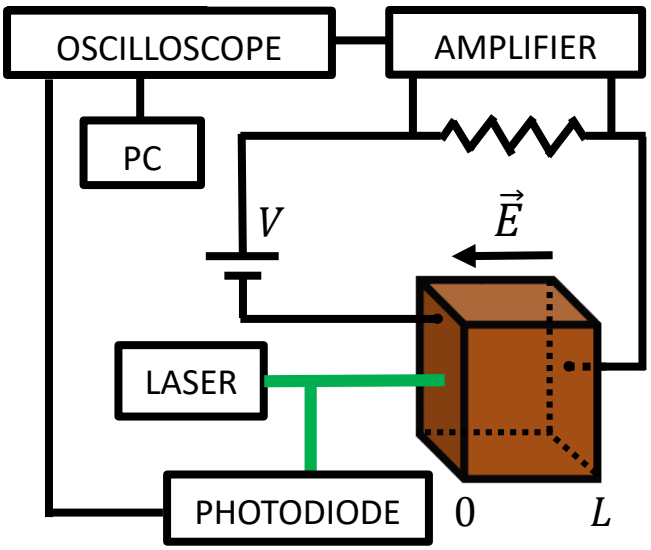

FIGURE 4.1 Transient Current Technique Experimental setup

The time profile of the laser is acquired by a photodiode and sent to the oscilloscope to be used as signal's trigger. The Current Transient signal crosses a low-pass filter (figure 4.2) composed of two operational amplifiers. The signal is then read from the oscilloscope and sent to the computer. A Matlab program acquires for each voltage approximately 10^4 signals to obtain an averaged signal to reduce the random noise by the further factor of 100.

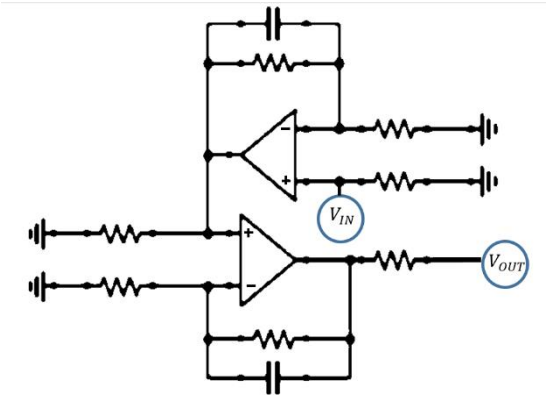

FIGURE 4.2 Amplifier's scheme

4.2 Full Area Detectors

Current transient measurements on full area detector allowed to obtain information about the transport properties of both electrons and holes, about the electric field profile, and to check the validity of the models presented in the thesis.

The measurements of full-area samples are divided into 3 groups:

1. CZT IMEM with *Au* contacts samples of different thickness
2. CZT REDLEN with *Pt* contacts (results on electrons and holes)
3. CdTe ACRORAD with *Pt* contacts

4.2.1 CZT IMEM Samples [Electrons]

Measurements have involved four samples of different thickness: [44]

$$Sample\ 1 \quad L = 270\ \mu m \qquad Sample\ 2 \quad L = 500\ \mu m$$
$$Sample\ 3 \quad L = 2.5\ mm \qquad Sample\ 4 \quad L = 4\ mm$$

Both measurements by Transient Current Technique (TCT) and Collected Charge Efficiency (CCE) are carried out to verify the agreement between results from two different experimental approaches. TCT measurements allow to obtain separately mobility and lifetime of the carriers and the profile of electric field; the measure of CCE leads to obtain only the $\mu\tau$ product, assuming a starting electric field profile (uniform or linear).

SAMPLE 1 CZT IMEM $L = 270\ \mu m$ [ELECTRONS]

In Figure 4.3 the transients show the typical initial spike due to the charge photo-generation with the laser, then a drift zone with the time decay due to trapping and the final part related to the arrival of electrons at the collecting electrode.

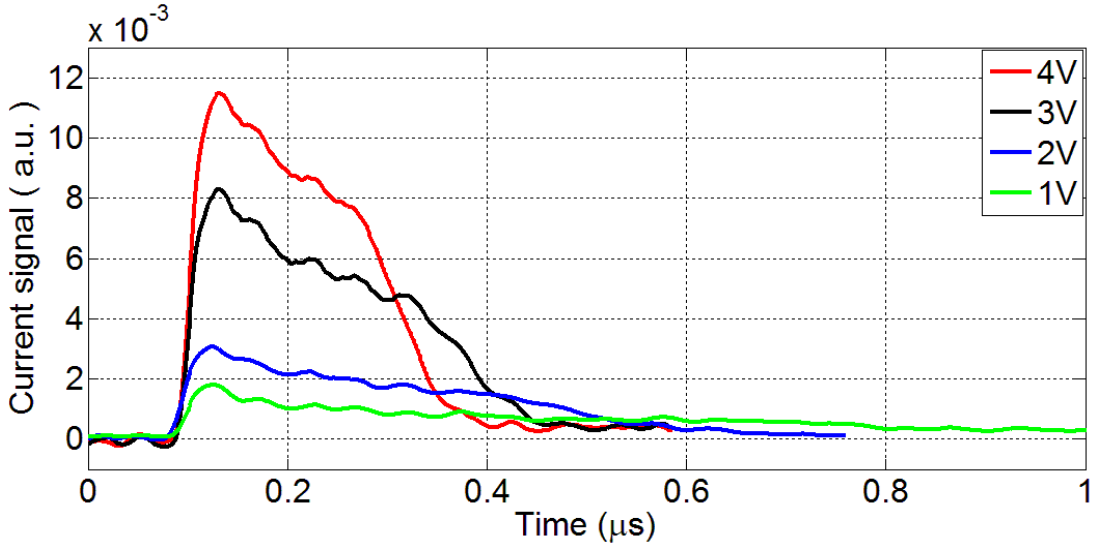

FIGURE 4.3 Electrons' Current signal at different voltages in CZT IMEM sample with 270 μm thickness

Starting from the flight times' acquisition for each transient it's possible, using the 2τ model, to find the lifetime, the mobility and, as shown in figure 4.4, the spatial electric field profiles:

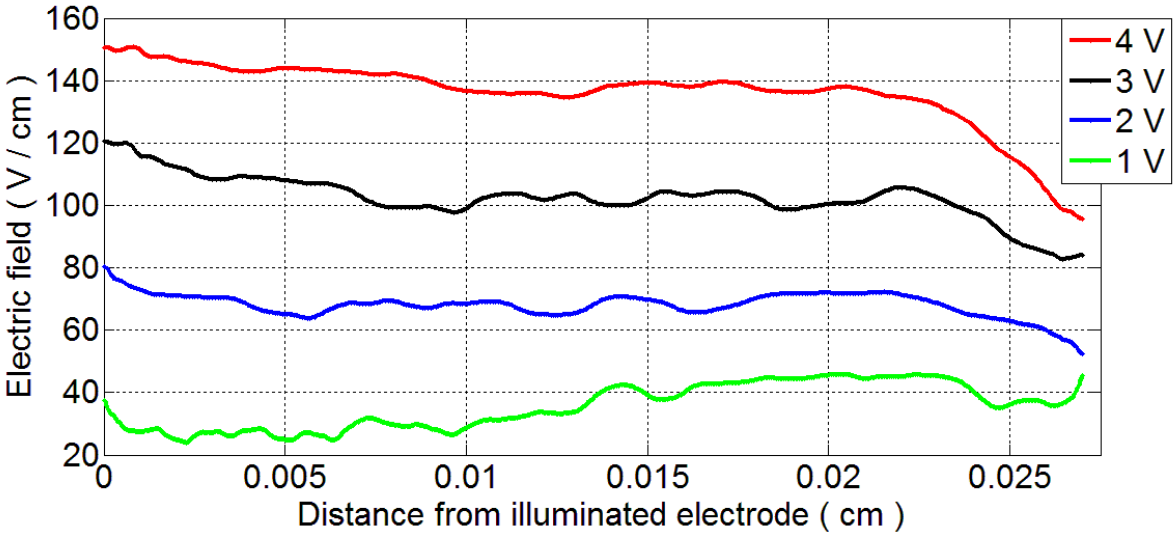

FIGURE 4.4 Electric fields at different voltages in CZT IMEM sample with 270 μm thickness

The analysis of a thin sample entails the use of very low voltages to be able to obtain times of flight at least comparable to the lifetime of carriers. Anyway the reconstructed electric fields show a uniform profile for all voltages.

The mobility of electrons and lifetime result:

$$\mu = (1040 \pm 40)\frac{cm^2}{Vs} \qquad \tau = (410 \pm 30)\, ns$$

In figure 4.5 the collected charge measured as a function of the applied voltage:

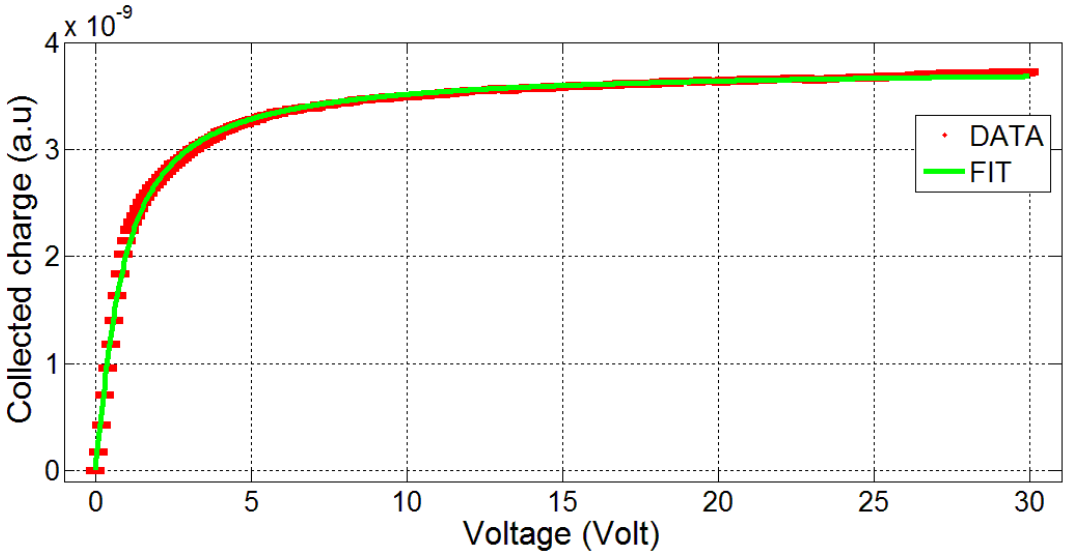

FIGURE 4.5 Collected charge as a function of applied voltages in CZT IMEM sample with 270 μm thickness

The "best-fit" curve that describe better the experimental data is the Hecht curve, that assumes a uniform profile, just like the one obtained with the transient measurements.

The value of the $\mu\tau$ product obtained with TCT and CCE technique are in good agreement:

TECHNIQUE	$\boldsymbol{\mu\tau}$ $\boldsymbol{(cm^2/V)}$	**Electric Field profile**
TCT	$(4.3 \pm 0.4)\ 10^{-4}$	Uniform (Experimental result)
CCE	$(5.1 \pm 0.6)\ 10^{-4}$	Uniform (Hecht model)

Table 4.1 Values of $\mu\tau$ product and electric field profile obtained with TCT and CCE techniques in CZT IMEM sample with 270 μm thickness.

SAMPLE 2 CZT IMEM $L = 500\ \mu m$ [ELECTRONS]

In figure 4.6 current signals show time uniform profiles during the drift region, probably due to the fact that the electric field probed in time increases as the number of carriers decreases.

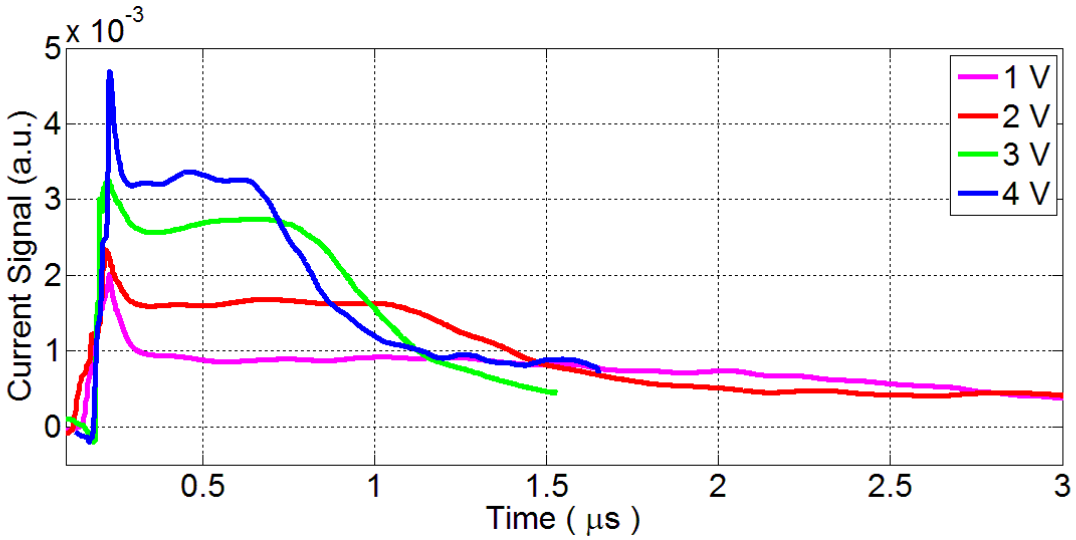

FIGURE 4.6 Electrons' signals at different voltages in CZT IMEM sample with 500 μm thickness

In figure 4.7 the electric fields in fact show an increasing linear profile.

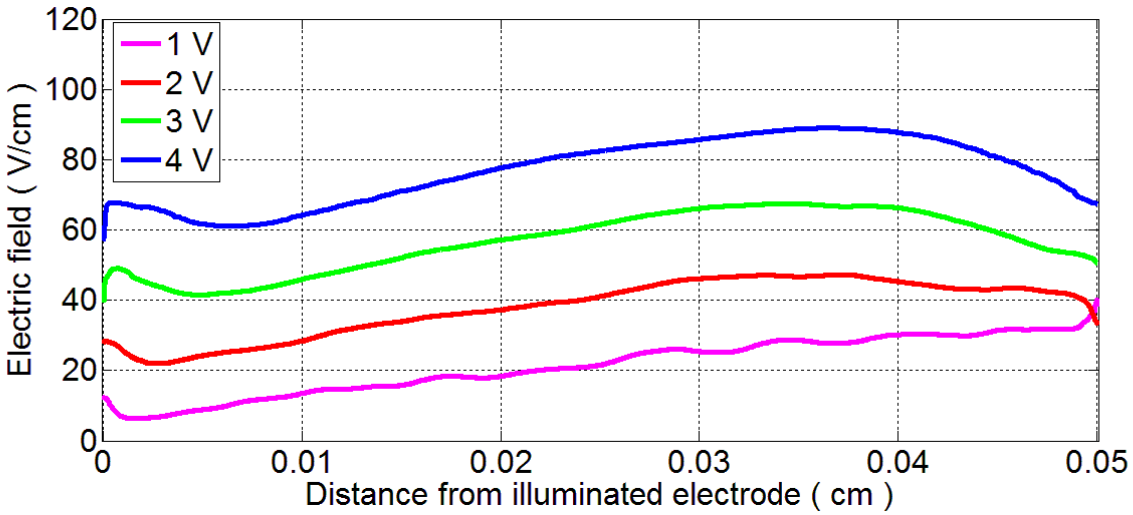

FIGURE 4.7 Spatial Electric field profiles at different voltages in CZT IMEM sample with 500 μm thickness

The mean slope of the electric field can also be calculated as:

$$\alpha = \Delta E / \Delta x$$

For example the field reconstructed from the transient at 1 volt (figure 4.7) show a variation of about 30 V/cm in the entire thickness $L = 0.05\ cm$, then the electric field slope results $\alpha = 600\ V/cm^2$.

The mobility and the lifetime calculated resulting from the application of the 2τ model:

$$\mu = (1170 \pm 60)\ \frac{cm^2}{V\ s} \qquad \tau = (510 \pm 40)\ ns$$

In figure 4.8 the "best-fit" curve that describe better the experimental data is the ModHecht curve, that assumes a linear (increasing or decreasing profile), as obtained from the transient measurements.

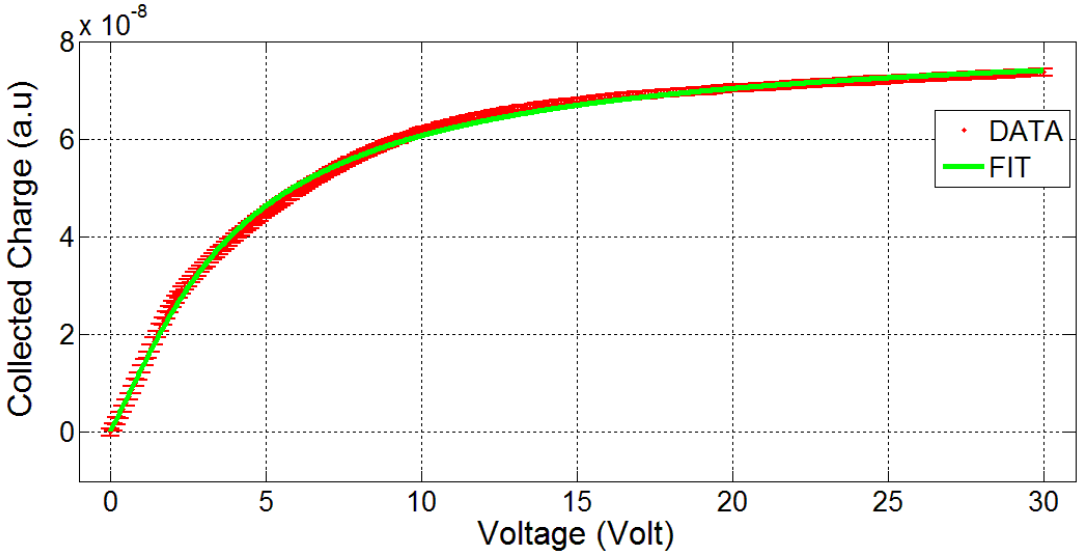

FIGURE 4.8 Collected charge as a function of applied voltages in CZT IMEM sample with 500 μm thickness

The value of the $\mu\tau$ product and the slope obtained with TCT and CCE technique are in good agreement:

TECHNIQUE	$\boldsymbol{\mu\tau\ (cm^2/V)}$	**Electric Field profile** $\boldsymbol{slope\ \alpha\left(\frac{V}{cm^2}\right)}$
TCT	$(6.0 \pm 0.5)\ 10^{-4}$	Increasing linear 600 ± 50
CCE	$(6.5 \pm 0.5)\ 10^{-4}$	Increasing linear (ModHecht) 700 ± 100

Table 4.2 Values of $\mu\tau$ product and electric field profile obtained with TCT and CCE techniques in CZT IMEM sample with 500 μm thickness.

SAMPLE 3 CZT IMEM $L = 2.5\,mm$ [ELECTRONS]

The current signals in sample CZT with 2.5 mm (figure 4.9) show decay profiles probably due to the electrons' trapping.

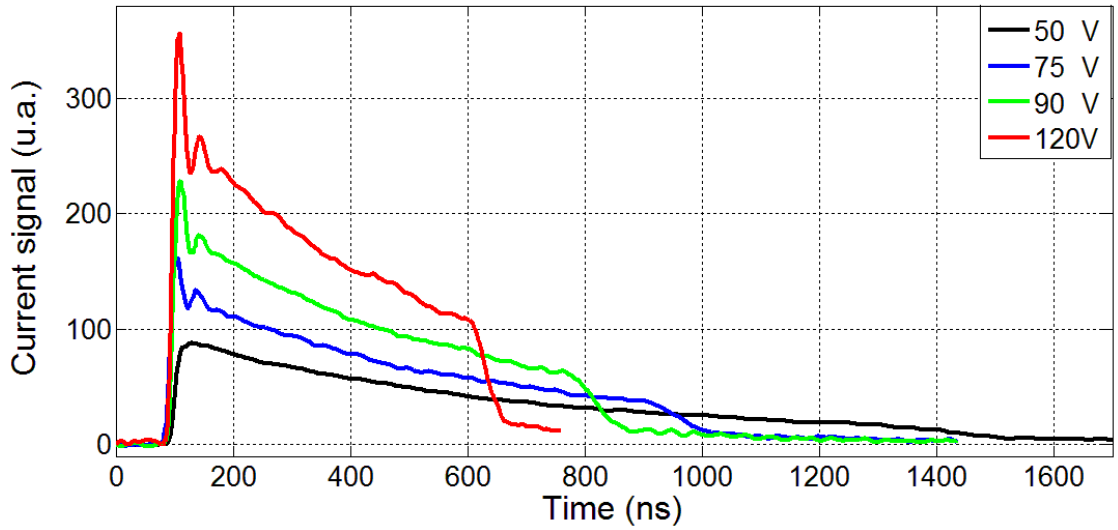

FIGURE 4.9 Electrons' Current signals at different voltages in CZT IMEM sample with 2.5 *mm* thickness

The application of the 2τ model show in figure 4.10 a reconstructed electric field with uniform profile in almost the whole sample.

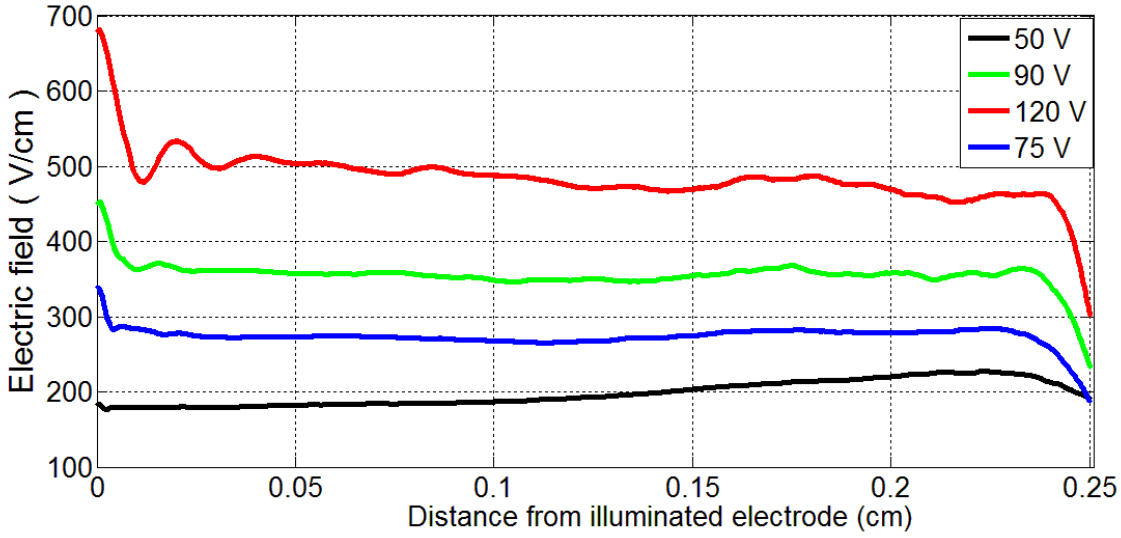

FIGURE 4.10 Electric fields at different voltages in CZT IMEM sample with 2.5 *mm* thickness

In this case carriers, probing the same electric field during the flight, move into the sample with a constant velocity proportional to the applied voltage and the current signal decay is only due to the trapping term.

The transport parameters calculated from the 2τ model result:

$$\mu = (1020 \pm 40)\ \frac{cm^2}{V\ s} \qquad \tau = (980 \pm 30)\ ns$$

The CCE technique allow to compare the $\mu\tau$ product with that measured with TCT technique. From the analysis of the collected charge as a function of the applied voltage (figure 4.11) it turns out that the curve that better describes better the experimental data is the Hecht curve, under the assumption of a uniform electric field profile.

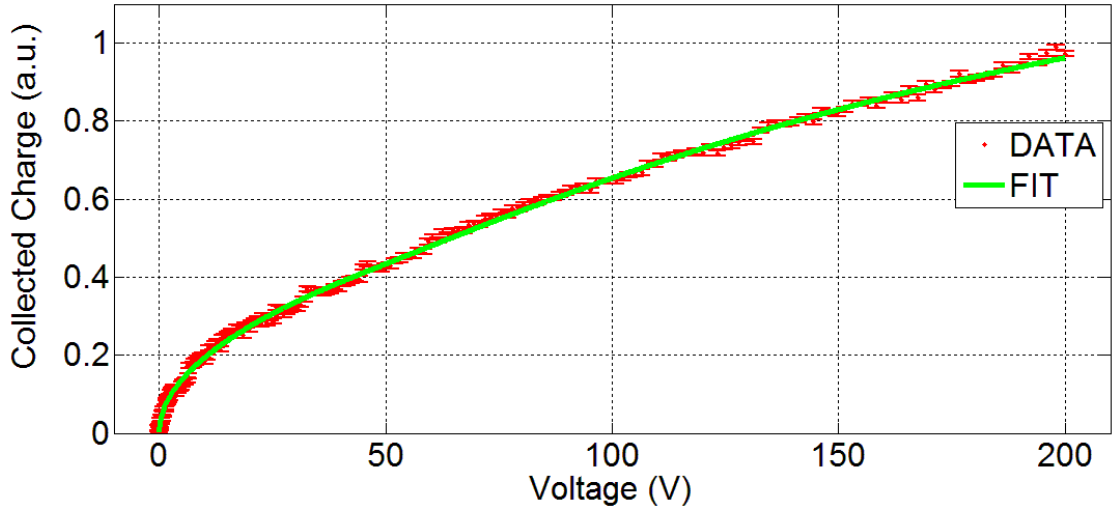

FIGURE 4.11 Collected charge as a function of applied voltages in CZT IMEM sample with 2.5 *mm* thickness

The value of the $\mu\tau$ product is shown on the table 4.3:

TECHNIQUE	$\boldsymbol{\mu\tau}$ $\boldsymbol{(cm^2/V)}$	**Electric Field profile**
TCT	$(1.0 \pm 0.1)\ 10^{-3}$	Uniform
CCE	$(1.1 \pm 0.3)\ 10^{-3}$	Uniform (Hecht)

Table 4.3 Values of $\mu\tau$ product and electric field profile obtained with TCT and CCE techniques in CZT IMEM sample with 2.5 *mm* thickness.

SAMPLE 4 CZT IMEM $L = 4\,mm$ [ELECTRONS]

The figure 4.12 shows the transient current profiles measured for voltages between 180 V and 320 V.

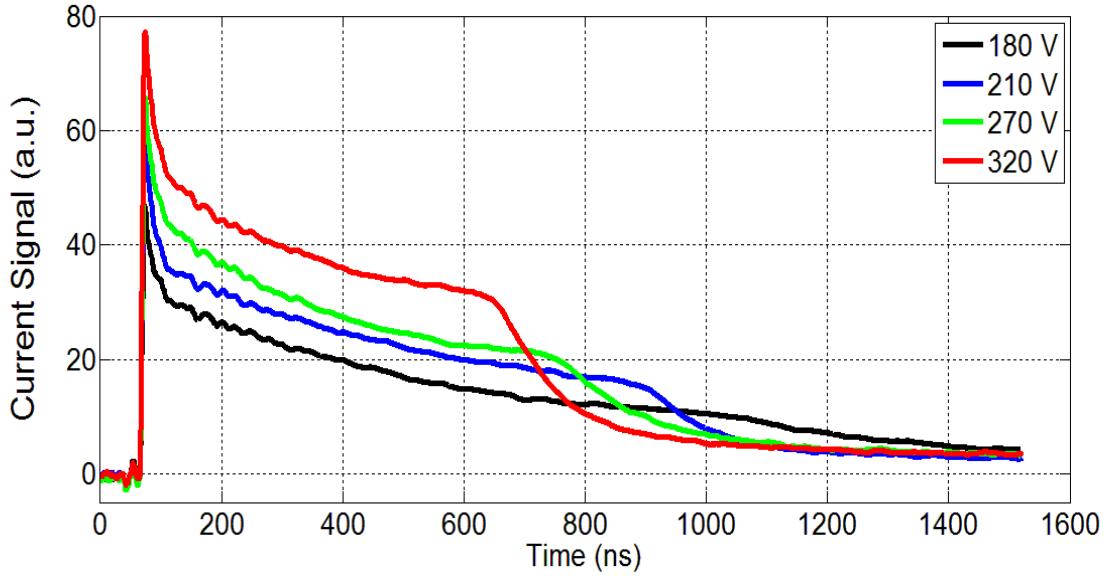

FIGURE 4.12 Electrons' Current signals at different voltages in CZT IMEM sample with 4 mm thickness

The electric fields profiles (figure 4.13) are reconstructed applying the 2τ model. The electric fields show a uniform profile in almost the whole sample, except in the proximity of the illuminate sample until depth of about 200 μm, where the electric field decreases.

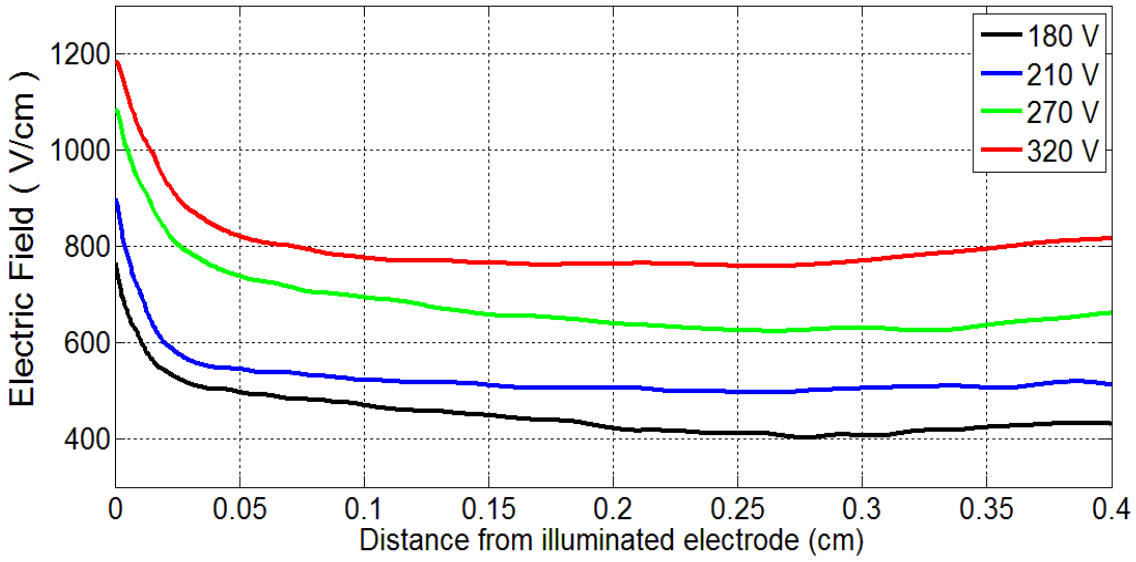

FIGURE 4.13 Electric fields at different voltages in CZT IMEM sample with 4 mm thickness

The transport parameters for electrons result:

$$\mu = (1050 \pm 30)\frac{cm^2}{Vs} \qquad \tau = (960 \pm 40)\ ns$$

Finally, the results can be compared to those obtained with the measurement of the collected charge efficiency. The best interpolating curve result the Hecht curve, assuming a uniform electric field profile.

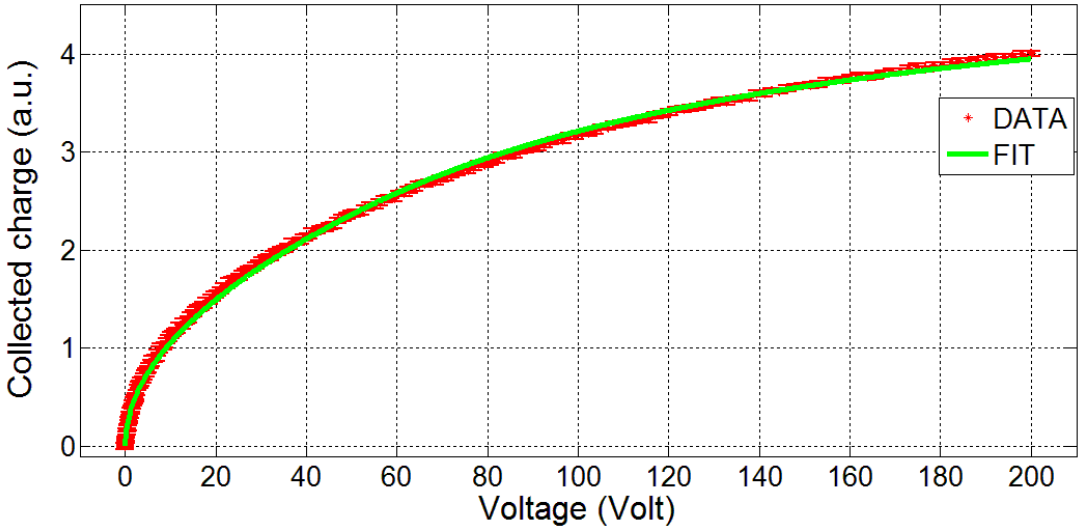

FIGURE 4.14 Collected charge as a function of applied voltages in CZT IMEM sample with 4 *mm* thickness

The $\mu\tau$ product is in good agreement with that calculated with TCT technique.

TECHNIQUE	$\boldsymbol{\mu\tau}$ $(\boldsymbol{cm^2/V})$	**Electric Field profile**
TCT	$(1.0 \pm 0.1)\ 10^{-3}$	Uniform
CCE	$(0.9 \pm 0.1)\ 10^{-3}$	Uniform (Hecht)

Table 4.4 Values of $\mu\tau$ product and electric field profile obtained with TCT and CCE techniques in CZT IMEM sample with 4 *mm* thickness.

4.2.2 CZT REDLEN [ELECTRONS AND HOLES]

1. ELECTRONS

In figure 4.15 the current signals increase in time very quickly, probably due to the fact that the electric field probed in time is predominant compared to the trapping decay. An exponential increase of the term $(E(x(t))$ indicates the presence of a linear increasing electric field.

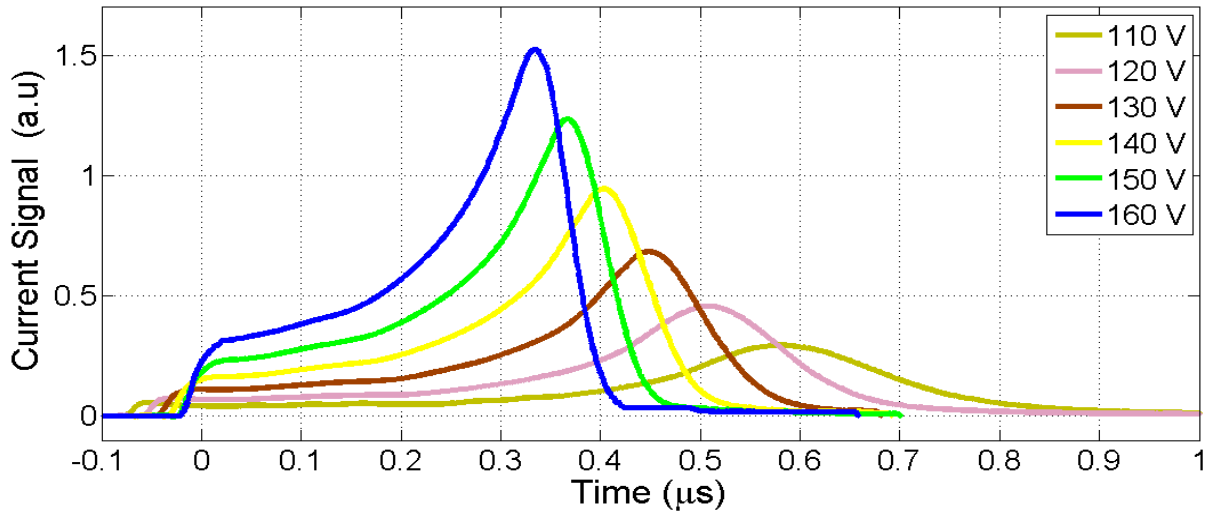

FIGURE 4.15 Electrons' current signals at different voltages in CZT REDLEN sample with 2 *mm* thickness

In figure 4.16 the electric fields show an increasing spatial profile, just as predicted from the current transients.

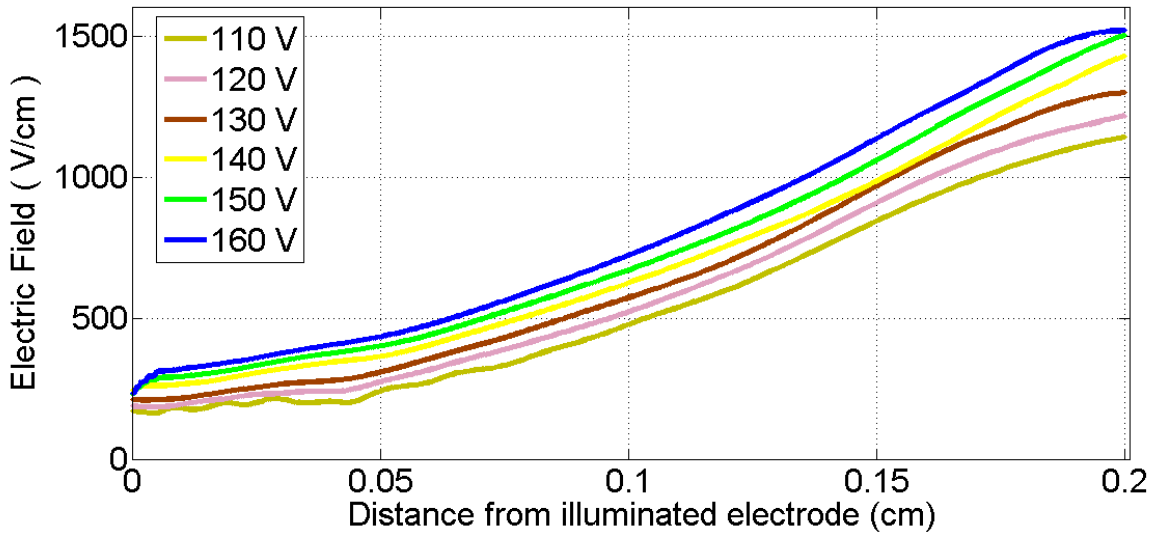

FIGURE 4.16 Electric fields at different voltages in CZT REDLEN sample with 2 *mm* thickness obtained from electrons' measurements

2. HOLES

The application of a voltage of opposite sign leads to the measure of the hole current transients. Actually the holes' signal is much lower that the electronic current due to the lower mobility of the holes. At the same voltage, the signal will thus be about 30 times less and, at the same time, 30 times more extended in time compared to the electrons' signal.

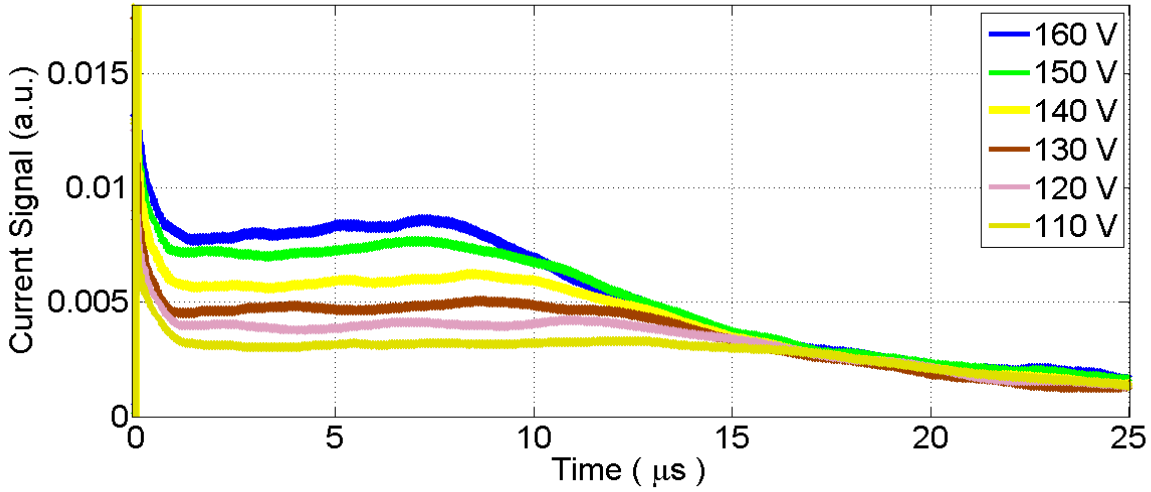

FIGURE 4.17 Holes' current signals at different voltages in CZT REDLEN sample with 2 *mm* thickness

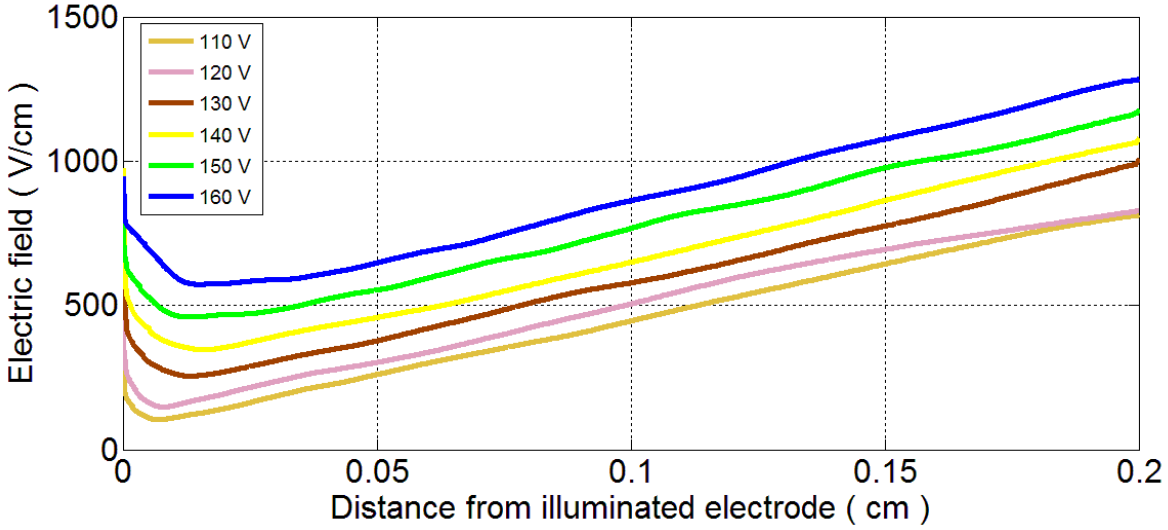

FIGURE 4.18 Electric fields at different voltages in CZT REDLEN sample with 2 *mm* thickness obtained from holes' measurements

The intermediate region of transients, in which holes drift, show a uniform profile in time. (figure 4.17). Times of flight result much greater than the electronic ones at the same voltage. For example, at 160 Volts the electronic and the hole transients show times of flight approximately equal to 0.35 and 9 microseconds, respectively, indicating a ratio between the mobility of electrons and holes equal to about 25. The mobility and the lifetime of electrons and holes are:

$$\mu_{EL} = (1150 \pm 50)\ \frac{cm^2}{Vs} \qquad \tau_{EL} = (1.1 \pm 0.1)\ \mu s$$

$$\mu_{HO} = (47 \pm 3)\ \frac{cm^2}{Vs} \qquad \tau_{HO} = (5.8 \pm 0.4)\ \mu s$$

The ratio $\mu_{EL}\ /\mu_{HO}$ results close to 25, as calculated before by means of the times of flight. The lifetime of holes has been calculated with the minimization procedure of the 2τ model. The Figure 4.19 shows two minimum of the two variances (5.5 μs *and* 6.1 μs) used for the determination of the lifetime of the holes. (Figure 3.21)

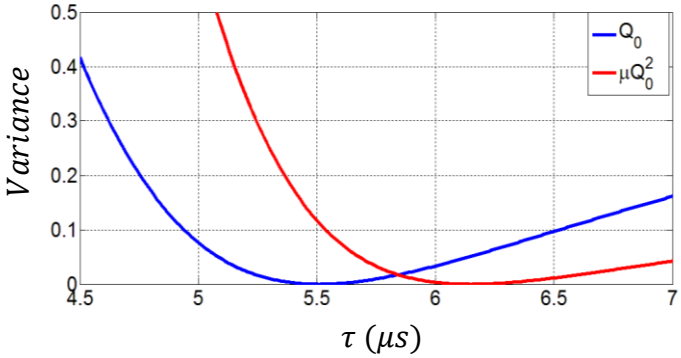

FIGURE 4.19 The minimum of the variances indicate the lifetime of the holes.

Starting from the times of flight acquisition is becomes possible to reconstruct the electric field profiles. The measurements of current transients for holes, performed at the same voltages used for electrons, allow a direct comparison between the reconstructed electric fields. They should be theoretically equal to each other.

The electric fields obtained for electrons and holes show an increasing linear profile with different mean slopes:

$$\alpha_{EL} \sim 5500\ V/cm^2 \qquad \alpha_{HO} \sim 4000\ V/cm^2$$

The difference between slopes can be probably due to the different trapping of the electrons and holes: also the free charge, once trapped, can change the electric field profile. The holes' lifetime results 5.3 times greater than the electrons' lifetime, then the trapping of the holes results low, just like the bending of the electric field.

4.2.3 CdTe Acrorad [Electrons]

In figure 4.20 the signals obtained with the TCT technique in CdTe sample show a decreasing profile different from the typical exponential decay (trapping), due to the concave and decreasing shape of the electric field (figure 4.21)

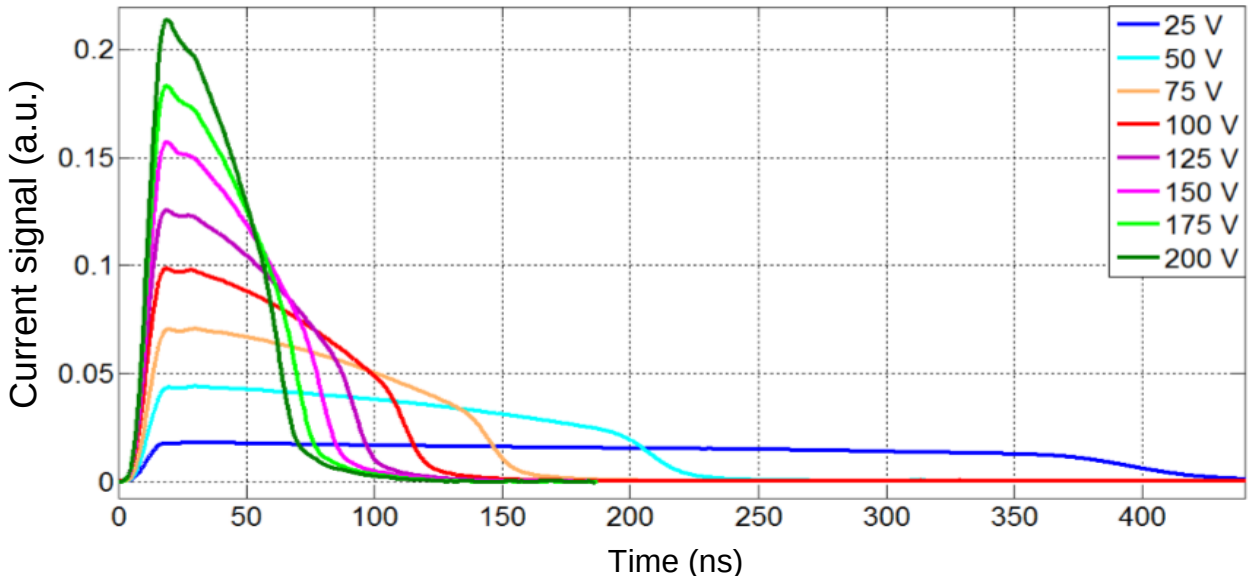

FIGURE 4.20 Electrons' signals in CdTe sample with *Pt* contacts and 1 *mm* thickness

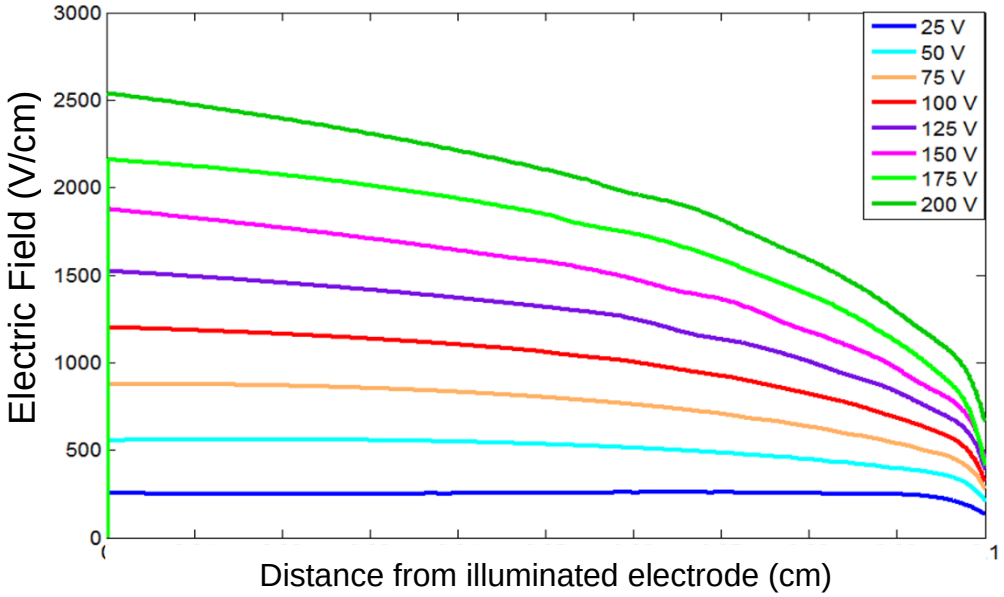

FIGURE 4.21 Electric field profiles in CdTe sample with *Pt* contacts and 1*mm* thickness

The application of the 2τ model allow also to obtain the electrons' transport parameters:

$$\mu_{EL} = (1050 \pm 20)\frac{cm^2}{Vs} \qquad \tau_{EL} = (950 \pm 30)\, ns$$

APPLICATION OF THE DIFFUSION MODEL

In the section 3.7.4 it was demonstrated how, starting from the current signals, it becomes possible to obtain information about the diffusion phenomenon. The procedure starts from the study of the time derivative of transients.

The time derivative (figure 4.22) in fact represent a "temporal photo" of the charge density. The final part of each transient shows a Gaussian profile, the width of which indicates the time needed to charge density, which is enlarged during the flight, to cross the collecting electrode. This crossing time is simply the ratio between the spatial spread of the charge density at the time of flight and the velocity of carriers.

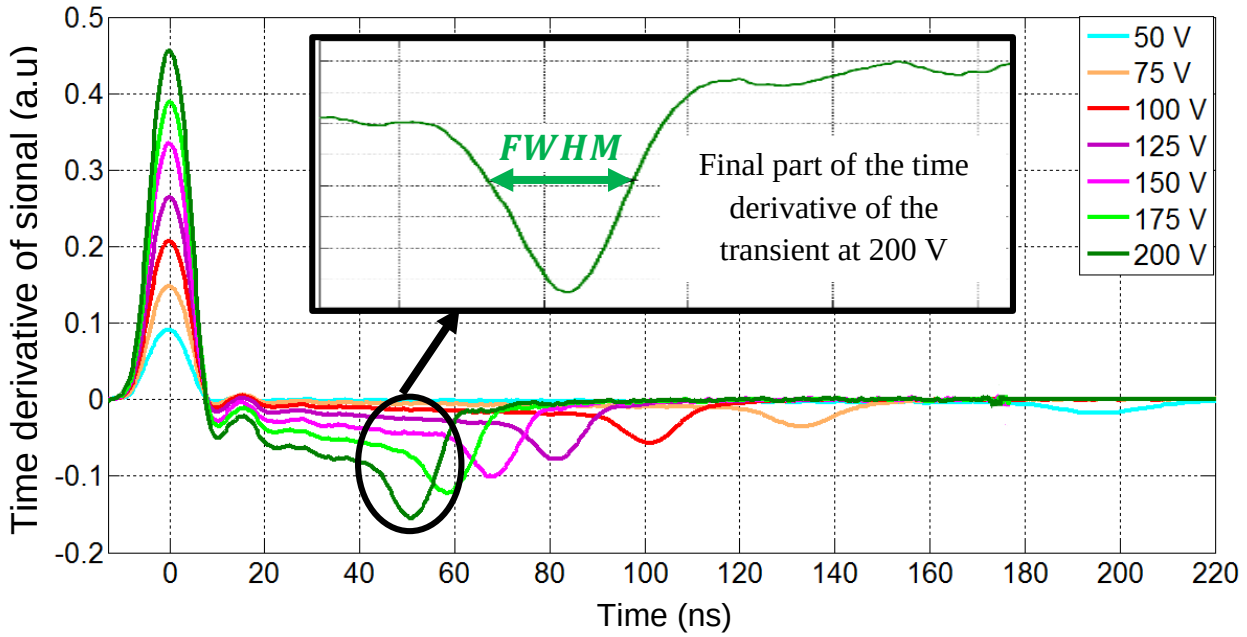

FIGURE 4.22 Time derivative of the transients (shown in figure 4.20) in CdTe sample

The temporal spread of the final part of the transient increases with the decrease of the applied voltage, because the diffusion can work for a longer time (high flight times for low voltages).

Looking at the final parts of the transients, from the highest to the lowest voltage, the spread of the carriers at different time instants can be drawn. The initial part of the curves shows that the temporal width of the time derivative is the same for all voltages and it represents the time duration of the laser pulse, equal to about 15 ns.

The Full Widths at Half Maximum of the Gaussian in the final part of the time derivatives are related to the flight times of the same transient: the crossing time of the charge density through the collecting electrode depends on the flight time T_R:

$$ln(FWHM) = 0.5\ ln\left(\frac{16ln(2)D}{L^2}\right) + 1.5\ ln\ (T_R)$$

The graph of the logarithm of the FWHMs as a function of the logarithm of times of flight and the relative linear interpolation allows to:

- Verify the validity of the model if a slope near to the theoretical value of 1.5 results from the interpolation
- Obtain the diffusion coefficient D from the y-intercept
- Obtain the mobility of the carriers, in a different way, by using the relation among the diffusion coefficient, the mobility and the thermic voltage ($26\ mV$ at RT) from the Smoluchwoski-Einstein relation $D = \mu\ V_{th}$

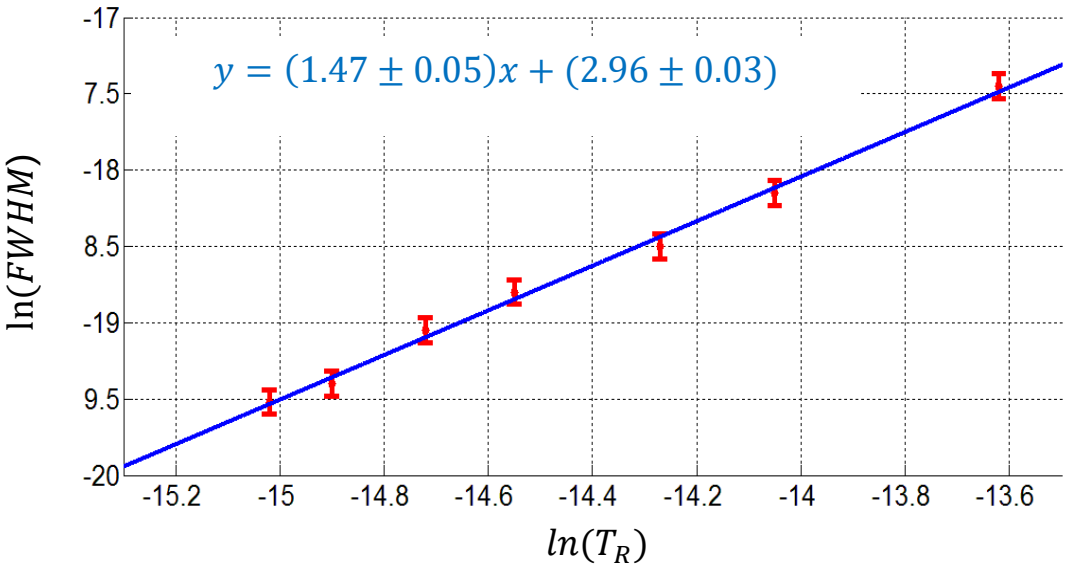

FIGURE 4.23 Full Width Half Maximum of the final part of the time derivatives of transients as a function of the flight times. The linear interpolation of the logarithm of the two quantities allow to obtain the value of the diffusion coefficient D

The slope obtained from the linear interpolation (figure 4.23) agrees with the ideal value equal to 1.5. The *y*-intercept value allows to obtain the diffusion coefficient *D* and the mobility:

$$D_{EL} = (27.1 \pm 0.3)\frac{cm^2}{s} \qquad \mu_{EL} = \frac{D}{V_{th}} = (1040 \pm 10)\frac{cm^2}{Vs}$$

The values of the electrons' mobility, calculated in two different ways, result in good agreement within the experimental error.

THE CHOICE OF THE CORRECT FLIGHT TIME

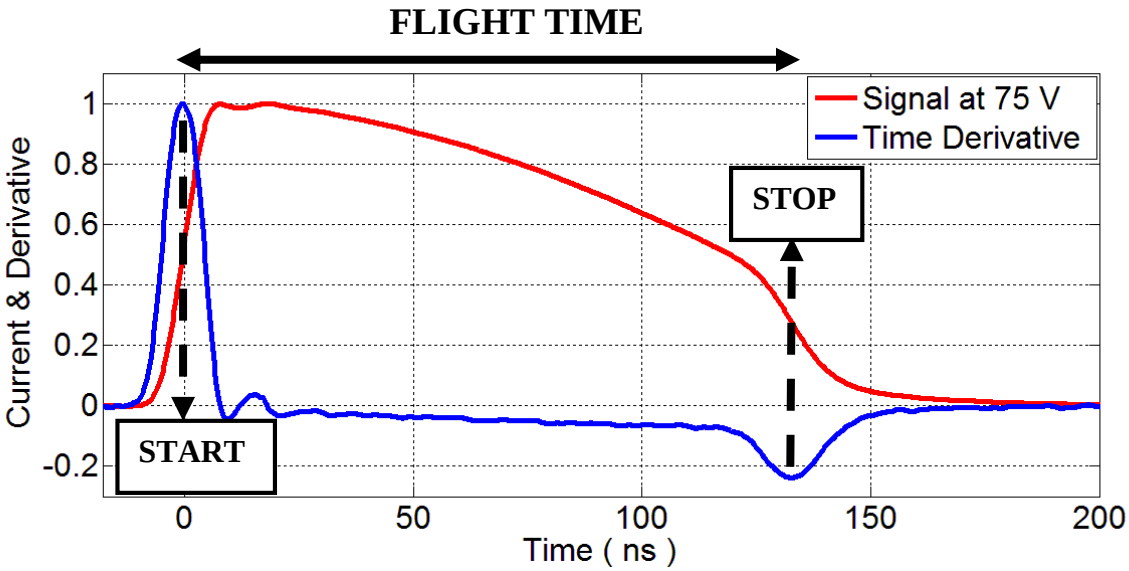

FIGURE 4.24 Transient at 75 V and its Time derivative (CdTe sample)

The time derivative of the current signals in important not only for the study of the diffusion. The correct time of flight anyway does not depend on the diffusion coefficient because it depends only on the law of motion and then on the electric field profile. The barycentre is the only point in charge cloud not affected by the diffusion.

The information about the departure of the barycenter from the illuminated electrode (START) and about its arrival at the collecting electrode (STOP) is found starting from the analysis of the time derivative of the transient current (figure 4.24). The initial and the final inflection points of the transient curves become a local maximum and minimum, respectively, in the time derivative and indicates the START and the STOP of the flight of the barycentre. Then the time of flight is the difference between the STOP and the START instants. This procedure was performed for all transients examined in the thesis.

4.3 PIXELATED DETECTORS

The samples analysed in this section have a non-symmetrical geometry of the contacts. While the illuminated electrode is full-area ($S\ x\ S$), the collection electrode, named pixel in the following, has a smaller and variable size ($P\ x\ P$) for different samples. The samples can differ for the thickness L, equal to the distance covered by carriers, generated near the illuminated electrode, to reach the pixel.

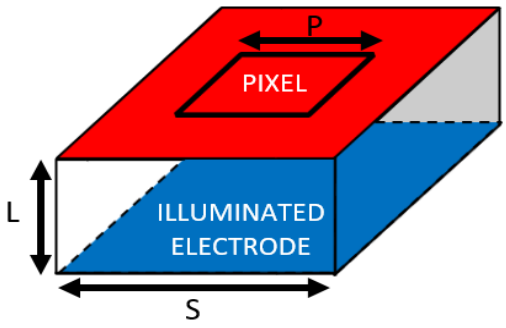

FIGURE 4.25
Geometry of a Pixelated detector

The pixelated samples studied are divided into 3 groups:

a. three CZT REDLEN samples, with *Au* contacts, with the same thickness and the same size of the illuminated contact, but with different pixel's size
b. CZT REDLEN sample with *Pt* contacts in which it has been possible to observe the holes' current
c. CZT IMEM sample with *Au* contacts

4.3.1 REDLEN CZT: DIFFERENT PIXEL SIZE [ELECTRONS]

The three REDLEN samples are characterized by:

- *Au* contacts
- Thickness $L = 2\ mm$
- Size of illuminated electrode $S = 5.4\ mm$
- Different pixel's size $P = (4\ ;\ 1.5\ ;\ 0.5)\ mm$

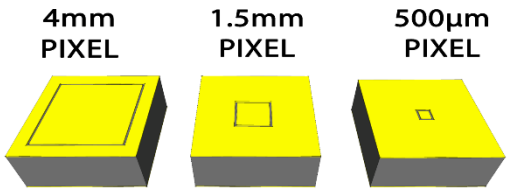

FIGURE 4.26 Different pixel's size for the three REDLEN samples

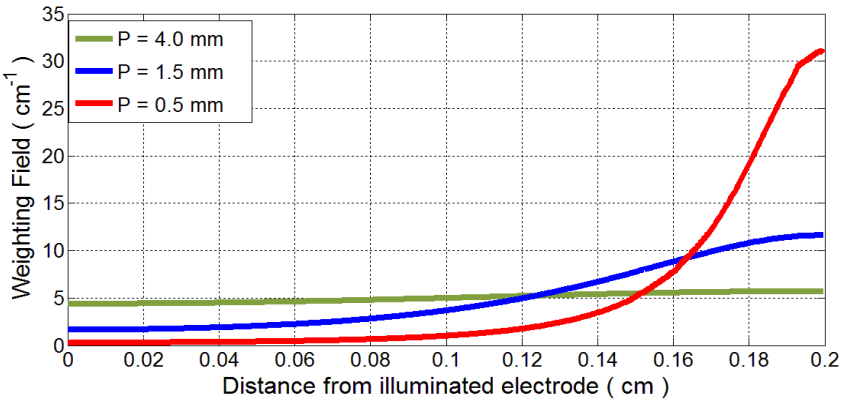

FIGURE 4.27 Spatial Weighting field profiles along Electric Field direction for samples with different pixel's size

WEIGHTING POTENTIAL AND WEIGHTING FIELD

The relative size of the pixel changes drastically the form of the lines of the weighting potential and the magnitude and the direction of the weighing field. In figure 5.3 this effect can be easily observed: if the pixel's size decreases, the lines of the weighting potential are more concentrated at the pixel, and in this region the weighting field increases considerably.

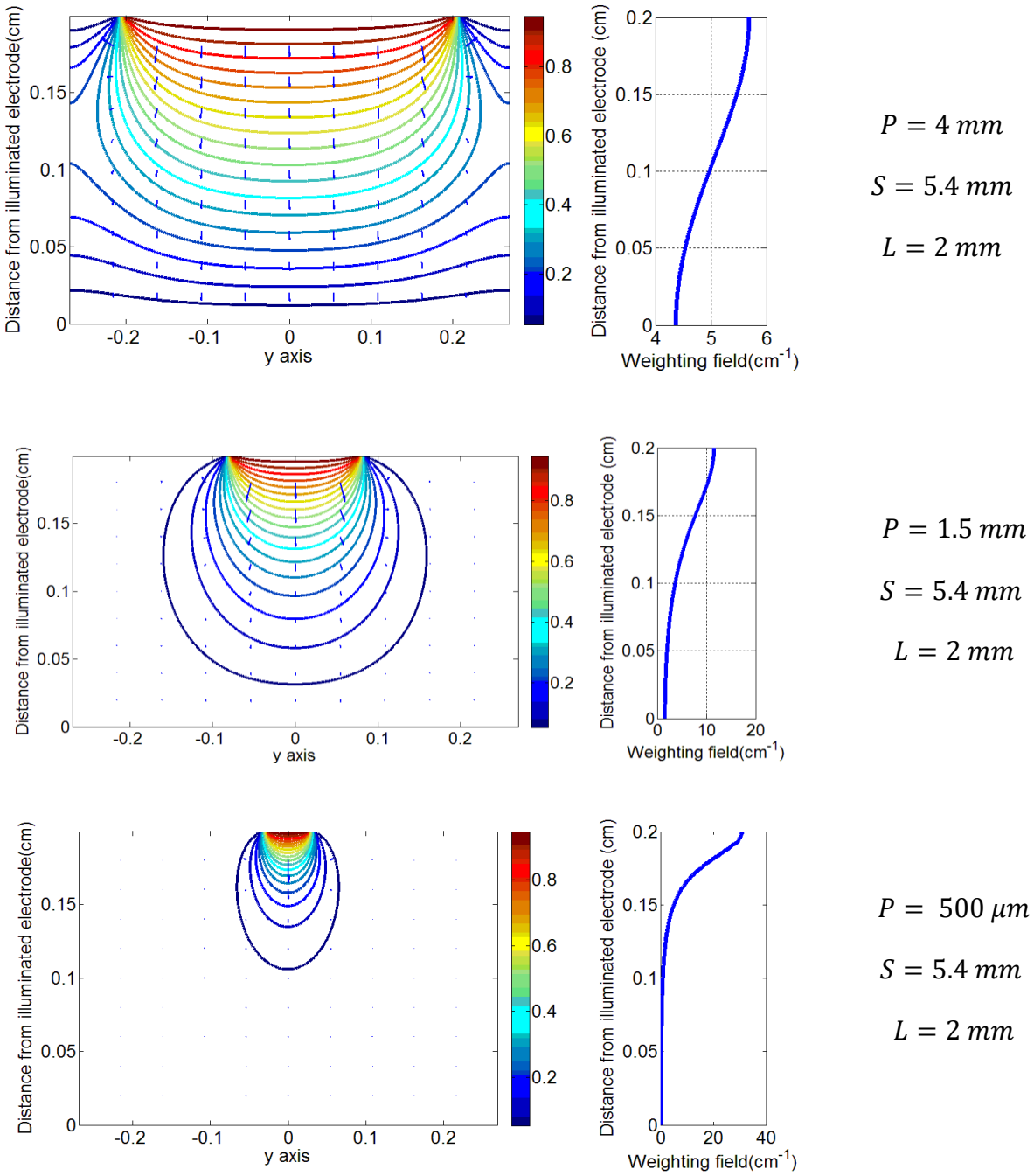

FIGURE 4.28 Weighting potential lines and weighting field for the three samples of different pixel size

CURRENT SIGNALS OF REDLEN CZT SAMPLES

The current measurements on the CZT REDLEN samples have allowed to obtain the value of mobility and lifetimes of electrons. The electric fields were finally reconstructed starting from the same current signal. The applied voltages start at 10 Volts to 100 Volts with a step of 10 Volts.

These sample belong to the same ingot but they differ for the pixel's size. It is reasonable to expect that the carriers' mobility, the lifetime and the electric field profile do not change dramatically with the geometry of the contacts. On the contrary, the time profile of the current can be different because of the "pixel effect" even if they should present the same time of flight at fixed voltage: the time of flight depends on the mobility and the spatial electric field profile, while it does not depend on the weighting field spatial profile.

1. CZT REDLEN with pixel's size $P = 4\ mm$ [ELECTRONS]

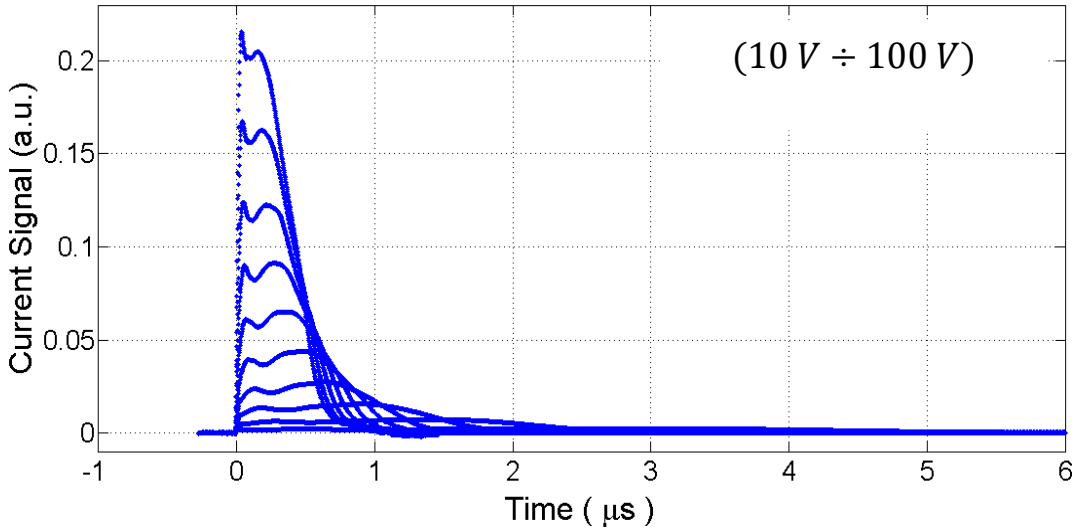

FIGURE 4.29 Current signals for different voltages ($from\ 10\ V\ to\ 100\ V\ with\ 10\ V$ step) in CZT REDLEN sample with thickness $L = 2\ mm$ and pixel's size $P = 4\ mm$

The current signals have the typical form of a transient signal:

- An initial spike (at $t = 0$) due the charge generation with the laser beam;
- A drift region due to the flight of carriers;
- A signal's fall due to the pixel's crossing by the electrons;
- At high voltages the carrier velocity increase and then the current, while the time of flight decrease.

After the acquisition of the signals, the carrier lifetime can be calculated by the minimization procedure (figure 4.30) described in section 3.6.3. The minimum of the variance of the calculated Q_{0i} represents the lifetime of the carriers. In this case the electrons' lifetime is about $\tau = 1.4\ \mu s$.

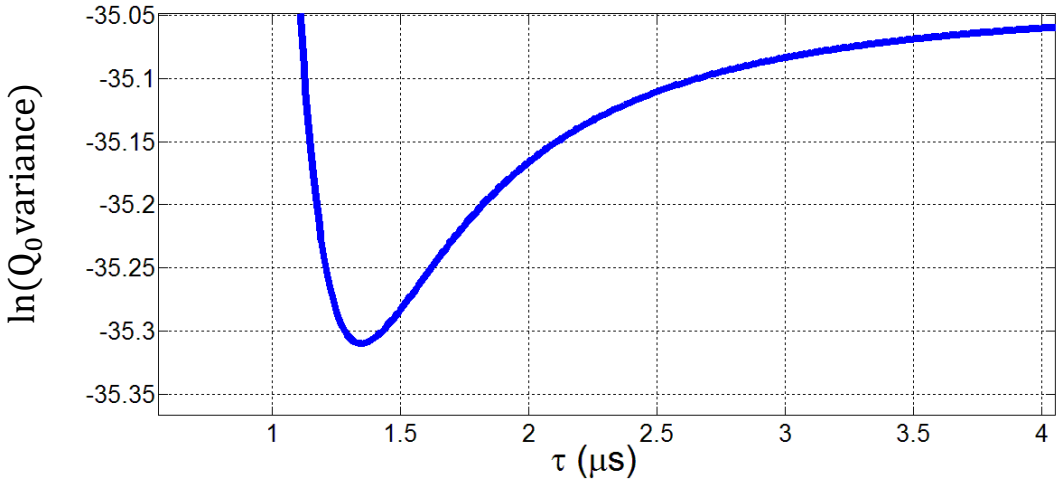

FIGURE 4.30 The lifetime of electrons is found with a minimization procedure. The figure shows the logarithm of the variance as a function of the τ candidates.

The electric fields are reconstructed (figure 4.31) after the calculation of mobility and laws of motion:

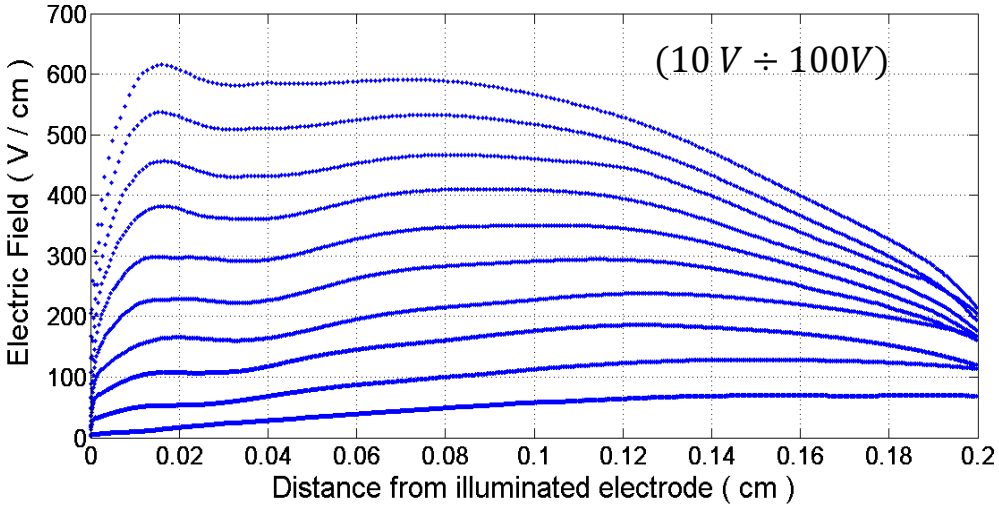

FIGURE 4.31 Electric fields for different voltages ($from\ 10\ V\ to\ 100\ V\ with\ 10\ V\ step$) in CZT REDLEN sample

In figure 4.31 the electric field show uniform spatial profiles at low voltages while on increasing the voltage, the electric field show a decreasing linear profile near the collecting pixel.

The lifetime and mobility of electrons result:

$$\tau = (1.35 \pm 0.05)\ \mu s \qquad \mu = (970 \pm 40)\ cm^2/(Vs)$$

$$\mu\tau = 1.3\ 10^{-3}\ cm^2/V$$

2. CZT REDLEN with pixel's size $P = 1.5\ mm$ [ELECTRONS]

The measurements of the current transient in the CZT sample with a pixel's size $S = 1.5\ mm$ are shown in figure (Figure 4.32):

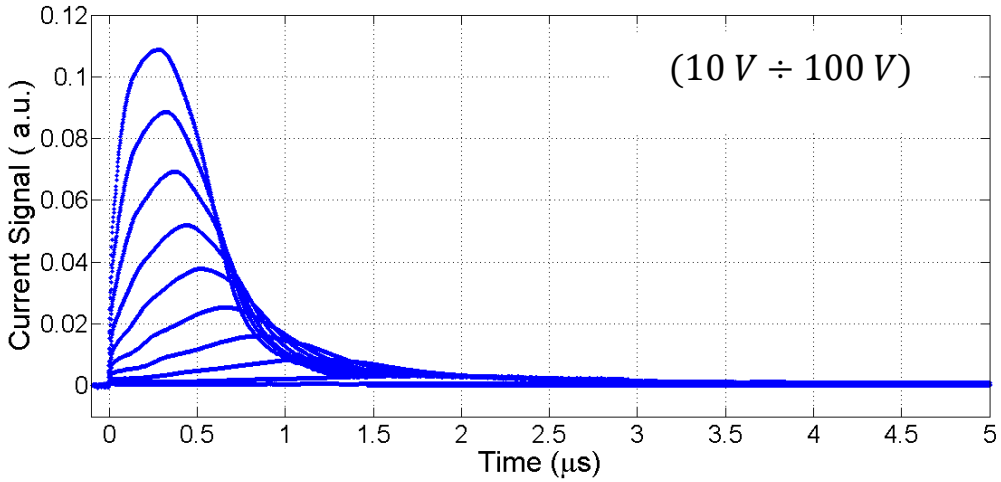

FIGURE 4.32 Current signals for different voltages ($from\ 10\ V\ to\ 100\ V\ with\ 10\ V\ step$) in CZT REDLEN sample with thickness $L = 2\ mm$ and pixel's size $P = 1.5\ mm$

The transients show the typical "pixel effect": the current increases while carriers travel towards the pixel. The term that increases in time is the $W(x(t))$ quantity: the weighting field probed in time by the carriers increases approaching to the pixel. This effect is only a geometric effect.

The calculation of the flight times, the procedure of minimization and the self-consistent approach described in the section 3.6.3 allow to obtain the transport parameters and the spatial electric field profile:

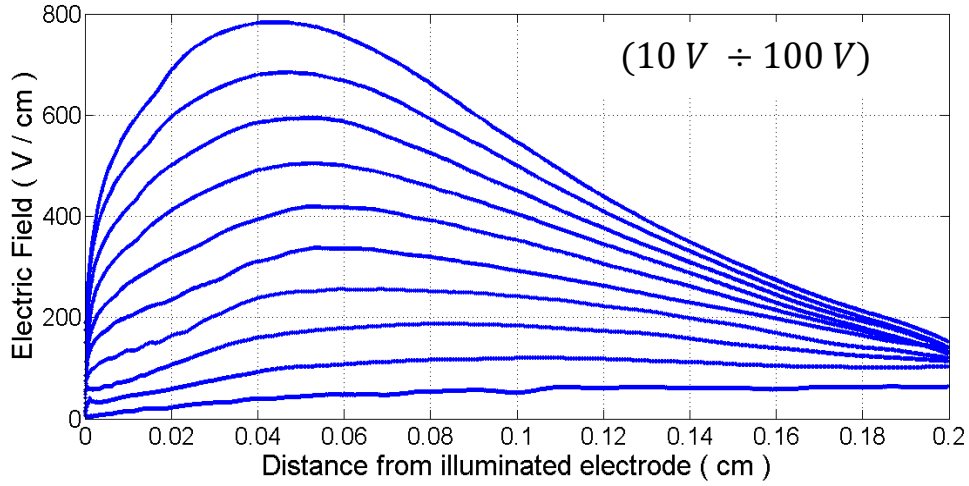

FIGURE 4.33 Electric fields for different voltages ($from\ 10\ V\ to\ 100\ V\ with\ 10\ V\ step$) in CZT REDLEN sample with thickness $L = 2\ mm$ and pixel's size $P = 1.5\ mm$

In figure 4.33, reconstructed electric fields show, as for sample with a 4 *mm* pixel, a uniform profile at low voltages, while the downward trend at high voltages is more pronounced. The decrease of the electric field is probably due to the presence of a positive fixed charge in the proximity of the collecting pixel.

The transport parameters result:

$$\tau = (0.98 \pm 0.07)\ \mu s \qquad \mu = (990 \pm 30)\ cm^2/(Vs)$$
$$\mu\tau = 0.97\ 10^{-3}\ cm^2/V$$

3. CZT REDLEN with pixel's size $P = 0.5\ mm$ [ELECTRONS]

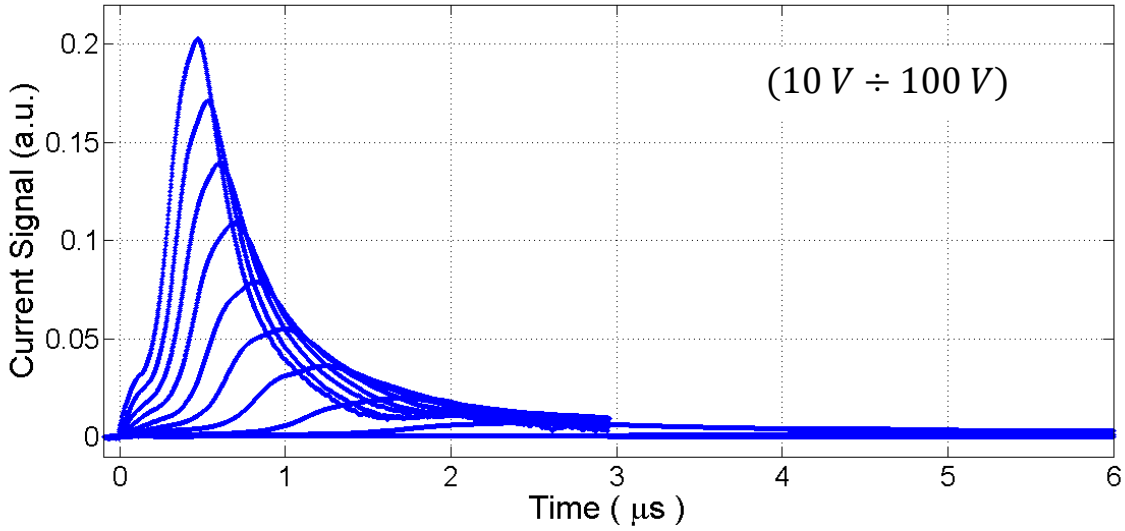

FIGURE 4.34 Current signals for different voltages $(from\ 10\ V\ to\ 100\ V\ with\ 10\ V)$ in CZT REDLEN sample with thickness $L = 2\ mm$ and pixel's size $P = 0.5\ mm$

In figure 4.34 the signals present a rapid increase due to the approach of the carriers to the pixel, where the weighting field is much greater than that probed at the beginning of the flight: the "pixel effect" is now widely clear.

The 1τ model's application allows to obtain the transport parameters and to reconstruct the electric fields:

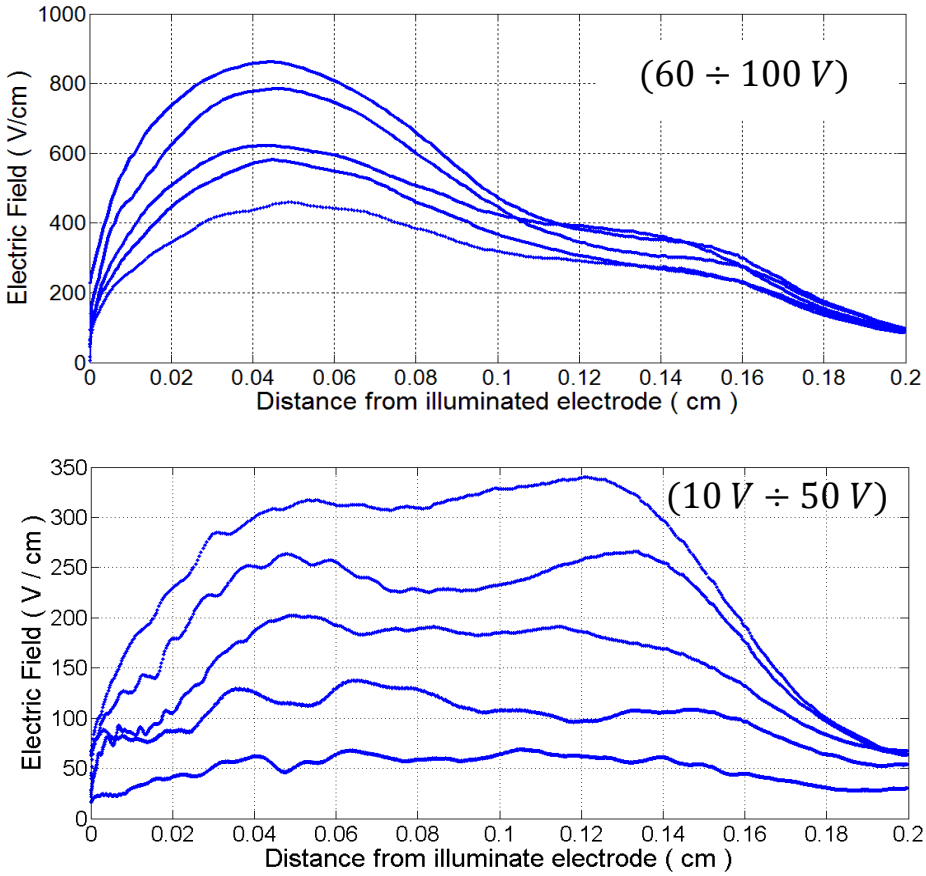

FIGURE 4.35 Electric fields for different voltages ($from\ 10\ V\ to\ 100\ V\ with\ 10\ V\ step$) in CZT REDLEN sample

The figure 4.35 shows the electric fields at high voltages, where the polarization effect near the pixel is greater. Instead, for lower voltages, as it happens on the other two samples, the electric fields show a nearly uniform profile.

The mobility and the lifetime of the electrons are equal to:

$$\tau = (1.4 \pm 0.05)\ \mu s \qquad \mu = (980 \pm 50)\ cm^2/(Vs)$$

$$\mu\tau = 1.37\ 10^{-3}\ cm^2/V$$

Measurements of current transient on three samples of the same ingot, where ideally the only difference lies in pixel size, showed that:

- the mobilities calculated for all three samples are in good agreement within experimental errors;
- the electric fields show a nearly uniform spatially profile at low voltages (from 10 to 50 Volts) while the electric fields show a descending profile in the proximity of the pixel for high voltages;
- the lifetime of electrons are very similar, about $1.3 - 1.4\ \mu s$, in samples with 4 and 0.5 *mm* pixel's size, while in the second sample the electron lifetime results $1\ \mu s$. We observe that also the slope of the electric field in the second sample is higher than in the others. The lifetime and the slope of the electric field could depend indeed on the presence of positive fixed charge. The fixed charge could bend the electric field and further it could increase the carriers' trapping, decreasing the lifetime. The application of 1τ model allows then to take into account of the contribution of the weighting field to the current. It is interesting to ask what would happen if we applied mistakenly the 2τ model, which assumes a uniform weighting profile, to the current transients. In this case, the choice of the model leads to a serious consequence on the electric field spatial profile. The assumption of a uniform weighting field induces the model to correlate the increase of the current to the increase of the electric field, even if the real increasing quantity is the weighting field. The transport parameters resulting from this mistaken assumption are wrong. It turns out that the lifetime does not change considerably using $1\tau - 2\tau$ model, because it's calculated starting from the same constraint (3.64) in both model. Instead the mobility changes significantly and it increases artificially with the decrease of the pixel size (Table 4.1)

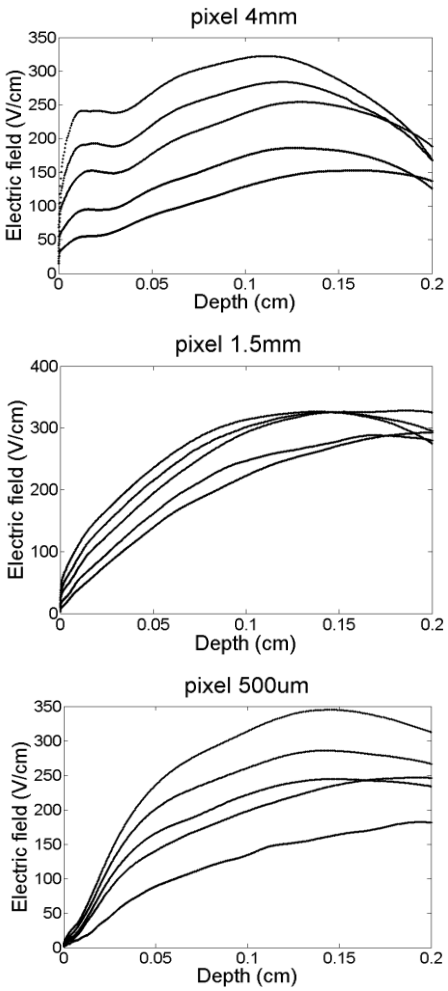

FIGURE 4.36 Electric field reconstructed using wrongly the 2τ model, for signals in pixelated detector.

PIXEL SIZE (mm)	***μ [CORRECT] (1τ model)***	***μ [WRONG] (2τ model)***
4	970	987
1.5	990	1070
0.5	980	1200

TABLE 4.1 Mobility values of the three sample with different pixel size obtained using the 1τ model (taking into account the non-uniform weighting field) and the 2τ model.

4.3.2 REDLEN CZT WITH *PT* CONTACTS [ELECTRONS]

It was observed before that the platinum electrodes enable the measure of signals from holes, in addition to electronic ones. The different work function between platinum and CZT is lower than that obtained with the junction Au-CZT. [45] This difference decreases the barrier for the escape of holes allowing to induce the current signal at the pixel.

The holes' mobility, 20-50 time less than electronic one, gives low induced signals nearly comparable to the thermal noise. For this reason, it is essential to use higher voltages than those used to obtain the electronic signals. In this sample, information related to the charge transport were obtained for both electrons that for holes, using two different ranges of voltages. Then the electric fields probed by carriers cannot be directly compared.

The CZT REDLEN sample with *Pt* contacts has:

- Thickness $L = 1.1\ mm$
- Size of the illuminated electrode $S = 5.5\ mm$
- Size of the pixel $P = 4\ mm$

In this case (figure 4.37) the weighting field does not differ significantly from the uniform profile, (being the relative difference of the weighting field between the two contacts is within 2%) because the sizes of the illuminated and pixel electrode are similar. A uniform weighting field, for a sample with a thickness equal to $L = 1.1\ mm$ should have a magnitude equal to $W = 1/L = 9\ cm^{-1}$.

Obviously the weighting field probed by electrons and holes are exactly the same.

The unique difference is the different sign of the applied voltage, while the geometry of the sample does not change.

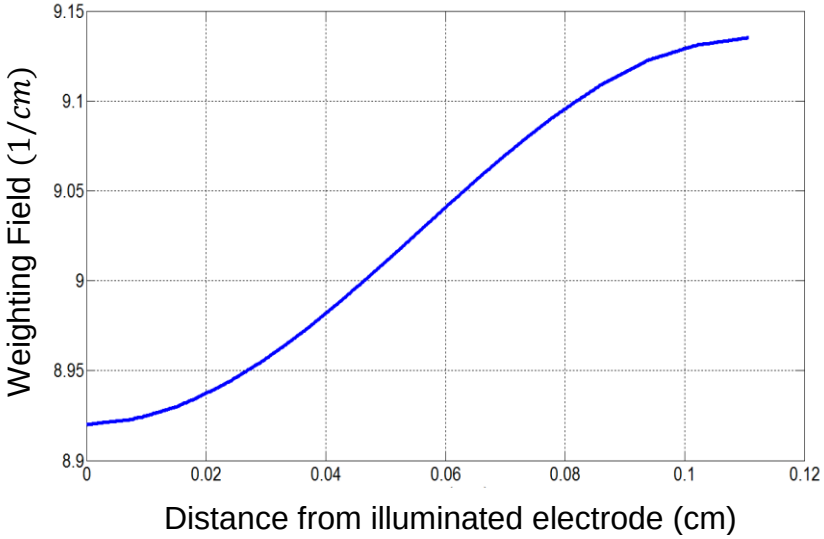

FIGURE 4.37 Weighting field for CZT REDLEN with $L = 1.1\ mm, P = 5.5\ mm\ and\ S = 4mm$.

SIGNALS ON CZT REDLEN WITH *PT* CONTACTS [ELECTRONS]

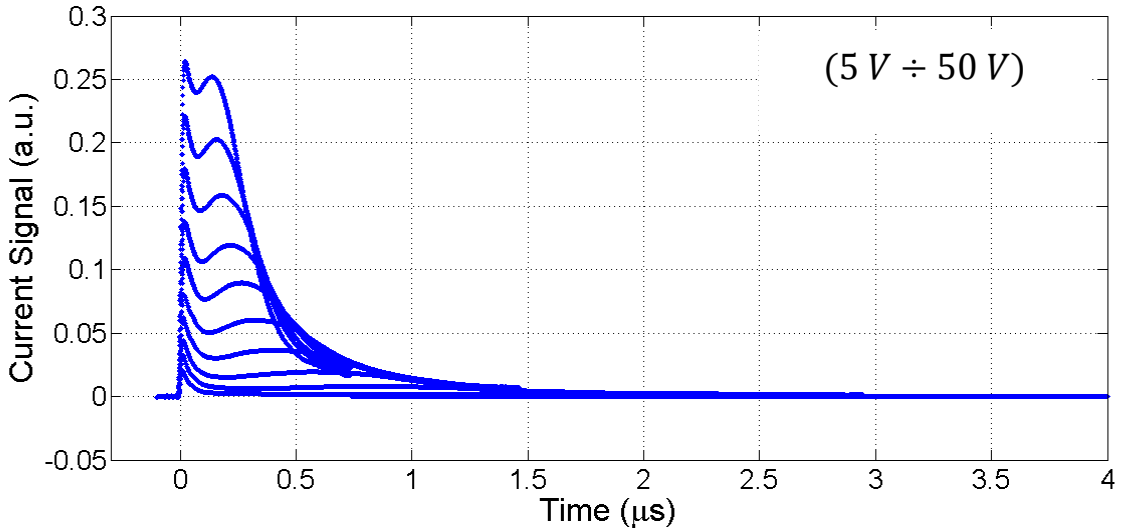

FIGURE 4.38 Signals of electrons for different voltages ($from\ 5\ V\ to\ 50\ V\ with\ 5\ V\ step$) in CZT REDLEN sample with *Pt* contacts with thickness $L = 1.1\ mm$ and pixel's size $P = 4\ mm$

With the application of the 1τ model, the electric fields (figure 4.39) for this range of voltages are obtained:

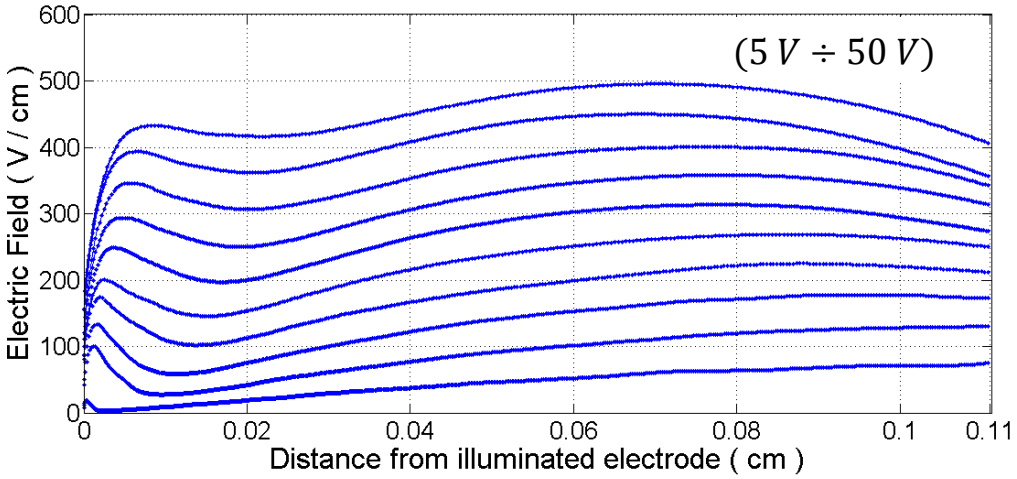

FIGURE 4.39 Electric fields for different voltages ($from\ 5\ V\ to\ 50\ V\ with\ 5\ V\ step$) in CZT REDLEN sample with *Pt* contacts with thickness $L = 1.1\ mm$ and pixel's size $P = 4\ mm$

The electric field show a uniform profile, proving that for low voltages the sample is not affected by the polarization phenomenon.

The transport parameters are equal to:

$$\tau = (0.60 \pm 0.08)\ \mu s \qquad \mu = (1030 \pm 60)\ cm^2/(Vs)$$

$$\mu\tau = 0.7\ 10^{-3}\ cm^2/V$$

SIGNALS ON CZT REDLEN WITH *PT* CONTACTS [HOLES]

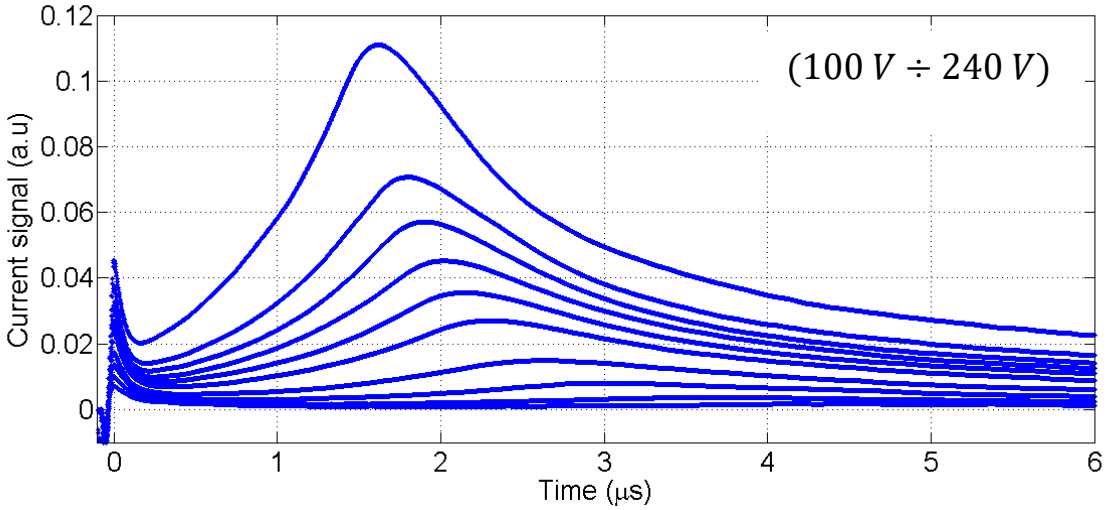

FIGURE 4.40 Signals of holes for different voltages ($from\ 100\ V\ to\ 240\ V\ with\ 20\ V\ step$) in CZT REDLEN sample with *Pt* contacts with thickness $L = 1.1\ mm$ and pixel's size $P = 4\ mm$

In figure 4.40 the currents show a time increasing profile, despite that the weighting filed does not increase so drastically in the vicinity of the pixel. The current should also decrease because of carriers' trapping. As a consequence, the unique quantity that can increase is the electric field probed by carriers during their flight.

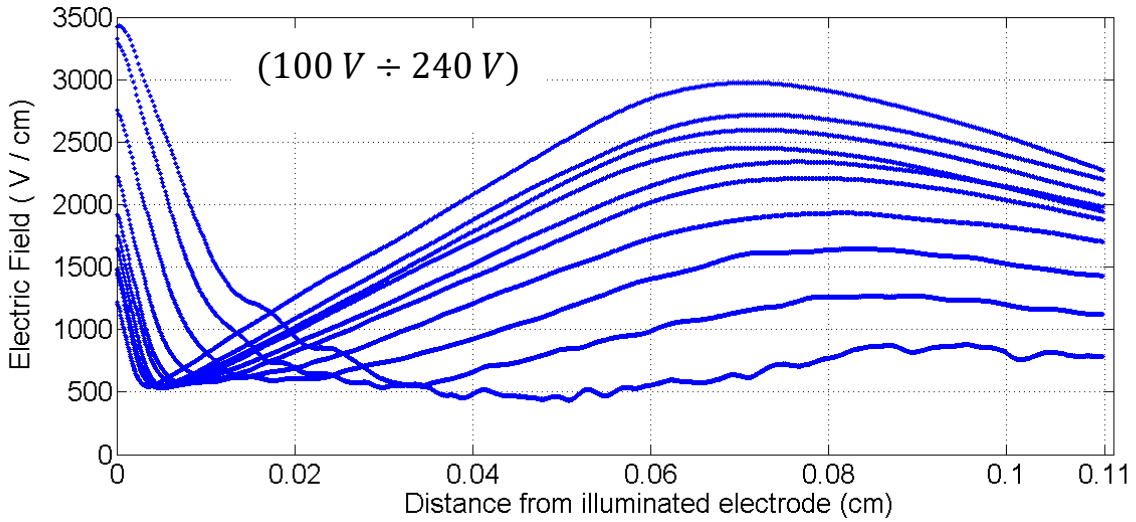

FIGURE 4.41 Electric fields for different voltages ($from\ 100\ V\ to\ 240\ V\ with\ 20\ V\ step$) in CZT REDLEN sample with *Pt* contacts with thickness $L = 1.1\ mm$ and pixel's size $P = 4\ mm$

The hypothesis of an increasing electric field is confirmed. Near the illuminated cathode, the electric field shows a decreasing profile, due probably to the holes trapped near this electrode. At distance higher than about $0.1\ mm$ from the illuminated electrode, the fixed charge changes in sign and electric field begins to increase.

In this case, the model was unable to give the lifetime of holes: the times of flight for the used voltages are much more short than the holes' lifetime. The only way to get the holes' lifetime would further lower the voltage to be able to fly the carriers for a longer time comparable to the lifetime. With our experimental setup, it is very difficult to measure transients because, for voltages lower than 100 volts, the signal becomes comparable with the noise and it is not possible to estimate the correct time of flight and the model results inapplicable. We can only assume that the lifetime is greater than the highest time of flight in our current signals. The holes' mobility instead results 35 times lower than electrons' mobility:

$$\tau > 5\ \mu s \qquad\qquad \mu = (28\ \pm 2)\ cm^2/(Vs)$$

4.3.3 CZT 43-IMEM [ELECTRONS]

The last pixelated detector studied in this thesis is a CZT IMEM detector with *Au* contacts.

The sizes of the sample are:

- Thickness $L = 2.8\ mm$
- Size of the illuminated electrode $S = 5.5\ mm$
- Size of the pixel $P = 3\ mm$

The current measurements show the pixel effect, while for low voltages the signal begins to decrease in time. Despite the increase of the weighting field, for low voltages the flight time becomes comparable with the lifetime of the carriers, and then the current begins to decrease because of the low number of electrons that arrives at the collecting pixel.

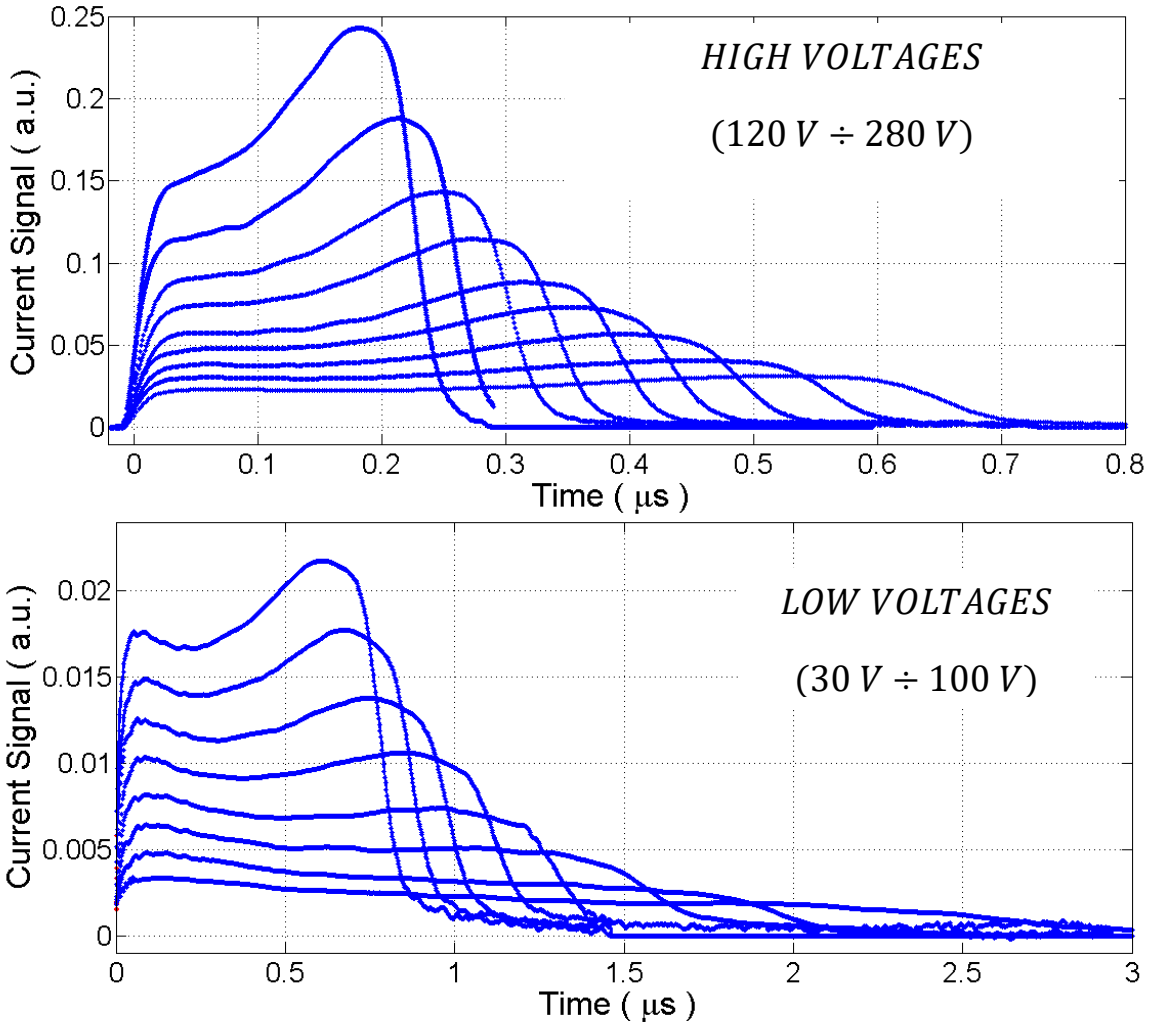

FIGURE 4.42 Current signals of electrons for two different ranges of voltages (HIGH VOLTAGE from 120 V *to* 280 V *with* 20 V step and LOW VOLTAGES from 30 V to 100 V with 10 V *step*) in CZT IMEM sample with *Au* contacts with thickness $L = 2.8\ mm$ and pixel's size $P = 3\ mm$

The profiles of the electric field reconstructed are shown in figure 4.43 for all range of voltages (HIGH VOLTAGE from 120 V *to* 280 V *with* 20 V step and LOW VOLTAGES from 30 V to 100 V with 10 V *step*).

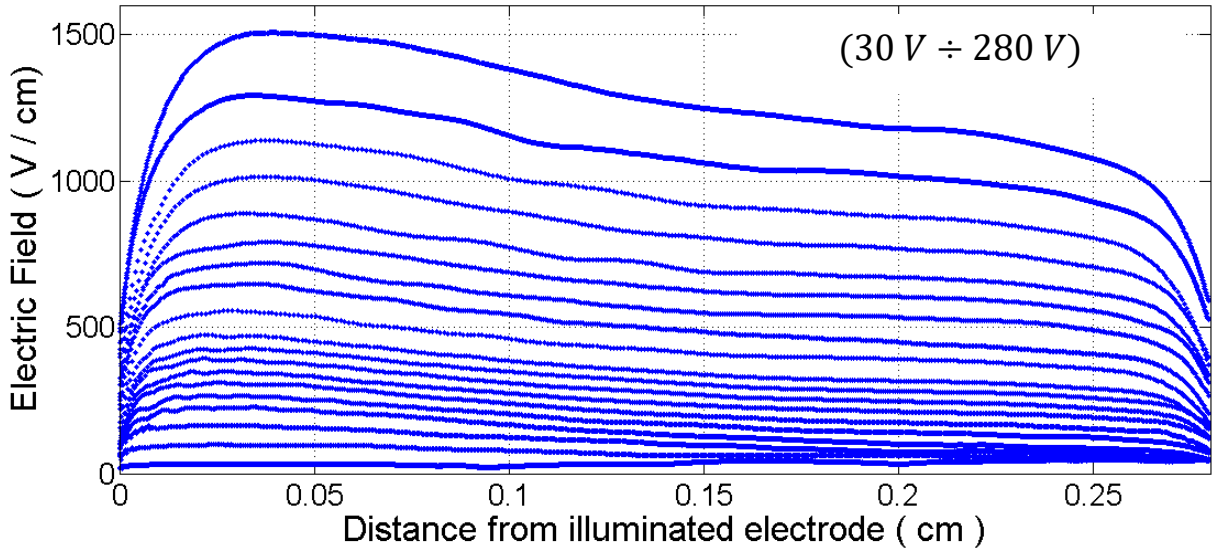

FIGURE 4.43 Electric field for different voltages (from 30 to 280 Volts) in CZT IMEM sample with *Au* contacts with thickness $L = 2.8\ mm$ and pixel's size $P = 3\ mm$

The transport parameters result:

$$\tau = (2.7 \pm 0.1)\mu s \qquad \mu = (1050 \pm 30)\ cm^2/(Vs$$

$$\mu\tau = 2.8\ 10^{-3}\ cm^2/V$$

5 CONCLUSIONS

In this thesis work we have proposed some transport models for the analysis of transient signal which have proved to be suitable for the study of the transport properties and the electric field in solid state X, γ rays photo-detectors. The thesis has involved the study of samples of different material ($CdTe$ and $Cd_{1-x}Zn_xTe$), thickness (form $250\,\mu m$ to $4\,mm$), type of contact (Platinum and Gold) and electrodes' geometry (full-area and pixel contact). All the models are based on the analysis of current transients induced by laser-beam, with the Laser Excited-Transient Current Technique (LE-TCT).

The application of 2τ model has allowed to obtain the transport properties of both electrons and holes and the spatial profile of the electric field in sample with full-area contacts. Furthermore, the measurements of Charge Collection Efficiency (CCE technique) allowed to compare successfully the $\mu\tau$ product obtained with the two different techniques, also with a good agreement regarding the electric field profile .

The pixelated detectors instead needed a preliminary study from a geometrical point of view, as the signal depends strongly on the weighting field, a vector field which depends only on the geometry of illuminated and collecting electrodes.

The 1τ model proposed a self-consistent procedure and minimization, enabling the possibility to measure μ, τ, and E directly on single devices. This method has been demonstrated useful for measuring both electrons and holes. The method has been validated on devices having different weighting field. The different geometric component leads to the so-called "pixel effect", an increase of the induced current in the proximity of the final part of the transients.

When the weighting field correction is not taken into account, a wrong value of μ and a wrong E profile is obtained.

A new method has been developed to study the spread of the charge cloud during the drift of carriers The diffusion coefficient has been deduced and a correct evaluation of the time of flight has been obtained through the study of the time derivative of the current transients.

Finally, this models could be used to obtain the transport properties and the electric field profiles of samples of different material such as $GaAs$ and Ga_2O_3.

BIBLIOGRAPHY

[1] W.E. Burcham. Nuclear Physics: An Introduction. Longmans, London, 1963.

[2] D.A. Neamen, “Semiconductor Physics and Devices: Basic Principles”. McGraw-Hill, 3th edition, 2003, pp. 189-196

[3] M.Guzzi, “Principi di Fisica dei semiconduttori”. Hoepli, 5th ed, 2008, pp.107-130

[4] G.F. Knoll. Radiation Detection and Measurement, 3rd Edition. Wiley and Sons Inc., 2000.

[5] T.E. Schlesinger, J.E. Toney, H.Yoon, E-Y. Lee, B.A. Brunett, L. Franks, R.B. James, "Cadmium zinc telluride and its use as nuclear radiation detector material", Material Science and Engineering, 32 (2001) 103-189 A review journal

[6] M. Fiederle, A. Fauler, A. Zwerger, "Crystal Growth and Characterization of Detector Grade (Cd,Zn)Te Crystals", IEEE Transactions on nuclear science, Vol. 54, N°. 4, AUGUST 2007, p 769.

[7] Glenn F. Knoll N. Peyghambarian, S.W. Koch, A. Msyrowicz, "Indroduction to Semiconductor Optics", Prentice-Hall, Englewood Cliff, 1993.

[8] A. Rose. "Concepts in Photoconductivity and Allied Problems". Wiley, New York, 1963.

[9] Tratto dal sito www.evproducts.com

[10] Robert Triboulet. Fundamentals of the CdTe synthesis. Journal of Alloys and Compounds, 371:67-71, 2004.

[11] F. Bissoli. "Preparazione e studio di CdTe per applicazioni elettroottiche". Tesi di Dottorato di Ricerca In STMI, 2002.

[12] C. Paorici. Crescita cristallina, crescita da liquidi. Enciclopedia del Novecento, Vol A-B Suppl III.

[13] R.B.James T.E.Schlesinger. "Semiconductors for room temperature applications". Academic Press, New York, 1995.

[14] J.J.Kennedy et al. Groth and characterization of $Cd_{1-x}\,Zn_xTe$ and $Hg_{1-x}\,Zn_xTe$. J. Crystal Growth, 86:93

[15] Csaba Szeles and Michael C. Driver. Growth and properties of semi-insulating CdZnTe for radiation detector applications. Technical report, eV Products a division of II-VI, Inc.

[16] S.Wen-Bin et al. Crystal growth and characterization of CdTe from melt under controlled cd partial pressure. Journal of Crystal Growth, 86:127-131, 1988.

[17] Cherng H.Y.O. Shin. Temperature-gradient-solution grown CdTe crystal for g-ray detectors. J. Crystal Growth, 186:67-68, 1998.

[18] E. Weigel, G. Müller-Vogt, "Comparison of Bridgam and THM method regarding the effect of In doping and distribution of Zn in CdTe", Journal of Crystal Growth, 161, 1996, pp 40-44.

[19] F. Seitz, Imperfections in nearly Perfects Crystal, Wiley, New York (1952)

[20] M.Hage-Ali, P.Siffert, Status of semi-insulating cadmium telluride for nuclear radiation detector, nuclear instruments and Methods in Physics Research A322(1992), pp. 313-323

[21] K. Nakagawa, K. Naeda, S. Takeuchi, Appl. Phys. Lett. 34 (1979) 574.

[22] C. Szeles, "Advances in the Crystal Growth and Device Fabrication Technology of CdZnTe Room Temperature Radiation Detectors", IEEE Trans. Nucl. Sci. Vol.51, N.3 (2004), 1242

[23] M. Avrami, J.Chem.Phys., 7 (1939), 1103

[24] H.F. Shaake and J.H. Tregilgas, J.Vac.Sci.Technol. A4 (1986), 2181

[25] M.Fiederle, C.Eiche,M.Salk,R.Schwarz and K.W.Benz. "Modified compensation model of CdTe", J Appl.Phys. Vol.84, No.12 (1998)

[26] G. A. Carini, A. E. Bolotnikov, G. S. Camarda, G. W. Wright, and R. B. James, "Effect of Te precipitates on the performance of CdZnTe detectors", Applied physics letters, 88, 143515, 2006 pp

[27] P. Rudolph et al. Defects in CdTe Bridgman monocrystals caused by nonstoichiometric growth conditions. Journal of Crystal Growth, 128:582{587, 1993.

[28] P. Rudolph et al. Distribution and genesis of inclusions in CdTe and (CdZnTe single crystals grown by the bridgman method and by the travelling heater method. Journal of Crystal Growth, 147:297{304, 1995.

[29] Robert Triboulet and Paul Siffert. CdTe and Related Compounds: Physics, Defects, Hetero and Nano-Structures, Cristal Growth, Surfaces and Applications. Elsevier, 2009.

[30] Ramo, S. (1939). "Currents Induced by Electron Motion". Proceedings of the IRE.27(9): 584–585.

[31] Shockley, W. (1938). "Currents to Conductors Induced by a Moving Point Charge". Journal of Applied Physics.9(10): 635.

[32] Štepán Uxa et al. "Determination of Electric-Field Profile in CdTe and CdZnTe Detectors Using Transient-Current Technique" IEEE TRANSACTIONS ON NUCLEAR SCIENCE, VOL. 59, NO. 5, OCTOBER 2012

[33] J. Fink et al. "Characterization of charge collection in CdTe and CZT using the transient current technique" arXiv:physics/0511184v2 [physics.insdet]. (2005)

[34] A. Santi, M. Zanichelli, G. Piacentini, M. Pavesi, A. Cola and I. Farella; "An original method to evaluate the transport parameters and reconstruct the electric field in solid-state photodetectors". Appl. Phys. Lett. 104, 193503 (2014).

[35] J.C. Erickson et al. "Time of Flight Experimental Studies of CdZnTe Radiation Detectors" Journal of Electronic Materials. Vol.29, No.6, 2000 (Received November 11, 1999; accepted December 12, 1999)

[36] A. E. Bolotnikov, S. E. Boggs, W. R. Cook, F. A. Harrison, S. M. Schindler."Use of a pulsed laser to study properties of CdZnTe pixel detectors" Space Radiation Laboratory, California Institute of Technology

[37] M.Zanichelli, A.Santi, M.Pavesi , A. Zappettini; "Charge collection in semi-insulator radiation detectors in the presence of a linear decreasing electric field" J.of Phys. D-Appl.Phys. 46,365103 (2013)

[38] J.D. Eskin, H.H. Barrett, and H.B. Barber, Signals induced in semiconductor gamma-ray imaging detectors, J. Appl. Phys. 85 (1999) 647.

[39] Y. Nemirovsky, M. Ifraimov, and A. Ludwig, Effect of the geometrical parameters on the electric field of pixelated two-dimensional arrays of γ-ray spectrometers, J. Appl. Phys. 88 (2000) 5388

[40] Z.He, "Rewiew of the Shockley-Ramo theorem and its applications in semiconductor gamma - ray detectors.". Nucl.Instr.Meth.A vol.463 (2001), pp.250-267

[41] K. Hecht, "Zum mechanismus des lichtelektrischen primrstomes in isolierenden kristallen" Zeitschrift fur physik A vol.77, pp.235-245,1932

[42] A. Many, "High - field effects in photoconducting cadmium sulphide" J.Phys. Chem. Solids, vol.26, pp.575-585,1965

[43] Maria Maksimow, Lavoro di Tesi. "Transient current technique characterization of silicon particle detectors".Helsinki university of technology Faculty of Electronics, Communications and Automation

[44] A. Santi, G. Piacentini, M. Zanichelli, M. Bettelli, A. Zappettini, and M. Pavesi "Comparison between two independent evaluation methods for electric field profile and transport parameters in solid-state CZT photodetectors". NSSMIC 2015

[45] Y. Nemirovsky, A. Ruzin, G. Asa, and J. Gorelik, "Study of Contacts to CdZnTe Radiation Detectors" J. El. Mat. vol. 26 No. 6, 1997, pp. 756-764.

[46] http://www.ks.uiuc.edu/Services/Class/PHYS498/LectureNotes/chp4.pdf

PUBLICATIONS AND CONGRESS

- **A.Santi**, G. Piacentini, M. Zanichelli, M. Bettelli, A. Zappettini, and M. Pavesi, "Evaluation of electric field profile and transport parameters in solid-state CZT detectors" Proc. Nuclear Science Symposium and Medical Imaging Conference (NSS/MIC) IEEE (2015)

- M.Zanichelli, **A.Santi**, M.Pavesi, A. Zappettini; "Charge collection in semi-insulator radiation detectors in the presence of a linear decreasing electric field". J. of Phys. D-Appl.Phys. 46, 365103 (2013)

- **A. Santi**, M. Zanichelli, G. Piacentini, M. Pavesi, A. Cola and I. Farella; "An original method to evaluate the transport parameters and reconstruct the electric field in solid-state photodetectors". Appl. Phys. Lett. 104, 193503 (2014).

Congress IEEE NSS-MIC-RTSD Congress October 2016 Strasbourg, France:

- Poster presentation: **A.Santi**, M. Bettelli, A. Zappettini, M.Zanichelli, M.Pavesi "Diffusion Coefficient and Drift Parameter Evaluation in Telluride Solid-State Detectors"

- Invited oral presentation: A.Zappettini, **A. Santi**, M. Bettelli, G. Piacentini, M. Zanichelli, and M. Pavesi. "Laser Induced Transient Current Technique as a Powerful Tool to Determine Charge Transport Properties, Electric Field and Weighting Field Distribution in CdZnTe Detectors"